

**Spatial and temporal distributions of magnetotactic bacteria in
control aquaria and a freshwater pond**

Kuang He

Dissertation zur Erlangung des Doktorgrades an der
Fakultät für Geowissenschaften
der Ludwig-Maximilians-Universität München

Vorgelegt von

Kuang He

Munich, 28. 11. 2017

Erstgutachter: Prof. Dr. Stuart Gilder

Zweitgutachter: Prof. Dr. William Orsi

Tag der mündlichen Prüfung: 09. 02. 2018

Contents

List of Figures.....	v
List of Tables.....	vii
Acknowledgements.....	viii
Abstract.....	1
Chapter 1 Introduction.....	3
Chapter 2 Constant flux of spatial niche partitioning from high resolution sampling of magnetotactic bacteria.....	14
2.1. Introduction.....	14
2.2. Materials and Methods.....	15
2.2.1. Sample Collection and Counting.....	15
2.2.2. Mapping.....	18
2.2.3. Oxygen Concentration.....	19
2.3. Results.....	20
2.3.1. Spatiotemporal variation of magnetotactic bacteria.....	20
2.4. Discussion.....	24
Chapter 3 Temporal and spatial variation of magnetotactic bacteria communities in a freshwater pond.....	31
3.1. Introduction.....	31
3.2. Methods.....	32
3.2.1. Study design and sampling.....	32
3.2.2 Measurement protocol: Oxygen, carbon and nitrogen concentrations, MTB quantification and magnetic properties.....	34
3.3. Results.....	37

3.4. Discussion	49
Chapter 4 Perspectives.....	56
Chapter 5 The relationship between magnetic field strength and remanence anisotropy through redeposition experiments.....	58
5.1 Introduction	58
5.2 Methods.....	60
5.2.1 Sample preparation	60
5.2.2 Magnetic measurements.....	63
5.3 Results and Discussion.....	65
References.....	84
Curriculum Vitae	97

List of Figures

Figure 2 - 1 Sketch of a sample placed on a slide in the magnetodrome	16
Figure 2 - 2 Image at the air-water interface seen under the optical microscope and scanning electro microscope	18
Figure 2 - 3 Number of MTB cocci counted as a function of time for 10 discrete samples	19
Figure 2 - 4 Oxygen profiles of nine samples in aquaria A and B on day 120	20
Figure 2 - 5 Horizontal distribution of MTB	21
Figure 2 - 6 Horizontal distribution of MTB (double normalized).....	22
Figure 2 - 7 Box plots of MTB abundance in aquaria A and B through time	24
Figure 2 - 8 Percentage of the three MTB species in aquaria A and B over time	29
Figure 2 - 9 Box plots of the change in MTB growth rate over time in aquaria A and B.....	30
Figure 3 - 1 The information of the Niederlippach pond	34
Figure 3 - 2 Temporal variation of environmental factors and MTB abundance	37
Figure 3 - 3 MTB concentrations at each site.....	40
Figure 3 - 4 Relationship between spirilla and cocci abundances at each site	43
Figure 3 - 5 Relationship between bottom water O ₂ and MTB concentrations of the three morphotypes.	44
Figure 3 - 6 Field cooled SIRM curves, temperature dependence of the magnetic remanence and susceptibility and FORCs.....	45
Figure 3 - 7 Magnetic and chemical parameters of the upper 1 cm of sediment from the pond...	46
Figure 3 - 8 Vertical distribution of magnetotactic bacteria abundance and magnetic parameters	50
Figure 3 - 9 Photos of the Niederlippach pond during different months in 2015.....	54
Figure 3 - 10 Photos of the Niederlippach pond during different months in 2016.....	54
Figure 3 - 11 Monthly averaged MTB concentrations in the pond	55
Figure 5 - 1 Redeposition experiment.....	62
Figure 5 - 2 The enrichment of MTB and set up of redeposition experiment produced by magnet.	62
Figure 5 - 3 The spatial distribution of external field strength and directions on the wood board	63
Figure 5 - 4 The electromagnet.....	64
Figure 5 - 5 Biplots of $\chi_{ARM}/SIRM$ vs. χ_{ARM}/χ	66
Figure 5 - 6 The average normalized AF demagnetization curves of NRM at different external field strength.....	67
Figure 5 - 7 Alternating-field demagnetization of the NRM of one sample at different field strength.....	69
Figure 5 - 8 Stereonet plots for NRM and AF 30 mT.....	71
Figure 5 - 9 Plot of SIRM versus χ for samples	72
Figure 5 - 10 The relationship between NRM/ χ and B.....	73
Figure 5 - 11 The relationship between NRM/ARM and B	73

Figure 5 - 12 The relationship between NRM/SIRM and B	74
Figure 5 - 13 The AARM ellipsoid at different field strength.....	74
Figure 5 - 14 The stereographic projection of principal susceptibility axes, P-Km plot and P-T plot of AMS	80
Figure 5 - 15 The relationship between F, L and B	81
Figure 5 - 16 The relationship between external field strength and P	81
Figure 5 - 17 SIRM normalized ARM acquisition versus the bias field applied during alternating field demagnetization for the redeposition samples.....	82

List of Tables

Table 2 - 1 Statistics on magnetotactic bacteria populations for aquaria A and B over time based on 36 measurements in each aquaria.....	28
Table 2 - 2 Correlation coefficients for each species between successive measurements.....	29
Table 3 - 1 Average magnetotactic bacteria cell populations and bottom water oxygen concentrations for the nine sites in the pond and in the control beaker	38
Table 3 - 2 Water depth and bottom water temperature at each site or control beaker (CB) for each month in 2015 and 2016.....	39
Table 3 - 3 Average (4 samples) magnetotactic bacteria cell populations for each site in 2015 (upper rows) and 2016 (lower rows).....	41
Table 3 - 4 Magnetic hysteresis and back field parameters for the nine sites in each month of 2016.....	47
Table 3 - 5 Carbon and nitrogen isotopic data for each sample at each site in January 2015 and August 2016 (data in figures are the averages of the two samples/site)	48
Table 3 - 6 Vertical distribution of magnetotactic bacteria abundance	51
Table 3 - 7 Vertical distribution of magnetic parameters.....	51

Acknowledgements

I thank Professor Gilder, who gave me the chance to finish my PhD studies in Munich. He taught me the right attitude to do scientific research. He also helped me to improve my scientific communication and writing skills. He always encouraged me to make progress patiently.

I thank Professor Petersen, who has huge interest on magnetotactic bacteria. He supplied me many interesting ideas about the experiments.

I thank Professor Orsi and Professor Egli, who gave me many useful suggestions to improve my paper.

I thank Professor Bachtadse, who wrote a recommendation letter for me to get the LMU completion grant. I thank Christoph Mayr, who helped me with the measurement of geochemical parameters and improving my paper.

I thank Xiangyu Zhao, Qingguo Wei, Yanjun Cheng and Xuegang Mao, Michael Wack, Michael Volk, Sophie Roud, Florian Lhuillier, Carina, Michael Eitel, Manuela Weiss, Edoardo, Gwenael, Stephan Eder, they helped me lot in my studies and life.

Finally, I thank my parents and my elder brother. They always supported and encouraged me.

The Chinese Scholarship Council helped support my studies in Munich, Germany. A LMU-Completion Grant supported me to finish writing the thesis.

Abstract

Magnetotactic bacteria (MTB) swim along magnetic field lines in water. They are found in aquatic habitats throughout the world, yet knowledge of their spatial and temporal distribution remains limited. To help remedy this, MTB-bearing sediment was taken from a natural pond, mixed into two replicate aquaria, and then the three dominant MTB morphotypes (cocci, spirilla and rod-shapes) were counted at high spatiotemporal sampling resolution: 36 discrete points in replicate aquaria were sampled every ~30 days over 198 days. Population centers of cocci and spirilla morphotypes moved in continual flux, yet they consistently inhabited separate locations displaying significant anti-correlation. Rod-shaped MTB were initially concentrated toward the northern end of the aquaria, but at the end of the experiment were most densely populated toward the south. That the total number of MTB cells increased through time during the experiment argues that population reorganization arose from relative changes in cell division and death and not from migration. The maximum net growth rates were 10, 3 and 1 day⁻¹ and average net growth rates were 0.24, 0.11 and 0.02 day⁻¹ for cocci, spirilla and rod-shaped MTB respectively; minimum growth rates for all three morphotypes were -0.03 day⁻¹. Our results suggest that cocci and spirilla occupy distinctly different niches--their horizontal positioning in sediment are anti-correlated and under constant flux.

Magnetotactic bacteria (MTB) synthesize ferrimagnetic crystals that contribute to the remanent magnetization in sediments, yet knowledge of how MTB populations vary in natural environments over time remained limited. One chapter in this thesis documents the abundances of three MTB morphotypes from nine sites collected and measured every month over a two-year period from a pond near Munich, Germany. Morphotype populations underwent coherent temporal trends among the nine sites. Spirilla populations attained maxima in the summer when temperatures were highest and oxygen concentrations were lowest. Spirilla and cocci exhibited relative antipathy in 2015 when both morphotypes reacted in distinctly opposite ways to oxygen levels. In 2016, they were positively correlated with each other but displayed no coherency with oxygen. Magnetic properties of the sediments varied with water depth: deeper sites, which were also lower in organic carbon, nitrogen and oxygen concentrations than shallower sites, had higher saturation magnetizations and were richer in single domain particles. Although absolute MTB concentrations differed in space, all three measured morphotypes underwent similar

relative changes in the time domain at the nine sites; hence, long-term trends of MTB populations in natural ecosystems are likely indicative of the ecosystem as a whole. This is in distinct contrast to artificial habitats in the laboratory that have not reached steady-state conditions.

Redeposition experiments were performed over a range of magnetic field intensities and inclinations using the magnetite-bearing, natural sediments from the pond near Munich. Remanent magnetization systematically increased with applied magnetic field, yet relative paleointensities from 25 repeat redeposition experiments performed at identical field conditions vary by a factor of two. The question arises as to what accounts for the variability and what can we do to diminish/remove the variability to improve the precision of relative paleointensity estimates? Recalling that the saturation magnetization (M_s) lies in the long axis direction of a magnetite grain, then the maximum axis of the magnetic anisotropy ellipsoid should parallel the paleomagnetic direction if the magnetization reflects a true depositional remanence acquired via torque. As higher external fields increase the remanence in sediments by tightening the alignment of the grains, the magnetic anisotropy ellipsoid should become increasingly prolate proportional to field strength. This effect is indeed demonstrated in new experiments using anisotropy of anhysteretic remanent magnetization (AARM): nearly all AARM indices vary in proportion with magnetic field strength. Conversely, anisotropy of magnetic susceptibility does not, as it is overwhelmed by the paramagnetic fraction that shows a sedimentary fabric. AARM thus holds promise to improve relative paleointensity estimates from sediments.

Chapter 1 Introduction

Magnetotactic bacteria (MTB) were first reported by *Bellini* [1963a; b], who found it is a microorganism which can swim along field lines. In 1975, *Blakemore* [1975] published a report about magnetotactic bacteria found in salt marshes. Afterwards, the unique characteristics of magnetosome biomineralization have attracted a broad interdisciplinary interest of scientists, such as biologists, geologists and engineers. MTB form membrane-bound intracellular magnetite or greigite or both. These particles are nanometre-sized (35-150 nm) aligned in one or several chains, which produce magnetic moments that force MTB to swim along magnetic lines. According to the phylogenetic identification, MTB can be divided into *Alphaproteobacteria*, *Gammaproteobacteria*, the *Deltaproteobacteria*, the *Nitrospira* phylum and the candidate division OP3 [*Faivre and Schüler*, 2008]. Magnetite magnetosomes strains mostly belong to alphaproteobacteria. *Desulfovibrio magneticus* strain RS-1, which belongs to the δ -Proteobacteria, has Fe_3O_4 magnetosomes [*Kawaguchi et al.*, 1995]. However, *Magnetobacterium bavaricum* with Fe_3O_4 magnetosomes, belong to *Nitrospira* phylum [*Spring et al.*, 1993]. Wild Fe_3S_4 magnetosomes strains belong to *deltaproteobacteria* [*DeLong et al.*, 1993].

MTB have a wide variety of morphotypes, including cocci, spirilla, rods, ovoids, vibrios and multicellular magnetotactic prokaryotes (MMPs). They can be found in freshwater or ocean habits, or even in soil [*Du et al.*, 2015; *Fassbinder et al.*, 1990; *Lin et al.*, 2013a; *Petermann and Bleil*, 1993; *Simmons et al.*, 2006; *Spring and Schleifer*, 1995]. They are microaerophilic or anaerobic. In the northern hemisphere, most of them are north seeking, which means they move in the same directions as the magnetic lines, supposedly to make them swim toward the oxic-anoxic transition zone (OATZ). In the southern hemisphere, most MTB are south-seeking [*Blakemore et al.*, 1980; *Kirschvink*, 1980]. However, *Simmons et al.* [2006] discovered south-seeking MTB in a salt pond in the US (northern hemisphere), and they concluded that high redox conditions caused the phenomenon. Because the magnetosome lie in the single domain size range [*Schüler and Frankel*, 1999], they can record the magnetic field. Several researchers found that biogenic magnetite contributes to the total magnetic remanence in sediments [*Petersen et al.*, 1986]. The morphology of magnetosome are octahedron, prismatic, bullet and tear-shaped [*Chang and Kirschvink*, 1989; *Moskowitz*, 1995]. Elongated-anisotropic magnetosomes strains belong to three phylogenetic groups of MTB: the *Deltaproteobacteria*, the

Nitrospirae phylum and the candidate division OP3. Magnetofossils also serve as potential proxies to reconstruct paleoclimate. Some researchers found that the morphology of magnetosome can be a potential proxy for oxygen concentration. *Yamazaki and Kawahata* [1998] found that uniaxial magnetofossils dominate during high oxic periods, while anisotropic magnetofossils dominate during anoxic periods. *Lean and McCave* [1998] found more isometric particles during glacial periods.

Multicellular magnetotactic prokaryotes (MMP) are marine, greigite-forming MTB [*Farina et al.*, 1990; *Mann et al.*, 1990]. The average diameter of the MMPs was $5.5 \pm 0.8 \mu\text{m}$ [*Zhou et al.*, 2013]. It usually contains 10-30 cells [*Rodgers et al.*, 1990]. The shape is roughly ovoid or spherical. The average swimming speed of MMPs is $55 \mu\text{m/s}$. The swimming speed of cocci is fastest, which can reach $300 \mu\text{m/s}$ [*Morillo et al.*, 2014]. The speed of spirilla is about $40\text{-}80 \mu\text{m/s}$ [*Martel et al.*, 2009]. *M. bavaricum* is slower, around $40 \mu\text{m/s}$ [*Spring et al.*, 1993].

Greigite-producing MTB were first detected in marine, estuarine and salt marsh environments [*Heywood et al.*, 1990; *Mann et al.*, 1990]. However, *Lefèvre et al.* [2011b] and *Wang et al.* [2013] discovered greigite-producing MTB in freshwater habitats. So far, only one MTB that forms greigite magnetosomes, *Candidatus Desulfamplus magnetomortis*, can be cultured [*Lefèvre et al.*, 2011b]. *Bazylinski et al.* [1993; 1995] found both iron oxide and iron sulphide magnetosomes were mineralized in one organism, but they could not be cultured.

There are several environmental factors that affect the morphology and type of magnetosomes. Iron uptake rates by MTB appear to change the morphology of the magnetite crystals [*Faivre et al.*, 2008]. *Faivre et al.* [2008] found that there is less biochemical control over the mineralization process when the iron uptake rates were higher. On the contrary, when the iron uptake rates were lower, the shape of the crystals were classical cubooctahedral. Sulfidic environments appear to favor the formation of greigite [*Bazylinski et al.*, 1995; *Lefèvre et al.*, 2011b]. *Lefèvre et al.* [2011b] found the mineral composition of the magnetosomes in strain BW-1, which is a large, rod-shaped, magnetite- and/or greigite- producing MTB, was controlled by levels of H_2S during their growth. For instance, when H_2S concentration was high in the cultured media, greigite was formed, whereas when H_2S levels were maintained at low levels, magnetite was synthesized [*Jermy*, 2012].

Faivre et al. [2008] also suggested that MTB can synthesize different morphologies of magnetosomes under different environmental conditions. Factors like pH can also effect the morphology of magnetosome. *Moisescu et al.* [2014] cultured *M. gryphiswaldense* MSR-1 in pH ranging from 5.0 to 9.0. They found that the shape of the majority of the magnetosome were immature and poorly developed, with superparamagnetic-sized particles appearing at pH 6.0. When the pH was 8.0, the morphology and size were similar to typical magnetosomes. At pH 9.0, the crystal size was even bigger (~45 nm) but still within the single domain (SD) particle size range.

Popa et al. [2009] suggested that oxygen concentration effected the magnetosome formation of *M. magneticum* (strain AMB-1). When MTB were cultured under higher oxygen concentrations (50–100 μM /150 rpm), magnetite synthesis was strongly inhibited. Euhedral, single domain crystals were mineralized when the MTB grew in totally anaerobic conditions (i.e., 0% O_2). *Li and Pan* [2012] replicated and confirmed the experiments of *Popa et al.* [2009]. *Li and Pan* [2012] demonstrated that MTB formed fewer magnetosomes with smaller grain sizes (33 ± 8.5 nm) when they grew in high oxygen environments (aerobic 120-rpm rotating cultures). Oxygen concentrations of 1% produced maximum Fe_3O_4 magnetosomes. The mineralization process was inhibited when oxygen concentrations $> 5\%$ [*Bazylinski and Frankel*, 2004]. Similarly, *Heyen and Schüler* [2003] revealed that oxygen effected the growth and type of magnetite magnetosomes in *M. gryphiswaldense*, *M. magnetotacticum* and *M. magneticum*. They found that magnetosome formation was only induced when the oxygen concentration was less than 20 mbar, and that the optimum oxygen concentration for magnetite formation was 0.25 mbar for these three *Magnetospirillum* strains.

Field strength can also effect the morphology of magnetosomes. *Frankel et al.* [1981] found MTB grown in weaker field strengths can produce larger magnetosomes. *Mandernack et al.* [1999] concluded that oxygen from water becomes incorporated into the Fe_3O_4 , yet the oxygen in Fe_3O_4 was not derived from molecular oxygen. Others found molecular oxygen effects the synthesis of protein which controls the magnetic particles size and morphology [*Sakaguchi et al.*, 1993; *Murat et al.*, 2010]. So far, the mechanism about how molecular oxygen affects Fe_3O_4 synthesis remains ambiguous.

Lin et al. [2012a] found that temperature can control the abundance and community composition of cocci. They found that when temperatures ranged between 9 and 26 °C, the MTB communities were not significantly different. When temperatures reached 37 °C, the abundance and diversity of cocci were significantly reduced. *Du et al.* [2015] found that the abundance of MMPs had a positive relationship with temperature. Spherical mulberry-like MMPs preferred relatively higher temperatures (14.2-27.4°C) than ellipsoidal pineapple-like MMPs (3.8-22.8°C). *Sobrinho et al.* [2011] found that MMPs preferred sediments with high iron (11.6 mmol/kg). *Lin et al.* [2012b] found salinity also influenced the biogeographic distribution of magnetotactic bacteria. They compared MTB communities from lagoons in Brazil and Germany, as well as different ecosystems across northern and southern China (19°N-40°N). Interestingly, all MTB communities can be grouped according to salinity through principal coordinates analysis of an unweighted UniFrac distance matrix (a measure of differences in bacterial community structure). Similarly, *Martins et al.* [2010] found that the distribution of MMPs was controlled by salinity in a hypersaline lagoon. *Lin and Pan* [2010] measured different anions (F⁻, Cl⁻, NO₃⁻, SO₄²⁻) and cations (Na⁺, K⁺, Mg²⁺, Ca²⁺) of pore water taken from Lake Miyun. They found that nitrate and genetic variability of MTB communities were strongly correlated (p<0.05). *Sobrinho et al.* [2011] and *Martins et al.* [2012] found that variations in MMP population density was related to the input of organic matter. Moreover, competition and predation can also influence the bacterial communities [*Lin et al.*, 2012b]. *Lin et al.* [2013b] suggested that field strength plays a key role affecting the distribution of MTB. They found community compositions of MTB populations in North America and East Asia varied according to the geomagnetic field intensity, which ranged between 44 to 55 μT.

Snowball et al. [1999] found a positive correlation between magnetosome concentration and the percentage of total organic carbon (TOC) in lake sediments. *Kodama et al.* [2013] concluded that the concentration of magnetofossils could be a potential proxy for reconstructing past rainfall variability. They found that the concentration of magnetosomes preserved in lake sediment correlated well with the past 70 years' rainfall record. The mechanism is that rainfall carries nutrients into the lake, stimulating the production of MTB. *Roberts et al.* [2011] found that iron fertilization causes unusually high MTB abundance. They assumed that high eolian dust flux adjusted biogenic magnetite abundances and played a key role in increasing primary productivity of surface waters. Therefore, more organic carbon enters into the seafloor thereby reducing iron

and dissolving detrital minerals. The soluble iron preserved in sediment serves as a resource for magnetosome formation. *Liu et al.* [2015] took a 8.5 m Holocene core from Dali lake, Inner Mongolia, China. They found that high magnetofossil abundance occurred into the Holocene Warm Period (HWP). Their biomagnetic record shows a good relationship with variation of summer insolation at high northern latitudes. *Savian et al.* [2016] found high concentrations of non-interacting biogenic magnetic minerals during the middle Eocene climatic optimum (MECO) event in response to increased aeolian iron fertilization. The sum of these results suggests that high magnetosome concentrations can be preserved during warm and wet periods. However, in a study of sediments deposited in the last 39000 years from the Ulleung Basin, *Suk* [2016] found that there were more magnetosome preserved during the marine isotope stage (MIS) 2 period (the Last Glacial Maximum). On the other hand, low abundances of magnetosomes were detected during the MIS 1 and 3 periods (warmer periods). *Suk* [2016] explained that the preservation conditions played a key role and concluded that sulphidic conditions were not suitable for the preservation of magnetosomes. In a 1.25 m deep piston core from Lake Ely, *Kodama et al.* [2013] found a significant decrease (from ~ 13 to ~ 1 mAm^2/kg) in magnetization at the deeper part (30-75 cm) of the core due to reductive diagenesis. However, the biogenic hard (BH) (24%) and biogenic soft (BS) components (17%) were still magnetically detectable at depths from 83 to 93 cm, which suggests that some magnetofossils survived reductive diagenesis.

Oxygen-18 isotope concentrations in magnetosomes can be a potential proxy to reconstruct paleotemperatures as *Mandernack et al.* [1999] demonstrated a temperature effect on oxygen isotope fractionation. This implies that the water temperature when magnetosome formed can be calculated. However, *Snowball et al.* [2002] found it was difficult to extract sufficient mass of the magnetosomes from the sediment for the analyses and that there is likely contamination from detrital magnetite. Oxygen isotope analyses on biogenic magnetite were consistent with other proxies like TEX-86 or carbonate oxygen isotopes in regards to paleotemperature *Schumann et al.* [2008].

Petersen et al. [1986] found magnetofossils in Quaternary to Eocene strata. *Vasiliev et al.* [2008] found biogenic greigite magnetofossils carry a primary magnetic signal in 5.3–2.6 Ma sediments from the Carpathian foredeep of Romania. They suggested that greigite magnetofossils reliably

recorded ancient geomagnetic field variations, and that they could also be a potential proxy to reflect anoxic/euxinic sedimentary environments.

There are several methods to diagnose the existence of biogenic magnetite in sediments such as rock magnetism, geochemistry and TEM or SEM observations. *Mandernack et al.* [1999] found no iron isotope fractionation in magnetosomes from two MTB strains (*Magneto- spirillum magnetotacticum* MS-1 and MV-1), whereas *Amor et al.* [2016] found iron isotope fractionation in *Magnetospirillum magneticum* AMB-1. The net Fe isotope fractionation between Fe sources in initial growth medium and magnetite ranged between 1.5 and 2.5‰. Therefore, Fe isotopes can potentially identify biogenic magnetite in the geological record.

Rock magnetic methods have the advantages of rapid detection and being non-destructive. *Moskowitz* [1993] found that there are four magnetic properties distinct of biogenic single domain magnetite particles in the form of intact magnetosome chains in sediments. First of all, the R_{df} value should be 0.5, where R_{df} is determined by the crossover point of direct field (DF) demagnetization and static or pulse field acquisition curves. Secondly, R_{af} should be bigger than 0.5. Similarly, R_{af} is determined by the crossover point of alternating field (AF) demagnetization curves and static field acquisition curves. Thirdly, the ratio between anhysteretic remanent magnetization (ARM) and saturation isothermal remanent magnetization (SIRM) should be between 0.15 and 0.25. Finally, δ_{FC}/δ_{ZFC} ratios should be larger than 2. $\delta = [J_{irm}(80) - J_{irm}(150)]/J_{irm}(80)$, where J_{irm} is the initial SIRM remaining at 80 or 150 K. Zero field cooled (ZFC) means the samples were cooled through the Verwey transition in a zero (null) field. Field cooled (FC) signifies the samples were cooled through the Verwey transition in a 2.5 T field.

Egli et al. [2010], *Roberts et al.* [2006; 2012; 2014] and *Heslop et al.* [2014] used high-resolution first-order reversal curve (FORC) diagrams to detect magnetofossils from lake and marine sediments. They found that non-interacting magnetite cause the existence of central ridges in FORCs. When the chains collapsed or the magnetosomes were oxidized to some extent, the central ridge became broadened. *Heslop et al.* [2013] found that FORCs could distinguish the relative contribution of biogenic magnetite from a Quaternary marine sediment core. The vector difference sum from natural remanent magnetization (NRM) demagnetization curves was calculated to detect the relative contribution of detrital particles and magnetosomes to the NRM.

Chang et al. [2016] found there are double Verwey transition temperatures which can discriminate biogenic and detrital magnetite; biogenic magnetosome had lower Verwey transition temperature (~100 K) than detrital magnetite (120 K).

Coercivity analysis of isothermal remanent magnetization (IRM) acquisition curves can also be used to distinguish detrital from biogenic magnetite [*Egli*, 2004]. According to the coercivity spectra, biogenic soft (BS), biogenic hard (BH), a mixture of extracellular, ultrafine magnetite and detrital magnetite can be distinguished. The coercivity of the biogenic soft (BS) fraction is ~35 mT and biogenic hard (BH) is ~70 mT, which [*Egli*, 2004] assumed reflected magnetofossils with different crystal morphologies. Lower coercivity component (25 mT) probably suggests a mixture of detrital magnetite and authigenic magnetite synthesized extracellularly [*Egli*, 2004].

Maher [1988] and *Oldfield* [2007] concluded that high values of χ_{ARM} , SIRM/χ and $\chi_{\text{ARM}}/\text{SIRM}$ in laminated sapropel units indicated the presence of stable SD grain size magnetic particles, when there is no significant superparamagnetic (SP) contribution. Here, χ_{ARM} is obtained by anhysteretic remanent magnetization (ARM) divided by the field strength. SIRM stands for saturation isothermal remanent magnetization. χ is magnetic susceptibility. *Yamazaki* [2009] concluded that $\chi_{\text{ARM}}/\text{SIRM}$ serves as a proxy to estimate the relative abundances of biogenic and terrigenous components in sediments. When $\chi_{\text{ARM}}/\text{SIRM}$ is higher, there are more biogenic components in sediments. *Snowball et al.* [2002] found that combining plots of $\chi_{\text{ARM}}/\text{SIRM}$ vs. χ_{ARM}/χ and SIRM/χ vs. χ_{ARM}/χ can better detect magnetosomes in sediment.

Ferromagnetic resonance spectroscopy (FMR) can also be used to detect magnetosome chains [*Kopp et al.*, 2006a; *Kopp et al.*, 2006b; *Weiss et al.*, 2004] for MTB cultured in the laboratory with α values < 0.25. Here, α values reflect the heterogeneity of ferromagnetic populations. Detrital sediments have high α values (typically > 0.40). For magnetofossil-bearing sediments, α values are typically between 0.25 and 0.35. However, sediments dominated by detrital particles can yield α values < 0.4. For complex sediments (different grain size, domain states, different kinds of magnetic minerals), additional measurement such as FMR at low temperature or spectral decomposition needs to be done. *Kopp et al.* [2007] used FMR to identify ancient biogenic magnetite, in sediments buried during the Paleocene–Eocene Thermal Maximum (PETM).

Gehring et al. [2011] found the decrease of the interaction-induced shape anisotropy in intact MTB can be expressed through FMR spectroscopy. Similarly, diagenesis can also reduce anisotropy of magnetofossils in sediment. Therefore, *Gehring et al.* [2011] concluded that low-temperature FMR results from intact MTB can be used as a potential tool to detect magnetofossils in natural environments. *Kind et al.* [2011] suggested that FMR and FORC results can be combined to identify magnetofossils based on alignment and interaction patterns of magnetic particles. *Gehring et al.* [2011] conclude that there are several groups of magnetite in lake sediments such as magnetite chains or chain fragments and dissociated bulk magnetite particles, all which have different anisotropy properties. FMR signal can distinguish them by empirical spectral separation.

Non-magnetic methods to observe the morphology and alignment of the magnetosomes in MTB include transmission electron microscopy (TEM) and scanning transmission electron microscopy (SEM) [*Kirschvink and Chang*, 1984]. Transmission Electron Microscopy Electron Dispersive X-ray Spectrometry (TEM-EDS) spectrum can analyze elemental compositions of magnetosomes [*Reinholdsson et al.*, 2013]. However, this method is time consuming and expensive. Moreover, only small sample masses can be analyzed.

Magnetotaxis, the ability to swim along magnetic field lines, in MTB can be exploited to quantify the abundance of live MTB in sediment, by counting them under an optical microscope. The method is called direct cell counting. In this method, a quantified drop is transferred to a glass slide using a pipette. A water drop is placed adjacent to the slurry. The slide is placed into magnetic field produced by Helmholtz coils, which induce the MTB to swim to the edge of water drop via magnetotaxis. *Flies et al.* [2005] used this method to determine the abundance of MTB. *Simmons et al.* [2007] used quantitative polymerase chain reaction (qPCR) assay targeting 16s rRNA genes to investigate the population dynamics of marine MTB in a salt pond. However, both qPCR and direct cell counts have disadvantages. For instance, results from qPCR may be overestimated due to differential amplification efficiency between samples and standard. For direct cell counts, the limit is that not all MTB may swim out of the sediment, which will also lead to underestimated abundances.

A common method to detect MTB species is via denatured gradient gel electrophoresis combined with sequence analysis of 16S rRNA genes [*Spring et al.*, 1992; *Spring et al.*, 1993].

In addition, *Lin et al.* [2009] found that restriction endonucleases (*MspI* plus *RsaI*) are the most effective means to distinguish MTB sequences and used the *MspI* plus *RsaI* restriction fragment length polymorphism analysis to investigate the diversity and change in MTB community compositions.

Mao et al. [2014b] used magnetosome-rich sediment to study the acquisition of detrital remanent magnetization. They found the NRM was proportional to the external field up to 160 μT , which led them to propose that magnetofossil chains can provide useful relative paleointensities. *Zhao et al.* [2016] confirmed that microorganisms play a role for post-depositional remanent magnetization (PDRM) acquisition in sediment. They also found DRM was progressively replaced by PDRM. This is helpful to reconstruct paleointensity on the basis of understanding how sediment becomes magnetized in the Earth's magnetic field.

Anhyseretic remanent magnetization (ARM), which is widely used to normalize relative paleointensity (RPI) records, is sensitive to SD grains and should therefore be sensitive to magnetosomes. Remanence anisotropy methods are shown to give unambiguous determinations of the degree and type of alignment [*Potter and Stephenson, 1988*]. Among these, the ratio of the intensity of anhyseretic remanent magnetization (ARM) to that of isothermal remanent magnetization, as well as their alternating field (AF) demagnetization curves are used as an indicator of the domain state of the particles [*Egli and Lowrie, 2002*].

This PhD thesis addresses the following questions:

- What is the horizontal spatial distribution of magnetotactic bacteria in sediment and how does the distribution changes over time in artificial environments (aquaria)?
- What is the temporal distribution of magnetotactic bacteria in a natural environment? What is the relationship between the abundance of MTB and environmental parameters such as temperature and oxygen concentration?
- How can we improve the precision of relative paleointensity estimates? What is the relationship between the anisotropy of ARM and external field strength?

In Chapter 2, I report measurements of three dominant magnetotactic bacteria morphotypes at 36 places in two replicate aquaria each month for seven months. I found that the spatial positioning

of population centers changed through time and that the two most abundant morphotypes (MTB-cocci and MTB-spirilla) occupied distinctly different niches in the aquaria. Maximum and average growth and death rates were quantified for each of the three morphotypes based on the 72 sites that were measured six times. To our knowledge, these rates are the first to be produced from a non-cultured environment for magnetotactic bacteria over such an extended time period. This work was published as: He, K., S. Gilder, W. Orsi, X. Zhao and N. Petersen (2017). Temporal and spatial distribution of magnetotactic bacteria in controlled aquaria, *Applied and Environmental Microbiology*, 83, e01382-17. Doi: 10.1128/AEM.01382-17. I prepared the experiment and made all the measurements for the study and wrote the first draft of the paper, which was then rewritten by S. Gilder and B. Orsi. X. Zhao gave me many useful suggestions to finish writing the manuscript. S. Gilder and N. Petersen designed the experiment.

Chapter 3 describes the temporal distribution of magnetotactic bacteria over 2 years in the Niederlippach pond, which is located 80 km northeast of Munich within the confines of our paleomagnetic laboratory in an isolated forest owned by LMU. It contains a high population density of MTB. We report that magnetotactic spirilla reached maximum populations in summer months when temperatures were highest and oxygen concentrations were lowest. Single domain magnetite (magnetosome) concentrations in the sediments varied with water depth but did not reflect living MTB abundances. Moreover, we found that relative variations in MTB morphotype abundances were consistent through two years at nine sites in a natural ecosystem. I did all the measurements and wrote the first draft of the paper. S. Roud did the partial magnetic measurements. S. Gilder and N. Petersen conceived and designed the experiments. C. Mayr made the geochemical measurements. R. Egli improved the rock magnetic description. The chapter has been submitted to *Geophysical Research Letters* as: He, K., S. Roud, S. Gilder, R. Egli, C. Mayr and N. Petersen. Seasonal variability of magnetotactic bacteria in a freshwater pond.

Chapter 4 gives perspectives on chapters 2 and 3 concerning the temporal and spatial distribution of MTB.

Chapter 5 describes an extensive series of redeposition experiments using magnetosome-rich sediments. Besides showing that sediments record the external field, we found a strong relationship between indices of the anisotropy of an anhysteretic remanent magnetization

(AARM) and field strength. This chapter is more preliminary in nature and will be submitted in the near future. As it is the first time a study could show that magnetic anisotropy can be used to estimate ancient magnetic field strength, I expect this chapter to have a high impact. I made all the measurements, S. Gilder conceived and designed the experiments, M. Wack developed the analytical infrastructure to make most of the measurements on the unique tool called the SushiBar, and J. Jezek will carry out the modelling.

Chapter 2 Constant flux of spatial niche partitioning from high resolution sampling of magnetotactic bacteria

The chapter has been published on Applied and Environmental Microbiology.

Abstract

Magnetotactic bacteria (MTB) swim along magnetic field lines in water. They are found in aquatic habitats throughout the world, yet knowledge of their spatial and temporal distribution remains limited. To help remedy this, we took MTB-bearing sediment from a natural pond, mixed the thoroughly homogenized sediment into two replicate aquaria, and then counted three dominant MTB morphotypes (coccus, spirillum, and rod-shaped MTB cells) at a high spatiotemporal sampling resolution: 36 discrete points in replicate aquaria were sampled every 30 days over 198 days. Population centers of the MTB coccus and MTB spirillum morphotypes moved in continual flux, yet they consistently inhabited separate locations, displaying significant anticorrelation. Rod-shaped MTB were initially concentrated toward the northern end of the aquaria, but at the end of the experiment, they were most densely populated toward the south. The finding that the total number of MTB cells increased over time during the experiment argues that population reorganization arose from relative changes in cell division and death and not from migration. The maximum net growth rates were 10, 3, and 1 day⁻¹ and average net growth rates were 0.24, 0.11, and 0.02 day⁻¹ for MTB cocci, MTB spirilla, and rod-shaped MTB, respectively; minimum growth rates for all three morphotypes were 0.03 day⁻¹. Our results suggest that MTB cocci and MTB spirilla occupy distinctly different niches: their horizontal positioning in sediment is anticorrelated and under constant flux.

2.1. Introduction

Almost all freshwater and marine environments host a broad spectrum of a special kind of bacteria, called magnetotactic bacteria (MTB) [Blakemore, 1975], that synthesize membrane-bound, single domain-sized (35 to 120 nm) magnetite and/or greigite crystals called magnetosomes [Bazylinski and Frankel, 2004; Lefèvre and Bazylinski, 2013; Lins et al., 2005]. Chains of magnetosomes that contain permanent magnetic moments are fixed within the cell,

which enable MTB to swim along magnetic field lines [Frankel *et al.*, 1997; Schüller and Frankel, 1999]. MTB host a wide variety of cell morphotypes including cocci, vibrios, spirilla, ovoids, rods and multicellular prokaryotes [Faivre and Schüller, 2008]. MTB generally live within the oxic-anoxic transition zone, yet they are also found in anoxic environments [Frankel and Bazylinski, 2004]. Upon death, they become entrained in the sediment column, where eventually through lithification the magnetosomes become important recorders of the geomagnetic field [Petersen *et al.*, 1986; Roberts *et al.*, 2012]. Magnetosome concentrations in sediments also serve as paleoclimate proxies [Kopp and Kirschvink, 2008; Snowball *et al.*, 1999; 2002; Yamazaki and Ikehara, 2012]. As they contain 2-4 dry wt% Fe [Flies *et al.*, 2005; Schüller and Baeuerlein, 1998], MTB could influence iron cycles in nature by acting to sequester Fe in sediments [Chen *et al.*, 2014]. Several studies have addressed the spatial-temporal variation of MTB along vertical profiles [Flies *et al.*, 2005; Jogler *et al.*, 2010; Postec *et al.*, 2012], yet much less is known about how their horizontal distribution varies in space and time. Specifically, we question how well MTB populations measured in a given place (a spatial niche) represent a particular environment through time; e.g., do the populations remain fixed in a limited area, move randomly from place to place, some combination of the two, and over what time-scales? We therefore carried out a relatively dense spatial and temporal sampling of decameter-sized environments and quantified natural MTB populations over a period of 198 days. This enabled us to map their distribution in space and to observe how the population evolved through time.

2.2. Materials and Methods

2.2.1. Sample Collection and Counting

We collected sediment from a natural pond situated in a forest near Landshut, Germany, 80 km northeast of Munich (48°35'14.98"N, 12°04'43.71"E) that hosts abundant and well characterized MTB [Mao *et al.*, 2014b; Zhao *et al.*, 2016]. Grain size analyses on five sediment samples showed log-normal distributions with maxima at 15-23 μm , whose dominant magnetic contribution comes from non-interacting single domain particles, probably in the form of intact magnetosome chains [Zhao, 2015]. On July 14, 2014 (considered as day 1, the start of the experiment) we took 4 liters of sediment from the sediment-water interface to a depth of 10 cm, thoroughly homogenized it, and then poured it into two, single-piece (seamless), glass aquaria

measuring 30 cm in length, 20 cm in width and 15 cm in height. The seamless glass aquaria were gas impermeable, and thus the only point at which oxygen could diffuse into the system was from dissolved O₂ in the water above the sediment in the aquaria. This preserved the oxic-anoxic redox gradient that naturally occurs in these sediments at a relatively shallow sediment depth (Figure 2-4). The sediment-water interface in the aquaria was at 5 cm height, with the rest filled with pond water up to 4.5 cm below the top of the aquarium. Constant water height was maintained throughout the course of the experiment.

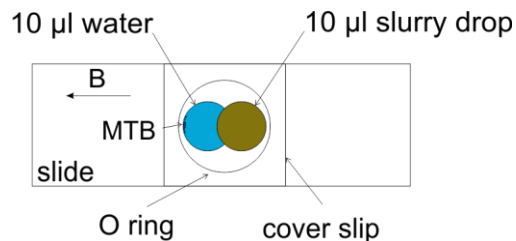


Figure 2 - 1 Sketch of a sample placed on a slide in the magnetodrome. B indicates the applied magnetic field direction in the horizontal plane.

The two replicate aquaria (A and B) were placed with their long axes parallel to the ambient geomagnetic field declination in a room whose temperature remained within 20-26°C. Plastic boards with small holes covered the aquaria to reduce evaporation. As the aquaria were not air tight, their covers inhibited contamination from aerosols in the laboratory. However, the environment was not exceptionally dissimilar to the natural state of the shallow pond that also received a constant influx of aerosols from the Munich suburban area. A total of 36 sites in each aquarium, spaced in rows every 4 cm in the long axis direction and 3 cm in the other, were sampled at roughly 30 day intervals beginning on day 7 by using a pipette to extract 200 µl of sediment at each site from the upper centimeter of the sediment column where the MTB are most concentrated [Jogler *et al.*, 2010]. A mark indicating the one-centimeter level on the pipette was visually placed at the sediment-water interface to within an accuracy of ±1.5 mm. Each site was defined as a 1×1 cm² area divided into two rows of three points whose position from one sampling to the next was systematically shifted to avoid disturbance: first in the upper left-hand corner, then in the upper right-hand corner, then in between the two upper corners, then in the lower left-hand corner, then in the lower right-hand corner, and finally in between the two lower corners— always the same for each site. On day 44, aquarium A was rotated 180° in the long axis direction. We used the viable cell count technique to quantify the MTB morphotypes [*Flies*

et al., 2005], which allows one to microscopically quantify each MTB morphotype without using more sophisticated methods such as qPCR [*Simmons et al.*, 2007], etc. High-throughput 16S rRNA gene sequencing (Illumina) of three replicate samples from the pond sediment identified uncultivated taxa corresponding to *Magnetococcus* and the rod-shaped *Candidatus Magnetobacterium bavaricum* and *Candidatus Magnetobacterium casensis* [*Coskun et al.*, 2017] similar to MTB recovered in other freshwater sediments from Germany, China, Russia, etc. [*Dziuba et al.*, 2013; *Jogler et al.*, 2010; *Lin and Pan*, 2009; *Lin et al.*, 2014]. The sediment was transferred to centrifuge tubes, then 4800 μ l distilled water was added to the 200 μ l of sediment (5 ml total) and homogenized by shaking. Although toxic on longer timescales, distilled water has the advantage when observing under the microscope in that it activates their propulsion. From day 120, the MTB population became so large at certain locations that we had to dilute 200 μ l sediment with 7.25 times more water for a total slurry of 35 ml. From the centrifuge tubes, 10 μ l of sediment+water slurry was placed on a glass slide and 10 μ l of distilled water was added beside the drop (Figure 2-1). An O-ring was placed on the slide and a cover slip was placed on the O-ring to inhibit evaporation. The slide was placed beneath an optical microscope in the center of Helmholtz coils (Petersen Instruments magnetodrome). Directing a horizontal magnetic field oriented toward the distilled water drop induced the MTB to swim out of the sediment and into the clear water where they were identified and counted via light microscopy (Olympus Model CKX41SF) at the air-water interface. The magnetic field strength produced by the coils was 0.6 mT, about 12 times the strength of the magnetic field intensity in Munich. The viable cell count technique allowed us to distinguish three general morphotypes: cocci (defined as round MTB with ca. 1-4 μ m diameters), spirilla (generally 2-3 μ m long, slightly concave shapes which included vibrios as the two are hard to distinguish) and rod-shaped (*Candidatus Magnetobacterium bavaricum* and/or *Candidatus Magnetobacterium casensis*, hereafter grouped and referred to as MTB-rods) that are easily distinguished by their rod shapes and dark appearance (Supplemental Figure 2-2) [*Petersen et al.*, 1989; *Spring et al.*, 1992]. Several different cocci and/or spirilla species exist in the sediment, but they cannot be distinguished optically and are thus grouped solely by morphotype. Figure 2-3 shows the number of MTB counted in ten different samples over time. From these data, we allowed the MTB to swim in an induced magnetic field for 20 minutes before counting each sample. The number of counted

bacteria was a minimum number since we cannot be sure that all of the MTB migrated out of the sediment.

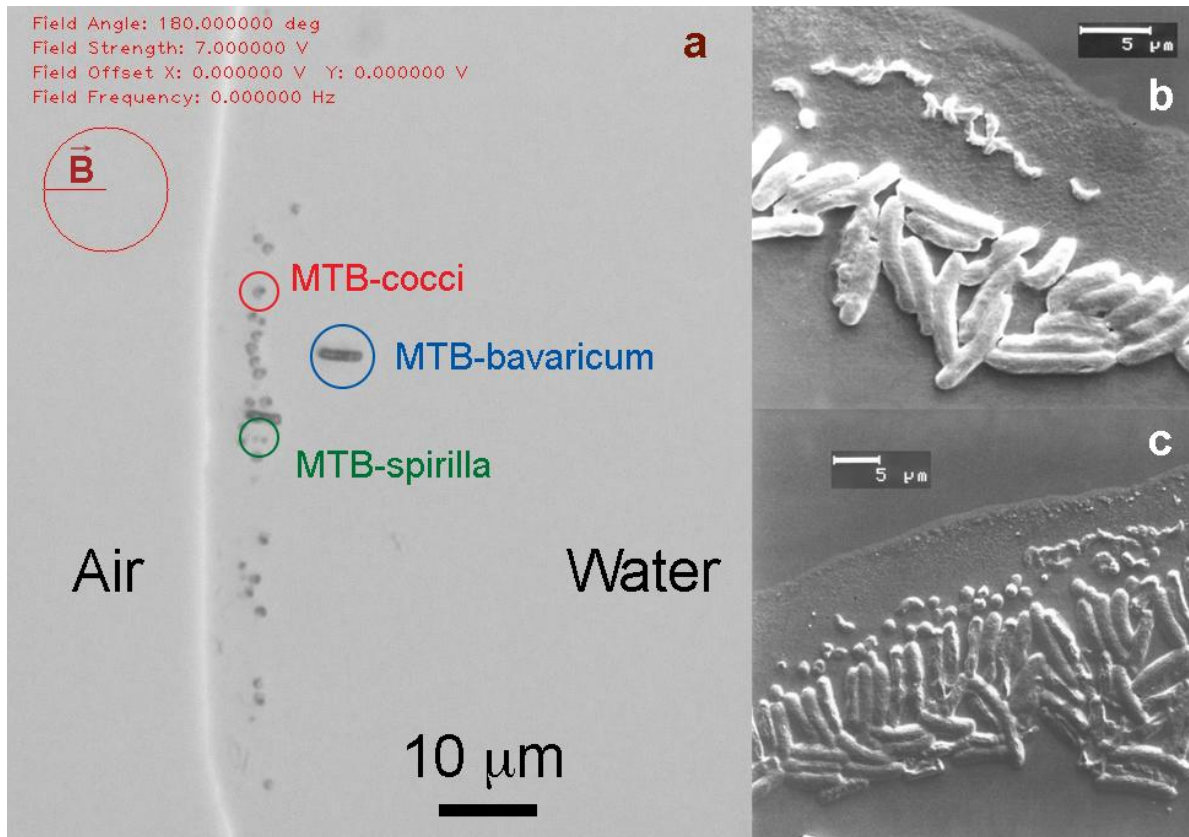


Figure 2 - 2 Image at the air-water interface seen under the optical microscope and scanning electron microscope. B is the applied field direction that points to the left in this example. The magnetic bacteria swim to the edge of the water drop under the influence of the magnetic field where the three common morphotypes are counted: MTB-cocci, MTB-spirilla and MTB-bavaricum (MTB-rods). (b and c) Scanning electron microscope images after allowing the water drop to dry out. (b) contains mostly spirilla (small) and rods (large) while (c) contains cocci (round), spirilla (small elongate) and rods (large elongate).

2.2.2. Mapping

Graphs of MTB distribution were made with Golden Software, Surfer 12 selecting the kriging method to contour the data [Vinatier *et al.*, 2011]. Plots in Figure 2-5 were made by calculating the average number of each morphotype from the 36 points in each aquarium, then subtracting the number of MTB morphotypes at each sampling position by the average number of that morphotype in the same aquarium for the day in question (e.g., the numbers are relative to the average with red colors being higher than average and green, lower). Figure 2-6 shows the same data except doubly normalized so that the minimum counts are 0 and maximum are 1. To test the

effect of the initial conditions (see below) on the MTB population, aquarium A was rotated 180° on day 44. The maps of aquarium A are shown in the same position relative to the start of the experiment (Figure 2-6). It took six days to count the MTB at the 72 sites (36 sites, 2 replicate aquaria), three days for each aquarium, with aquarium A being counted first and then B; “day” in our study goes according to the first day when counting began on aquarium A.

2.2.3. Oxygen Concentration

Magnetotactic bacteria are microaerophilic and sensitive to O₂, thus they prefer to live near the oxic-anoxic interface in sediments where O₂ levels are low [Lefèvre *et al.*, 2014]. For this reason, O₂ profiles were measured at nine locations in each aquarium using a Unisense OX50 oxygen microsensor (tip diameter = 50 µm) with a 0.3 µmol/l detection limit on day 120. The sensor was fixed on a computer-driven micromanipulator mounted on a heavy laboratory stand. Three seconds were required to reach stable readings. Three north-south transects were spaced at 6 cm intervals, 8 cm apart in the east-west axis. Measurements were made every 1 mm depth, starting 5 mm above the sediment water interface until 10 mm below it. Oxygen concentrations in water ranged from 100 to 150 µmol/l, while O₂ disappeared by 3 mm depth in the sediment (Figure 2-4).

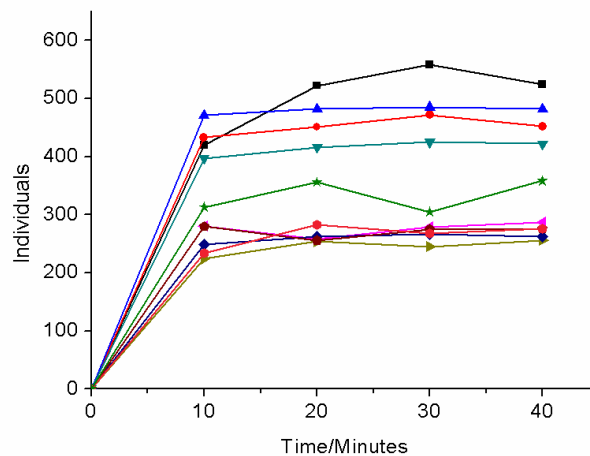


Figure 2 - 3 Number of MTB cocci counted as a function of time for 10 discrete samples

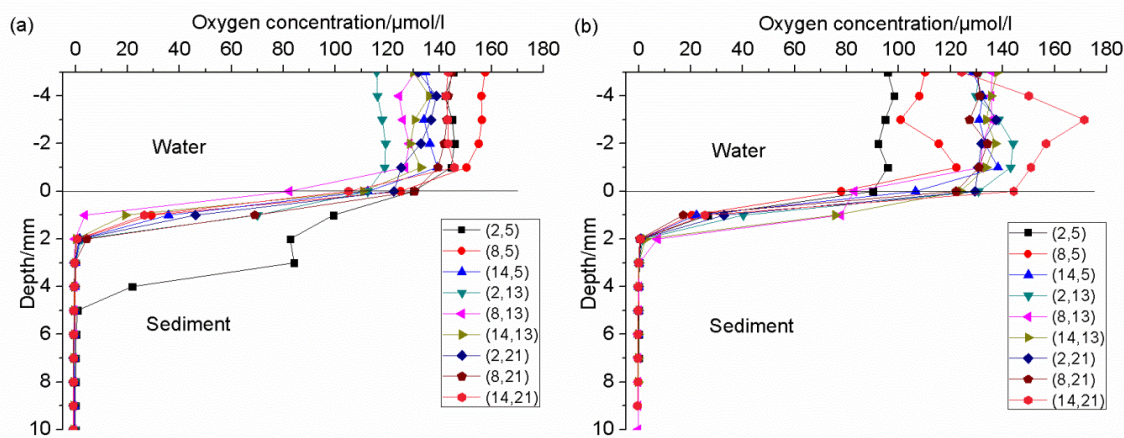


Figure 2 - 4 Oxygen profiles of nine samples in aquaria A and B on day 120. 0 lies at the sediment-water interface. Their coordinates along the east-west axis are 2, 8 and 14 cm, respectively, whereas those along the north-south axis are 5, 13 and 21 cm, respectively.

2.3. Results

2.3.1. Spatiotemporal variation of magnetotactic bacteria

Figure 2-7 shows box plots of the total population of the three MTB morphotypes in the two aquaria through time (data in Table 2-1). Between day 7 and 37, the total quantity of MTB-spirilla and MTB-rods decreased whereas the total quantity of MTB-cocci slightly increased. After day 67 until day 150, all counted MTB morphotypes increased with the exception of MTB-rods in aquarium A. The rotation of aquarium A at day 44 was done to test the influence of the starting conditions relative to magnetic north.

Figure 2-6 shows the horizontal distribution of the three dominant MTB morphotypes in each aquarium over time. The plots contour the number of bacteria at each site relative to the average value for the morphotype at the given day of measurement separately for each aquarium. Initially (day 7), MTB-cocci and MTB-rods concentrated toward the north, which might be due to mixing and pouring the sediment into the aquaria in the ambient, northward-directed field. On day 37, MTB-cocci began to grow at the corners of the aquaria. Population densities remained stable for MTB-cocci from day 7 through day 120 in aquarium B and initially for MTB-rods in both aquaria over days 7 to 67. This is supported through a Pearson correlation analysis where significance is indicated at the 0.05 and 0.01 probability level (Table 2-2). Interestingly, when

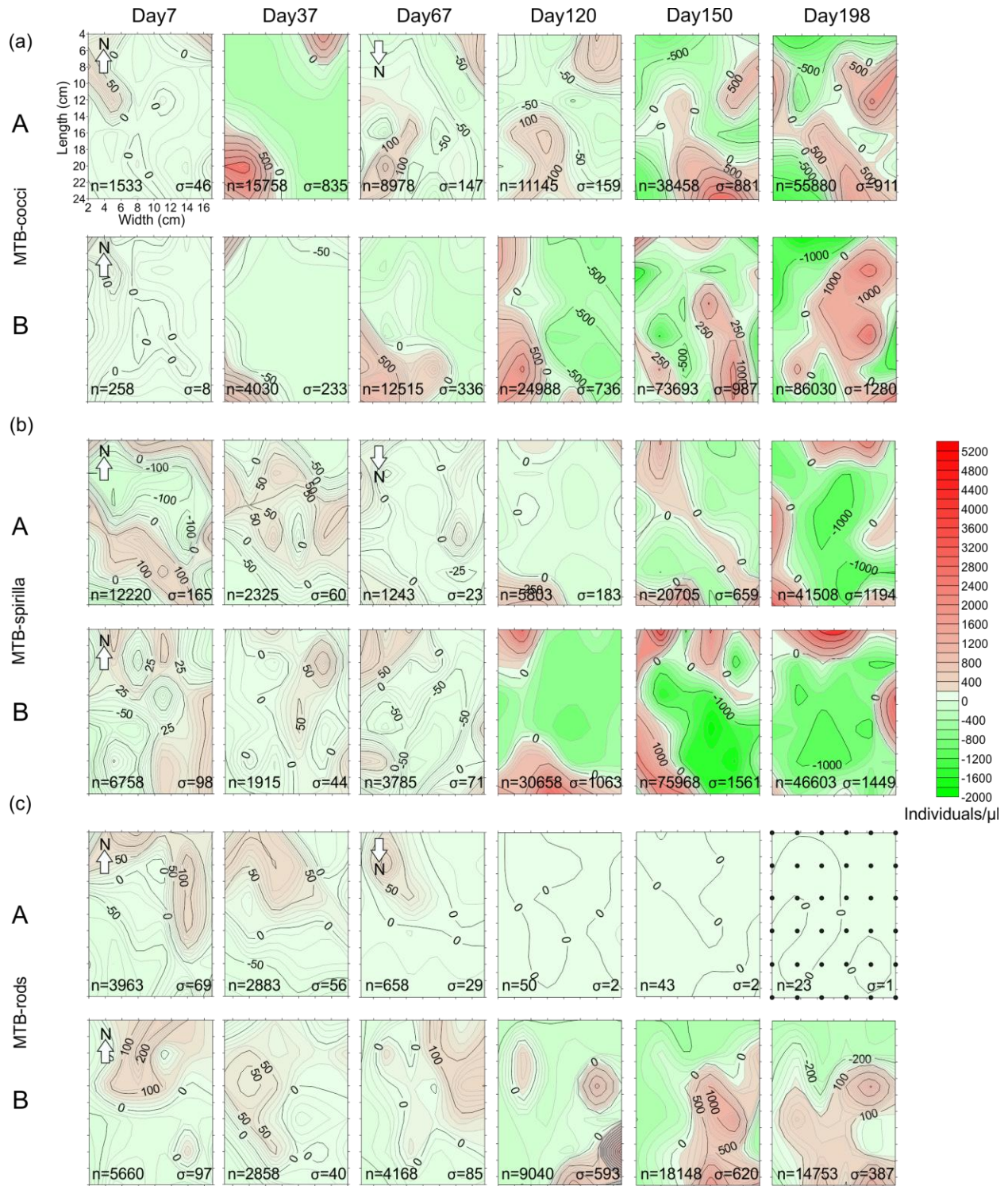


Figure 2 - 5 Horizontal distribution of MTB (a) MTB-cocci (b) MTB-spirilla and (c) MTB-rods in aquaria A and B from day 7 to day 198. Values at each point represent the difference with respect to the average number of a given species at a given day. The color scale is with respect to the maximum distribution. The total number and single standard deviation about the average are listed in each plot. The plot at day 198

for MTB-rods in aquarium A shows the distribution of the sampling sites. Plots were truncated at the edges of the sampling points to avoid extrapolation effects from the contouring.

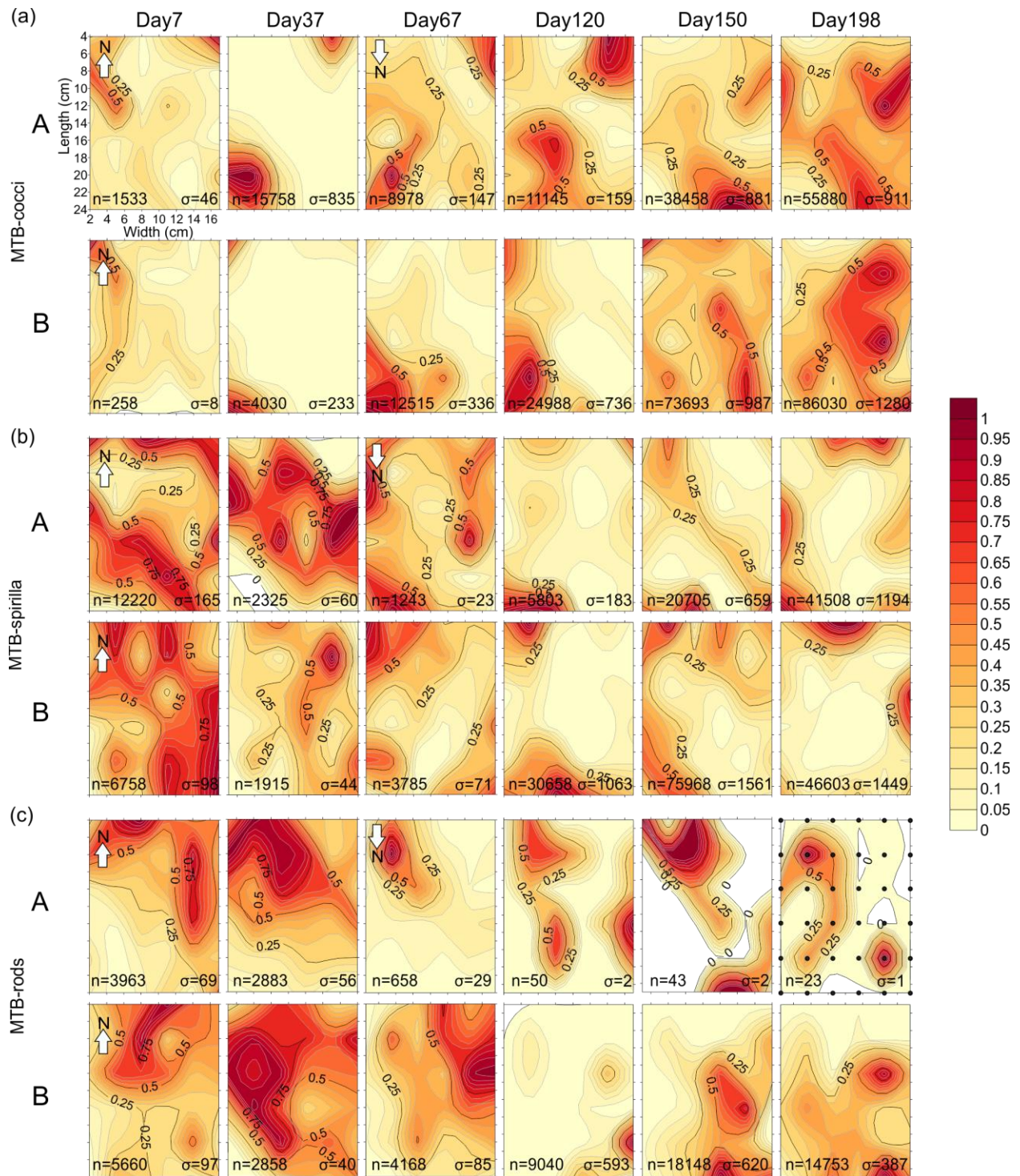


Figure 2 - 6 Horizontal distribution of MTB (double normalized).The color scale reflects relative variations instead of absolute variations as in Figure 2-5. Caution should be exercised when interpreting these plots

as aquaria with low numbers of MTB (e.g., MTB-rods in Aquarium A at day 120, 150 and 198) as the relative variability is given equal weight as in aquaria with high numbers of MTB.

MTB-cocci had higher correlation values between successive measurements, there was no correlation in the same period for MTB-spirilla, and vice versa. In most other cases, it appeared that the relative number of MTB-morphotypes did not increase or decrease at the same places, but rather maxima (above average numbers colored red in Figure 2-6) and minima (below average numbers colored green in Figure 2-6) in population varied in time. On the other hand, the relative variability (single standard deviation / mean) tended to stabilize after day 37 for MTB-cocci and remained fairly constant for MTB-rods and MTB-spirilla, although relative variability for the latter could be argued to have slightly increased with time (Table 2-1). In general, the data suggest that the MTB populations observed were relatively copiotrophic--changes in population tended to boom or bust heterogeneously in space, despite changes in absolute numbers. A general rule taking a relative variability of 1.0 as a typical number means that the number of MTB at any place in a given microcosm is likely representative to within \pm the average. A bootstrap analysis suggests the uncertainty about the relative variability remains stable to within 20% until N decreases from 36 to 20. This should be interpreted with caution as the population generally increases for all MTB-morphotypes except for MTB-rods in aquaria A (see below), so the populations are not at a steady state.

Toward the end stages of the experiment, MTB-spirilla generally inhabited the perimeter of the aquaria while MTB-cocci populated more toward the center. That the two morphotypes consistently preferred to live in distinctly separate places was one of the most important observations of our study. One problem with the way to visualize the changes in MTB in Figure 2-5 is that the color scale is optimized for relatively high cell counts. One sees a different view when doubly normalizing the data (Figure 2-6), which is exaggerated when cell numbers are low, like for MTB-rods, yet has the advantage of weighing each morphotype and time equally.

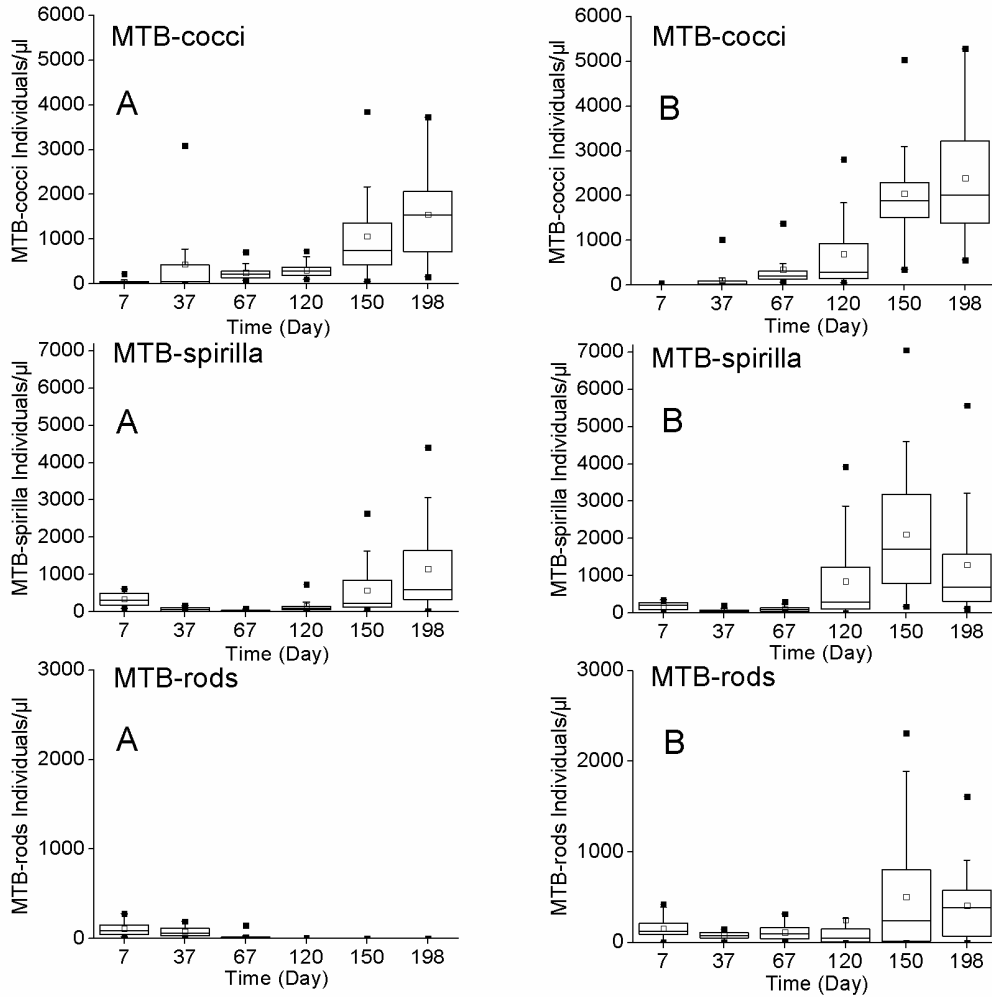


Figure 2 - 7 Box plots of MTB abundance in aquaria A and B through time. The bars in the boxes represent the sample median, boxes themselves show the upper and lower quartiles, the vertical bars show the range; asterisks represent extreme values.

2.4. Discussion

There are few studies on the horizontal distribution of MTB in sediment microcosms over time. We find a mostly non-uniform and constantly varying horizontal distribution of MTB, consistent with *Jogler et al.* [2010] who also found uneven population distributions of MTB-rods in seven habitats. *Simmons et al.* [2004] found sharp changes in abundance of MTB-cocci and a greigite (iron sulphide) producing MTB over small length scales in a natural pond. MTB-rods and MTB-cocci initially concentrated in the northern part of the aquaria. After aquarium A was rotated 180° on day 44, MTB-rods did not flourish in the “new” northern part of the aquarium or die off toward the south. Because the sediment was mixed into the aquaria in the magnetic field,

and because MTB swimming velocities are faster in water than in sediment [Mao *et al.*, 2014b], the fact that MTB-rods concentrated in the north could indicate that pouring the sediment into the aquaria in the ambient field might have biased the initial results. On the other hand, that MTB-rods died off in aquarium A and not in B, whereas MTB-cocci and MTB-spirilla were less affected by the rotation suggests the change in magnetic environment influenced the MTB-rods community. Mao [2013] found that the abundance of MTB-rods dropped after lowering the ambient magnetic field to near null, whereas they recovered to normal concentrations after restoring the geomagnetic field. Lin *et al.* [2013b] analyzed more than 900 MTB 16S rRNA gene sequences from 25 locations around the world based on the UniFrac and Sørensen indices. They found that geomagnetic field strength influenced MTB activity and diversity to the same extent as salinity, sulfate, temperature and Eh. The fact that only MTB-rods showed a response to the 180° rotation of the aquarium may also be due to the fact that MTB-rods has a magnetic moment that is a factor of 10 larger than that of MTB-cocci [Hanzlik *et al.*, 1996]. Correspondingly, higher sensitivity of MTB-rods to magnetic field changes could be expected. To test whether morphotype populations correlated with O₂ concentration, we measured nine O₂ profiles in each aquarium on day 120 (Supplemental Figure 2-4). Oxygen concentrations in water ranged from 100 to 150 µmol/l; O₂ disappeared by 3 mm depth in the sediment. A Pearson correlation analysis revealed no significant relationship between bacteria abundance and O₂ concentration at 1 mm depth. A similar analysis based on the O₂ concentration in water just above the sediment also yielded no significant degree of correlation. MTB populations were uncorrelated with local O₂ conditions in the aquaria environment in the plane parallel to the surface. Flies *et al.* [2005] found that MTB distributions in the vertical dimension were restricted to a narrow sediment layer overlapping or closely below the maximum oxygen penetration depth. Different species showed variable preferences within vertical gradients, but over 60% of MTB were detected within the suboxic zone, which begins ~1-2 mm below the sediment-water interface in our study. Our sampling integrates a volume of $h \cdot \pi \cdot r^2$ ($r = 2.5$ mm, $h = 10$ mm) spanning the oxic-anoxic transition zone where most bacteria should live. That the MTB numbers do not correlate with O₂ might not be surprising considering that O₂ restricts the MTB to live in a specific region in the vertical direction, but does not control the absolute numbers of MTB within that region. Our experiments would suggest that the absolute numbers of MTB could vary considerably if one measured them in the horizontal plane at a given depth or constant horizon of chemical activity.

MTB-cocci initially grew in the corners of the aquaria and ended up more concentrated in the center of the aquaria toward the end of the experiment. That the total number of MTB increased through time suggests that the changes in horizontal distribution do not stem from migration, but rather to changes in cell division (growth) and death rates, and then trended toward relatively equal numbers at the latter stages of the experiment in both aquaria. This is consistent with the observations of *Mao et al.* [2014b], who found MTB move via a slightly biased random walk in the external magnetic field in the sediment. While the swimming velocity of MTB-cocci in water can reach 112 $\mu\text{m}/\text{sec}$ [*Lin and Pan*, 2009], their swimming velocity in sediment is unknown. Another way to quantify changes in MTB population is to examine the relative population over time (Figure 2-8). Viewed in this way one sees that MTB-cocci and MTB-spirilla populations were generally anti-correlated at the beginning stages of the experiment. Seeking correlations with other studies needs to be made with caution as there are multiple morphotypes of cocci and spirilla [*Faivre and Schüller*, 2008; *Lefèvre and Bazylinski*, 2013], and each might respond differently to a given microenvironment. The horizontal distribution of MTB-cocci and MTB-spirilla population centers were in continuous flux during the incubation, and the spatial positioning of these centers was consistently anti-correlated (Fig. 3). Initially, MTB-rods and MTB-spirilla predominated, but MTB-cocci became the dominant group after day 37, which has been found in natural habitats [*Flies et al.*, 2005; *Lin and Pan*, 2010; *Martins et al.*, 2012; *Postec et al.*, 2012]. Moreover, when MTB-cocci had a similar spatial distribution between adjacent counting days, MTB-spirilla concentrated in different places between those same adjacent counting days, and vice versa. A Pearson correlation analysis suggests MTB-cocci and MTB-spirilla were significantly anticorrelated on day 198 in aquarium B ($r = -0.523$), with a lower probability of anticorrelation in aquarium A ($r = -0.301$). The anti-correlation between MTB-cocci and MTB-spirilla leads us to conclude that the two morphotypes occupy spatially distinct niches whose horizontal positioning undergoes constant flux. We calculated the relative growth rate (k) of MTB using the formula $k = (N_{n+1} - N_n) / [N_n \cdot (t_{n+1} - t_n)]$, where N_{n+1} and N_n are the amount of MTB at time $n+1$ (t_{n+1}) and time n (t_n) (Figure 2-9). MTB-cocci had a higher average growth rate between day 7 and 67, whereas MTB-spirilla and MTB-rods in aquarium B had higher growth rates since day 120. The maximum growth rate at all 72 sites in both aquaria for MTB-cocci, MTB-spirilla and MTB-rods were 10, 3 and 1 day^{-1} , respectively. Average relative growth rates (k) were 0.24, 0.11 and 0.02 day^{-1} , respectively. The minimum growth rate

was -0.03 day^{-1} . In comparison, the generation time of cultured magnetotactic spirilla is between 6 and 26 hours [Ardelean *et al.*, 2009], which corresponds to k values of 15 and 1 day^{-1} ; hence, significantly larger than our average growth rates, but on the same order as the maximum growth rates. Nutrient availability and/or predator-prey relationships between natural sediment and culture environments likely accounts for the difference. The two aquaria experienced identical environmental conditions and parallel initial conditions. The spatial distribution of MTB-cocci and MTB-spirilla were fairly similar in each aquarium, independent of the rotation at day 44. Changes in the distribution of MTB cannot be related to temperature, light or O_2 concentration, as was also concluded by Jogler *et al.* [2010]. Lin and Pan [2010] speculated that the variation of nitrite-oxidizing and ammonia-oxidizing bacteria could change the concentration of nitrate in sediment, which may have had an effect on spatiotemporal distribution of MTB communities. Different areas of the sediment may contain different predators like phages or eukaryotic grazers [Jogler *et al.*, 2010], which could account for the uneven distribution of MTB. On the other hand, some workers found that the abundance of spherical, mulberry-like magnetotactic multicellular prokaryotes correlated with the concentration of organic matter [Du *et al.*, 2015; Simmons *et al.*, 2007; Simmons and Edwards, 2007]. This could explain our results if local depletion in organic matter led to population decreases whereas population booms represent exploitation of new sources of organic matter, although other variables like nitrite, phosphate, etc., could play equally significant roles. Sobrinho *et al.* [2011] found iron and bioavailable sulfur concentrations regulate the magnetotactic multicellular prokaryote density at the Araruama Lagoon in Brazil. Other workers found salinity, nitrate and sulfate correlates with the amount of MTB [Flies *et al.*, 2005; Lin and Pan, 2010; Lin *et al.*, 2012b; Postec *et al.*, 2012]. We observed worms and small aquatic plants living in the sediment. Bioturbation through invertebrate burrowing as well as the roots of aquatic plants can increase the heterogeneity of microenvironments. In our particular case, the aquaria likely had an uneven distribution of nutrients. The method of counting MTB has some limitations, as only highly motile MTB swam out of the sediment into the water drop and only live cells were counted. Nevertheless, the relative changes we observed should be robust as the same method was applied across all samples and time points. The anti-correlation of MTB-cocci and MTB-spirilla population centers cannot be attributed solely to migration or swimming speeds. Rather, changes in the growth and death rates of MTB must be a contributing factor, with the population centers undergoing

constant flux throughout the time period. These results suggest that many MTB lie dormant and then wake up at different times, either in a stochastic fashion [Buerger *et al.*, 2012] or in response to newly available nutrients such as iron [D'Onofrio *et al.*, 2010]. This appears to vary on the cm scale, given the anti-correlation of the fluxes in growth and death rates of the two morphotypes. Our study suggests that quantifying the presence and abundance of MTB in nature should be carried out at high-resolution sampling in space and time. The highly dynamic niche partitioning shown here implies that results based on environmental samples taken from a single point in space (e.g., for metagenomics or 16S rRNA gene sequencing) from benthic ecosystems should be interpreted with caution.

Table 2 - 1 Statistics on magnetotactic bacteria populations for aquaria A and B over time based on 36 measurements in each aquaria

Species	Day	Aquarium A				Aquarium B			
		Total	Mean	σ	RV	Total	Mean	σ	RV
MTB-cocci	7	613	17	18	1.1	103	3	3	1.2
	37	6303	175	334	1.9	1612	45	93	2.1
	67	3591	100	59	0.6	5006	139	134	1.0
	120	4458	124	64	0.5	9995	278	294	1.1
	150	15383	427	352	0.8	29477	819	395	0.5
	198	22352	621	364	0.6	34412	956	512	0.5
MTB-spirilla	7	4888	136	66	0.5	2703	75	39	0.3
	37	930	26	24	0.9	766	21	18	0.8
	67	497	14	9	0.7	1514	42	28	0.7
	120	2321	64	73	1.1	12263	341	425	1.3
	150	8282	230	264	1.2	30387	844	625	0.7
	198	16603	461	478	1.0	18641	518	579	1.1
MTB-rods	7	1585	44	27	0.6	2264	63	39	0.6
	37	1153	32	23	0.7	1143	32	16	0.5
	67	263	7	11	1.6	1667	46	34	0.7
	120	20	1	-	-	3616	100	237	2.4
	150	17	0	-	-	7259	202	248	1.2
	198	9	0	-	-	5901	164	155	0.9

σ , single standard deviation about the mean of the MTB from 36 sites; RV, relative variability = σ/mean .

Table 2 - 2 Correlation coefficients for each species between successive measurements

MTB-cocci	Day 37	Day 67	Day 120	Day 150	Day 198
Day 7	0.023, 0.405*				
Day 37		0.377*, 0.648**			
Day 67			0.277, 0.649**		
Day 120				0.223, 0.026	
Day 150					0.621**, 0.183
MTB-spirilla	Day 37	Day 67	Day 120	Day 150	Day 198
Day 7	-0.082, 0.484**				
Day 37		0.051, 0.003			
Day 67			0.445**, 0.177		
Day 120				0.543**, 0.367*	
Day 150					0.040, 0.232
MTB-rods	Day 37	Day 67	Day 120	Day 150	Day 198
Day 7	0.469**, 0.365*				
Day 37		0.564**, 0.336*			
Day 67			-, 0.128		
Day 120				-, 0.112	
Day 150					-, 0.464**

* and ** indicate significance at the 0.05 and 0.01 probability level, respectively. Blue (green) color stands for Aquarium A (B).

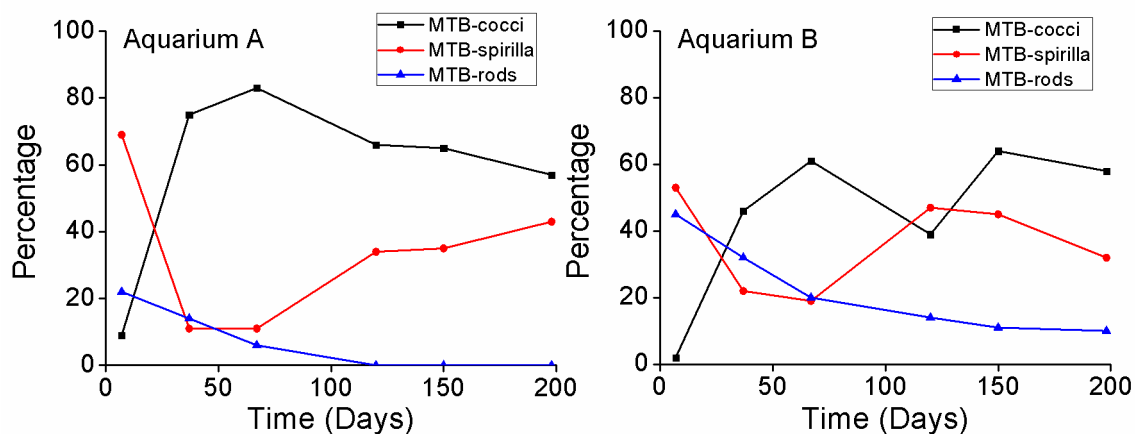


Figure 2 - 8 Percentage of the three MTB species in aquaria A and B over time

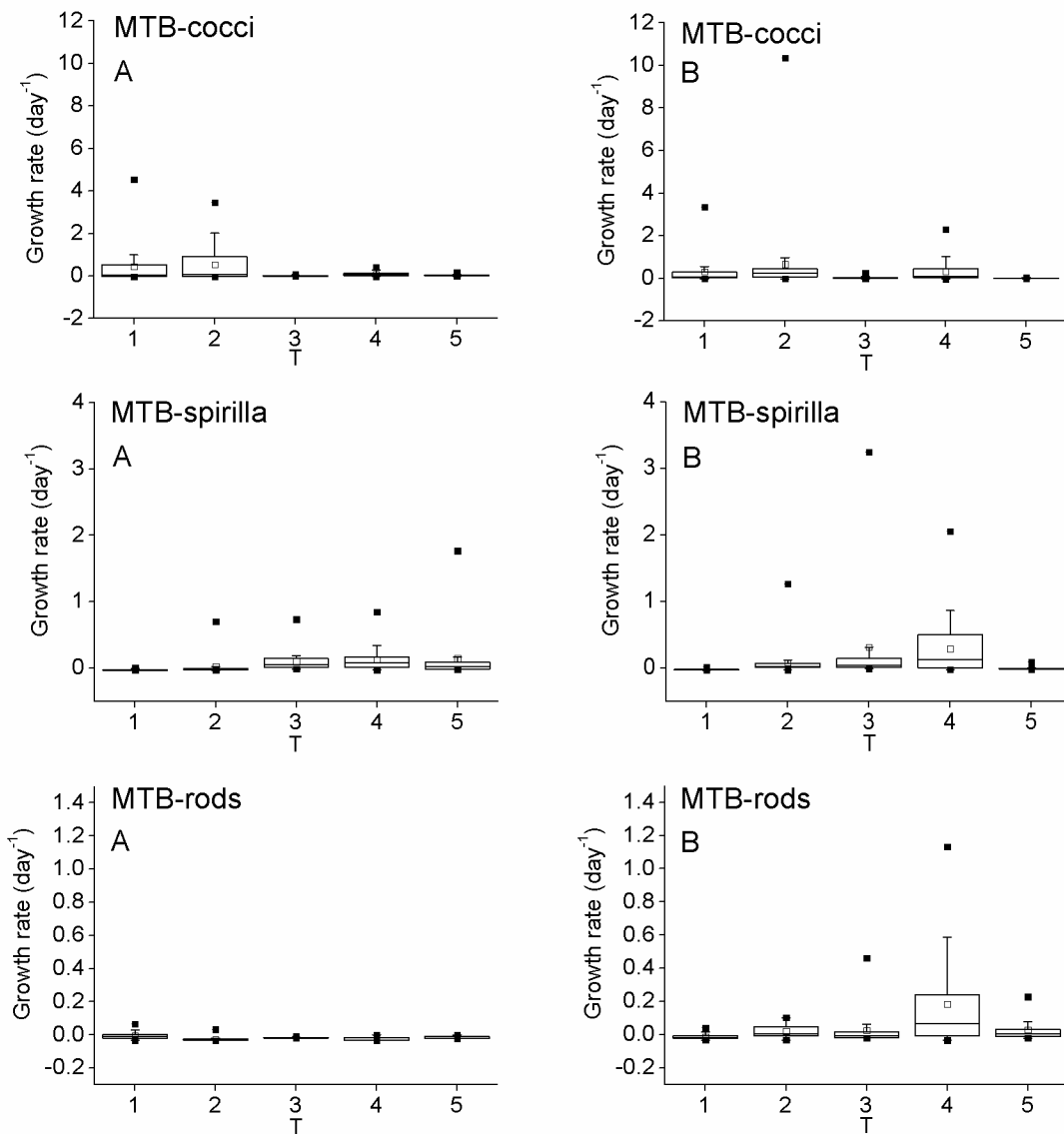


Figure 2 - 9 Box plots of the change in MTB growth rate over time in aquaria A and B. The bars in the boxes represent the sample median, boxes show the upper and lower quartiles, the vertical bars show the range; asterisks represent extreme values.

Chapter 3 Temporal and spatial variation of magnetotactic bacteria communities in a freshwater pond

The chapter is in revision for Geophysical Research Letters.

Abstract

Magnetotactic bacteria (MTB) synthesize ferrimagnetic crystals that contribute to the remanent magnetization in sediments, yet knowledge of how MTB populations vary in natural environments over time remained limited. We report abundances of three MTB morphotypes from nine sites collected and measured every month over a two-year period from a pond near Munich, Germany. Morphotype populations underwent coherent temporal trends among the nine sites. Spirilla populations attained maxima in the summer when temperatures were highest and oxygen concentrations were lowest. Spirilla and cocci exhibited relative antipathy in 2015 when both morphotypes reacted in distinctly opposite ways to oxygen levels. In 2016, they were positively correlated with each other but displayed no coherency with oxygen. Magnetic properties of the sediments varied with water depth: deeper sites, which were also lower in organic carbon, nitrogen and oxygen concentrations than shallower sites, had higher saturation magnetizations and were richer in single domain particles.

3.1. Introduction

Magnetotactic bacteria (MTB) are found in most fresh and saline water habitats [Blakemore, 1975; Du *et al.*, 2015; Lin and Pan, 2010; Pan *et al.*, 2005; Petermann and Bleil, 1993; Schüler, 2006; Simmons and Edwards, 2007; Spring *et al.*, 1993]. They are micro-aerobic to anaerobic organisms that live in the oxic-anoxic transition zone where chemical gradients are high [Frankel *et al.*, 1997]. MTB belong to gram-negative phylogenetic groups [Uebe and Schüler, 2016] and host a wide variety of cell morphotypes including cocci, vibrios, spirilla, ovoids, rods and multicellular prokaryotes [Lefèvre *et al.*, 2011a; Spring and Schleifer, 1995; Wenter *et al.*, 2009]. They produce 30 to 120 nm sized crystals of membrane-bound, ferrimagnetic magnetite and/or greigite magnetosomes that are aligned in chains [Kopp and Kirschvink, 2008]. The

magnetosome chains are fixed to the cell, which compels MTB to move along magnetic field lines [Blakemore and Frankel, 1981].

It is well established that fossil magnetosomes preserved in sedimentary rocks can serve as recorders of the paleomagnetic field. The morphology and abundance of magnetosomes can also reflect environmental conditions and have been used as paleoenvironmental proxies [Chang and Kirschvink, 1985; Hesse, 1994; Lean and McCave, 1998; Moisesescu et al., 2014; Paasche et al., 2004; Roberts et al. 2011; Snowball et al., 2002; Yamazaki, 2012]. MTB cells contain 2 to 4% (dry weight) Fe, so they likely influence iron cycles in nature by sequestering Fe in sediments [Chen et al., 2014]. Relationships between temperature and MTB abundance have been observed, which could make them potentially useful temperature proxies [Du et al., 2015; Lin et al., 2012a]. MTB are also sensitive to local chemical factors such as total organic carbon (TOC), dissolved iron and nitrate concentrations [Du et al., 2015; Lin and Pan, 2010; Roberts et al., 2011; Zhou et al., 2013].

Despite their importance to paleomagnetic and environmental studies, few studies have been dedicated to understanding natural environmental factors governing MTB life cycles. Simmons et al. [2004] measured MTB abundances at a single site in a chemically stratified coastal salt pond three times over a four-month period. Du et al. [2015] studied MTB at two sites in a brackish water environment every two weeks for 15 months. Although some long-term microcosm studies have been carried out [e.g., He et al., 2017; Postec et al., 2012], MTB populations growing in temperature-controlled microcosms versus those in nature are likely quite different [Flies et al., 2005]. A high MTB population density and broad diversity of magnetic microorganisms live in a pond within the confines of an isolated forest owned by LMU-Munich. Here, we report MTB abundances, as well as temperature, dissolved O₂ and magnetic properties from nine sites in the pond measured at a one-month frequency over a two-year period. These results are compared against a control beaker kept in a laboratory. Vertical profiles of MTB and magnetic hysteresis loops, as well as carbon and nitrogen concentration of the surface sediments, were also measured at a few discrete places and/or times.

3.2. Methods

3.2.1. Study design and sampling

The pond, 30 m in length and 7 m in width, lies at the edge of a forest, 80 km northeast of Munich (48°35'15"N, 12°04'43"E) (Figure 3-1). A small stream feeds the pond whose source water percolates out of permeable bedrock from several different places in the forest. A golf course abuts one side of the stream for 1.5 km and contributes run off to the stream; no discharge from nearby farms enters the pond. We built an aqueduct system that modulated the water stand, although strong rainstorms or sudden warming in winter months that abruptly melted the surrounding snowpack occasionally flooded the entire area. When we began the experiment in January 2015, the water was ~60 cm deep near the pond's outlet and ~30 cm near the inlet (Figure 3-1b).

Twenty-nine meter rails lay parallel to the long axis on both sides of the pond. A bridge that rolls on the rails suspends a carriage over the water that supports people and equipment, so that a person can access any location of the pond from above with minimal disturbance to the environment. We selected nine sites to extract cores (Figures 3-1b and 3-1c), with each sampling site comprising an area of 100×60 cm² spanning the two-year period ensuring that each extraction did not disturb the sedimentary environment of successive cores. Cores to obtain vertical profiles of MTB and magnetic parameters were collected in June, August and November 2016 at the sites indicated in Figure 3-1b.

Before sampling, we measured the height of the sediment and water surfaces relative to a constant reference to obtain sediment accumulation rates and water depth (Figure 3-2a). It was necessary to break a hole in the ice to access the sediment in the winter. Water temperature was measured at each site every 5 cm from the air-water interface until 1-4 cm above the water-sediment interface. For sampling, plastic pipes, 5 cm diameter and 20 cm in height, were inserted ~10 cm into the sediment. A rubber stopper sealed the top of the pipe, the pipe was removed from the sediment, and then a second rubber stopper blocked the bottom of the pipe. The nine pipes were carried ca. 100 m to the nearby laboratory with minimal disturbance. In January 2015, we also sampled the upper 10 cm layer of the sediment near the inlet of the pond (Figure 3-1b) and thoroughly mixed it into a two-liter glass beaker. The beaker was stored in the laboratory and studied monthly over the same two-year period as the pond.

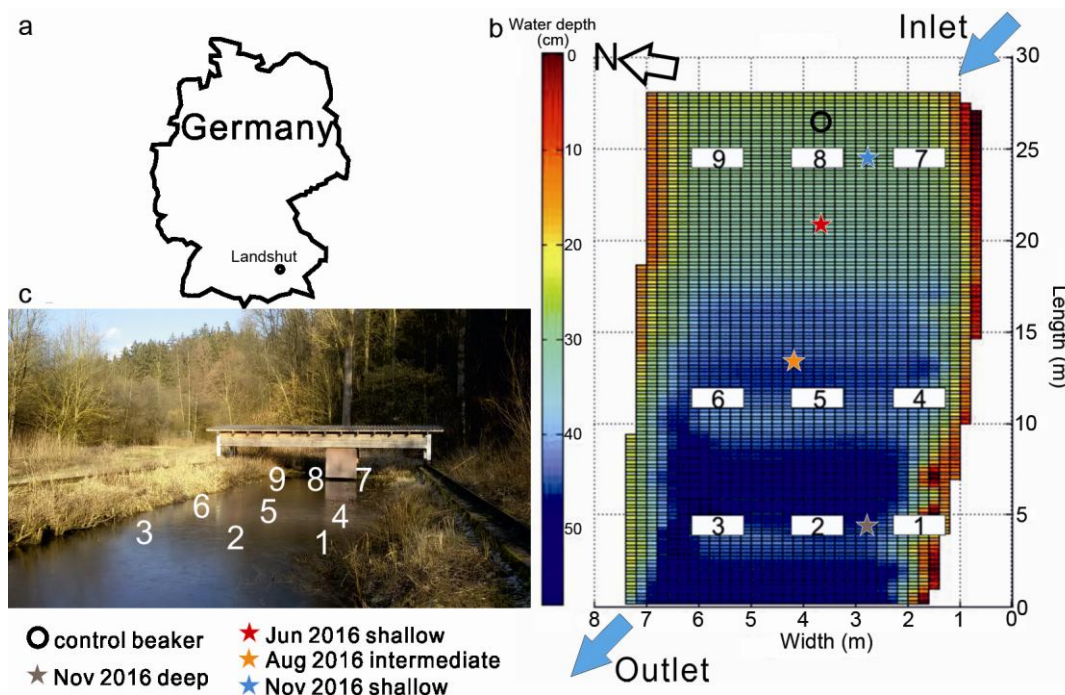


Figure 3 - 1 The information of the Niederlippach pond. **a)** General location map of the pond located near Landshut, Germany. **b)** Water depth (in September 2011) and distribution of the sampling sites. **c)** Photo of the pond with bridge that rolls on rails along the pond's long axis. A cabin suspended on the bridge moves back and forth on a rope-pulley system enabling a single user to access any point in the pond with sampling/analytical equipment.

3.2.2 Measurement protocol: Oxygen, carbon and nitrogen concentrations, MTB quantification and magnetic properties

Within five minutes after transporting the cores to the laboratory, oxygen (O_2) profiles were measured starting 10 mm above the water-sediment interface using a Unisense oxygen-50 microsensor (tip diameter = 50 μm , detection limit = 0.3 μM). The sensor was fixed on a computer-driven micromanipulator mounted on a heavy laboratory stand. We used the viable cell count technique to quantify the MTB morphotypes using the instrumentation and methodology of *He et al.* [2017]. We extracted 200 μl from the upper 10 mm of the sediment cores and of the control beaker, diluted each subsample with distilled water to a total of 5 ml or 35 ml depending on the MTB concentration and homogenised the slurry. For counting the cells, 10 μl of homogenised slurry was placed on a glass slide with 10 μl of distilled water placed next to it. The drop was then sealed with an O-ring and a cover slide to prevent evaporation and placed in a 0.6 mT horizontal magnetic field within a Petersen Instruments magnetodrome (optical microscope with Helmholtz coils surrounding a non-magnetic stage). The magnetic field induced

motile MTB to swim out of the sediment slurry toward the clear edge of the drop where the MTB were counted after 20 min when their numbers reached a steady state.

Morphotypes were classified into three categories based on easily recognizable traits: (1) rods that are large ($>5 \mu\text{m}$), elongate and mostly opaque in transmitted light, (2) cocci based on their rounded morphology, fast swimming behavior and small ($\sim 1\text{-}4 \mu\text{m}$) sizes, and (3) spirilla, which are generally $2\text{-}3 \mu\text{m}$ long and slightly concave. 16S rRNA sequencing of the pond sediment identified several cocci species and two rod-types [*Coskun et al.*, 2017], but species cannot be distinguished under the microscope so they are grouped according to morphotype. Vibrios would be counted as spirilla, as the two cannot be distinguished optically. Two subsamples were prepared from each core and the control beaker every month and two drops were counted per subsample. The number of MTB morphotypes per site and time was taken as the average of the four drops. For the vertical profile measurements, only one sample was extracted and one drop was counted for each layer.

Magnetic hysteresis loops and backfield curves were measured with a Princeton Instruments vibrating sample magnetometer (MicroMag 3900) on air-dried sediments (uppermost 1 cm from the cores) from all nine cores taken each month in 2016 to calculate the saturation magnetization (M_s), the remanent magnetization after saturation (M_{rs}), the coercive force (B_c) and the coercivity of remanence (B_{cr}). Total organic carbon and total nitrogen (TN) were measured in the same sediment samples that were used to count MTB in January 2015 and August 2016. Analyses of the freeze-dried, homogenized samples took place at Erlangen University using a Carlo Erba NC 2500 elemental analyzer coupled to a Thermo-Finnigan, Delta Plus isotope-ratio-mass spectrometer following the methods described in *Mayr et al.* [2011]. Mass percentage (TOC) and isotope ratios ($^{13}\text{C}/^{12}\text{C}$) of organic carbon were measured from samples decalcified with 20% HCl in silver cups; TN content and isotope ratios ($^{15}\text{N}/^{14}\text{N}$) were determined from chemically untreated samples. Isotopic ratios are reported in the common delta notation ($\delta^{15}\text{N}_{\text{TN}}$, $\delta^{13}\text{C}_{\text{TOC}}$) versus the international standards AIR and VPDB, respectively. Carbon-to-nitrogen ratios are reported as molar ratios and were calculated from TOC and TN values. Internal standards used for element content determinations were cyclohexanone-2,4-dinitrophenylhydrazone and atropine; for isotope calibration, a peptone

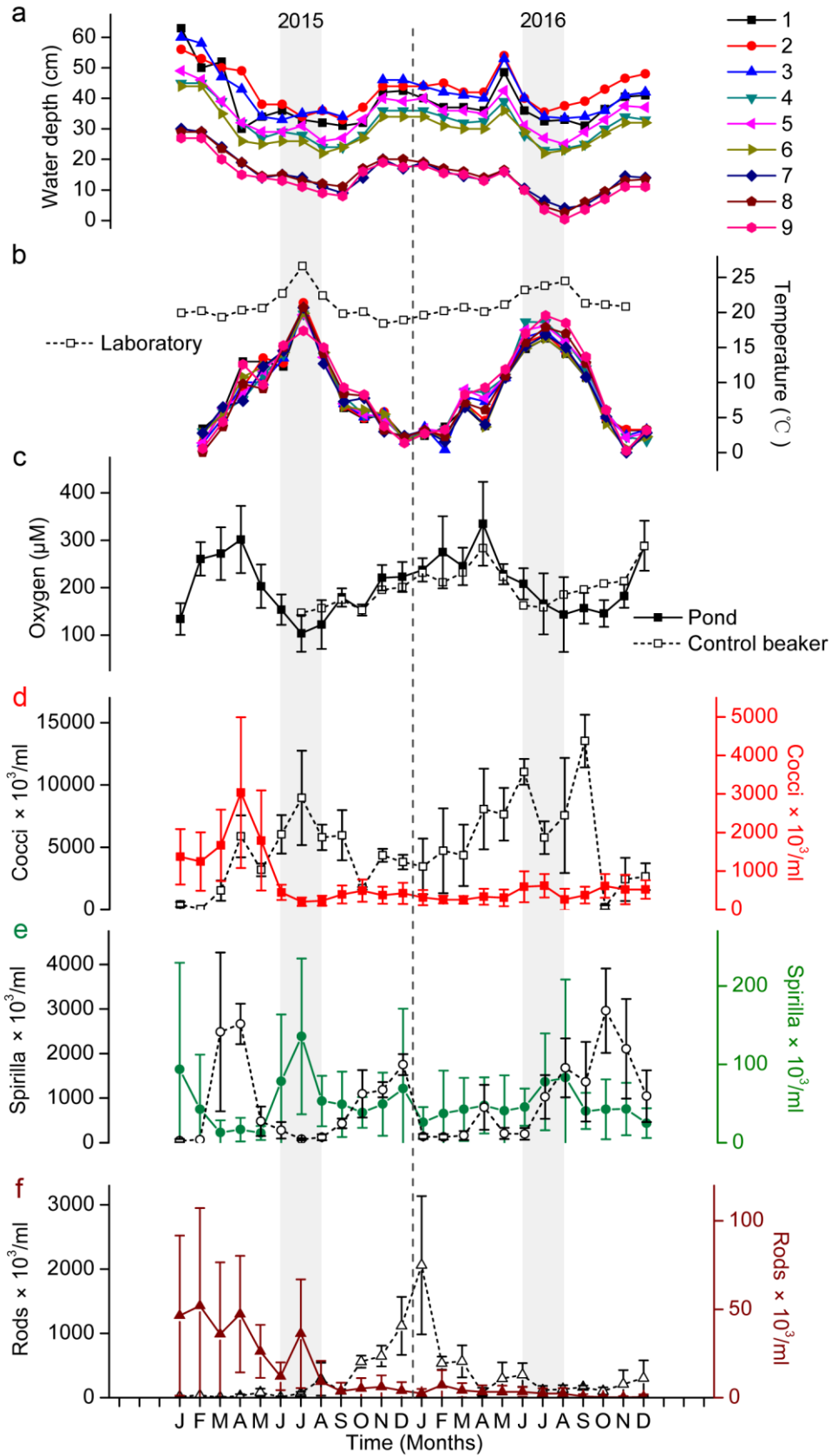


Figure 3 - 2 Temporal variation of environmental factors and MTB abundance. Temporal variation of (a) water depth at sites 1-9, (b) bottom water temperature at each site (legend in a) together with the temperature of the water in the laboratory used for the O₂ calibration measurements, (c) average and single standard deviation of nine oxygen concentration measurements made 3 mm above the sediment-water interface (d-f) average and single standard deviation (nine sites) of magnetotactic bacteria population for each of the three morphotypes. Open symbols with dashed lines are from the control beaker with scale on left. Data in Tables 3-1 to 3-3.

laboratory standard was used. The error was less than 5% for TOC and TN determinations, and less than 0.2‰ (one standard deviation) for isotope analyses.

3.3. Results

Figures 3-2a to 3-2c show the water depth, bottom water temperature and dissolved O₂ over the two-year period. Although the water inflow was regulated via the aquifer, the level varied throughout the observation period with lowest water stands in summer. Bottom water temperatures reached highs of 16-21°C in summer and lows of ~0°C in the winter. Bottom water O₂ concentrations generally waxed in spring (max. 300 μM or ~100-120% saturation) and waned in late summer (min. 44 μM or 16% saturation). A strong horizontal gradient in O₂ occurred in summer 2016 with hypoxic bottom waters at the deepest sites and O₂ saturated waters at the shallowest sites. The maximum penetration depth where O₂ disappeared in the sediment over the two years ranged from 2 to 7 mm, which correlated well on average ($r = 0.72$, $n=24$) with the bottom water O₂ concentration that ranged from 103-335 μM. Floating plants (*Lemnoideae* = duckweed) covered the pond's surface from June to September. These plants reduced the light at depth, thereby limiting O₂ production. Surprisingly, the beaker in the temperature-controlled environment (between 20 and 25°C) underwent similar annual trends in O₂ as the pond (Figure 3-2c), independent of temperature correction, suggesting common O₂ respiration and production mechanisms.

Figures 3-2d to 3-2f show the temporal variation of MTB morphotype abundances averaged over the nine sites. Cocci dominated the MTB community, being 10× on average more abundant than spirilla and 100× more abundant than rods. Generally the growth and death phases coincided among the different sites in the pond, although the total abundance from site to site varied up to an order of magnitude (Figure S1). Consistency among the deeper water sites was higher, with centrally located sites 2 and 5 showing the highest correlation in seasonal trends.

Table 3 - 1 Average magnetotactic bacteria cell populations and bottom water oxygen concentrations for the nine sizes in the pond and in the control beaker

Month	Pond						Control beaker						O ₂ μM		
	Cocci	σ	Spirilla	σ	Rods	σ	Cocci	σ	Spirilla	σ	Rods	σ			
	cells/μl						cells/μl								
													μM		
J-2015	1370	722	94	136	46	45	134	33	408	201	47	38	20	13	--
F	1242	759	43	70	52	55	261	35	25	0	68	0	35	0	--
M	1666	927	13	16	36	41	272	56	1514	807	2485	1781	6	8	--
A	3038	1958	17	15	47	33	302	71	5870	1683	2665	452	25	30	--
M	1791	1301	12	9	26	15	203	46	3181	508	481	329	83	58	--
J	444	200	78	85	12	8	154	32	6042	1543	280	184	9	10	--
J	202	110	136	99	36	31	103	39	8960	3794	79	23	70	20	147
A	227	128	53	32	9	12	122	51	5793	1021	123	67	289	256	157
S	388	232	49	42	4	5	179	19	5959	2012	433	110	101	30	175
O	490	286	39	20	5	6	153	12	1711	98	1098	533	560	95	152
N	371	222	49	40	6	6	221	27	4349	525	1190	172	648	161	195
D	418	279	69	102	4	5	223	32	3806	586	1754	237	1116	451	201
J-2016	308	200	26	20	2	3	237	25	3456	2228	140	55	2061	1076	232
F	255	99	37	55	7	9	275	76	4712	3410	131	60	538	101	212
M	250	99	43	40	4	4	245	39	4349	2464	162	100	564	251	232
A	332	207	48	36	3	4	335	89	8068	3234	796	503	88	69	284
M	304	216	41	45	3	4	228	21	7648	2106	210	126	298	250	223
J	587	402	45	24	3	3	208	33	11056	1024	197	131	354	182	162
J	615	304	78	62	2	3	166	65	5766	1307	1028	492	114	68	158
A	260	278	83	125	2	3	144	79	7551	4620	1680	660	131	61	185
S	371	216	41	23	1	1	157	32	13523	2113	1369	894	162	26	196
O	612	306	43	38	0	1	145	28	171	170	2962	945	101	60	208
N	520	381	43	34	0	1	182	24	2419	1728	2109	1118	210	217	214
D	519	241	25	19	0	1	288	53	2638	1079	1046	579	302	278	288

Table 3 - 2 Water depth and bottom water temperature at each site or control beaker (CB) for each month in 2015 and 2016

Month	Water depth (cm)									Bottom water temperature (°C)									CB
	1	2	3	4	5	6	7	8	9	1	2	3	4	5	6	7	8	9	
J-2015	63.0	56.0	60.0	45.0	49.0	44.0	30.0	29.0	27.0	--	--	--	--	--	--	--	--	--	20.0
F	50.0	53.0	58.0	45.0	46.0	44.0	29.0	29.0	27.0	3.4	1.4	1.3	3.0	1.4	2.8	2.8	0.0	0.6	20.3
M	52.0	50.0	47.0	39.0	39.0	35.0	24.0	23.5	20.0	5.9	6.1	5.0	5.8	6.4	5.6	6.5	3.7	4.4	19.4
A	30.0	49.0	43.0	32.0	32.0	26.0	19.0	19.0	15.0	13.0	9.4	10.0	7.6	8.3	10.8	7.4	9.8	12.6	20.4
M	34.0	38.0	34.0	27.0	29.0	25.0	14.0	14.5	14.0	13.0	13.5	10.1	11.1	11.7	12.3	12.3	9.1	9.7	20.7
J	36.0	38.0	33.0	29.0	29.0	26.0	15.0	15.0	13.0	12.3	12.8	13.5	14.0	14.6	14.3	14.5	15.0	15.3	22.8
J	33.0	34.0	35.0	28.0	31.0	26.0	14.0	13.0	11.0	20.7	21.4	19.9	19.8	19.7	19.9	20.7	20.7	17.4	26.7
A	32.0	36.0	36.0	24.0	26.0	22.0	11.0	12.0	9.0	14.6	14.5	14.6	13.8	13.6	14.3	12.7	14.1	15.0	22.5
S	31.0	33.0	34.0	24.0	27.0	24.0	9.0	11.0	8.0	6.4	6.6	7.0	8.0	7.0	6.6	7.3	8.4	9.3	19.9
O	32.0	37.0	--	28.0	33.0	27.0	14.0	17.0	16.0	4.8	4.9	5.1	5.4	5.5	6.1	7.8	8.1	8.3	20.2
N	42.0	44.0	46.0	36.0	40.0	34.0	20.0	20.0	19.0	5.5	5.8	5.6	4.8	5.0	5.5	3.0	3.2	3.8	18.5
D	42.5	44.0	46.0	36.0	39.0	34.0	17.0	20.0	17.5	2.2	1.6	1.6	2.0	2.0	1.8	2.4	2.2	1.4	19.0
J-2016	40.0	44.0	44.0	36.0	40.0	34.0	19.0	19.0	18.0	2.4	3.3	3.6	2.8	3.4	2.7	3.2	3.2	2.7	19.7
F	37.0	45.0	42.0	34.0	36.0	31.0	16.0	17.0	15.5	3.7	2.4	0.4	3.4	3.0	2.2	1.6	2.3	3.3	20.3
M	37.0	42.0	41.0	32.0	36.0	30.0	14.5	16.0	15.0	6.5	7.1	8.0	8.8	9.0	7.1	6.5	7.1	8.3	20.8
A	36.0	42.0	40.0	32.5	35.0	30.0	13.3	14.0	13.0	3.8	4.6	7.3	8.6	7.8	3.7	4.0	6.1	9.3	20.2
M	48.5	54.0	53.0	39.0	42.5	36.0	16.0	16.5	16.0	10.7	10.9	10.7	10.8	10.9	10.7	10.7	10.9	11.9	21.2
J	36.0	40.0	40.0	28.0	31.0	29.0	10.5	10.0	10.0	14.8	15.7	16.5	18.7	17.5	14.9	15.2	15.7	17.0	23.3
J	32.5	35.5	34.0	23.0	27.0	22.0	6.5	4.5	3.5	16.3	16.9	17.4	18.6	18.1	16.3	16.8	17.9	19.6	23.9
A	33.0	37.5	33.5	23.5	25.0	23.0	4.0	2.5	0.4	14.1	14.4	14.8	15.9	15.8	14.2	15.0	17.0	18.5	24.6
S	31.0	39.0	34.0	25.0	29.0	24.5	5.0	6.0	3.5	10.7	10.8	11.1	12.0	12.6	10.8	10.8	12.7	13.7	21.4
O	36.5	43.0	36.0	30.0	33.0	28.5	9.0	9.5	7.0	4.8	4.9	5.3	5.9	5.9	4.1	5.1	6.1	6.1	21.2
N	40.5	46.5	41.0	34.0	37.5	32.0	14.5	13.0	11.0	3.2	3.3	2.4	2.3	2.2	0.6	0.0	0.3	0.3	20.9
D	41.0	48.0	42.0	33.0	37.0	32.0	14.0	13.5	11.0	3.2	3.3	3.3	1.7	2.8	2.3	2.8	3.3	3.2	--

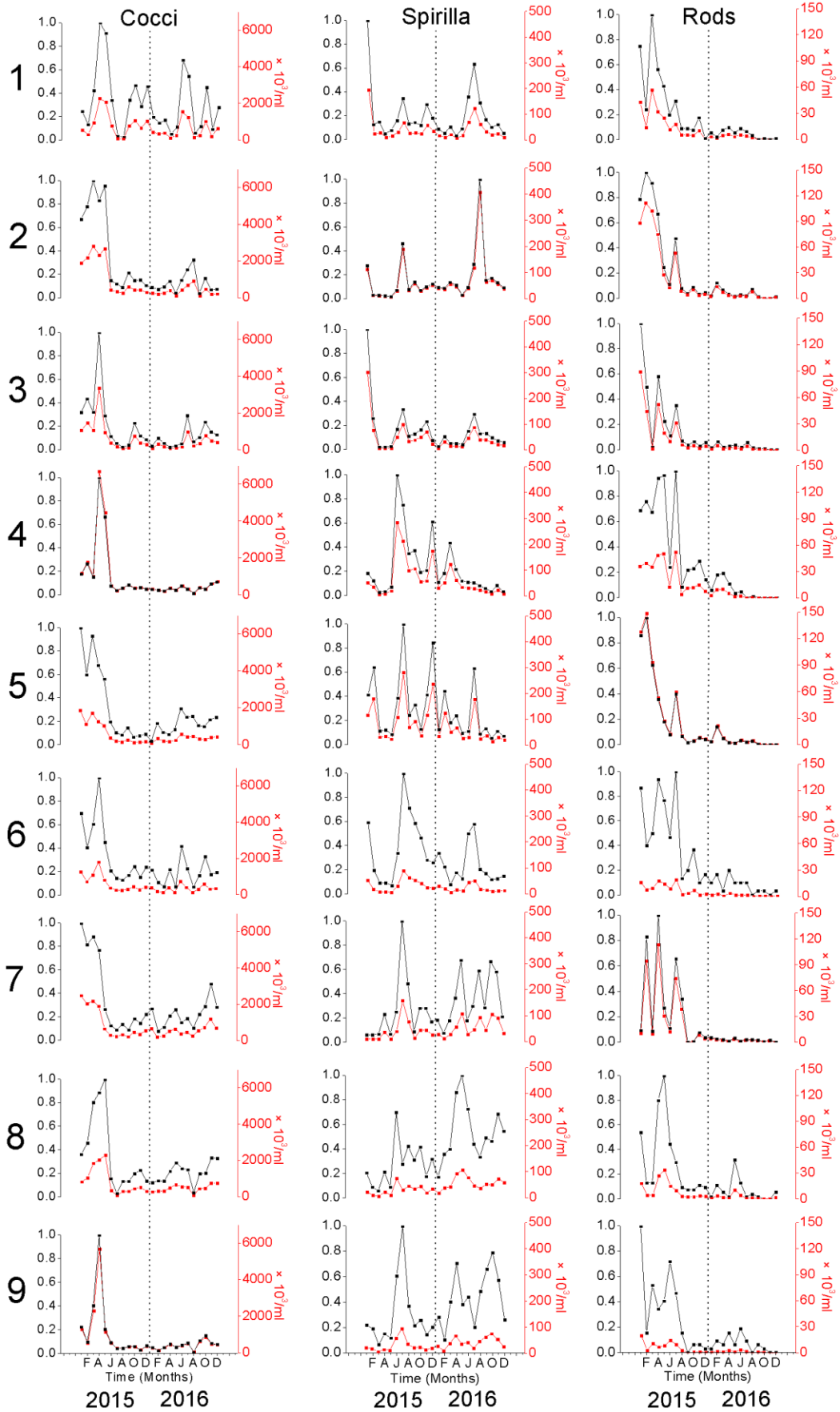


Figure 3 - 3 MTB concentrations at each site (1-9) normalized (to maximum) on the left and in absolute numbers at the same scale for each morphotype on the right.

Table 3 - 3 Average (4 samples) magnetotactic bacteria cell populations for each site in 2015 (upper rows) and 2016 (lower rows)

Site	Cocci (cells/ μ l)											
	J	F	M	A	M	J	J	A	S	O	N	D
1	553	297	957	2264	2060	769	75	54	771	1055	648	1033
2	1879	2181	2803	2326	2671	410	328	246	598	411	423	289
3	1075	1466	1085	3376	971	381	181	75	131	759	393	293
4	1176	1778	1014	6709	4468	503	248	384	561	371	409	319
5	1851	1105	1716	1256	1040	368	195	156	269	125	146	170
6	1252	724	1089	1798	806	370	258	230	300	434	273	427
7	2483	2023	2189	1903	654	309	225	338	219	457	363	552
8	833	1054	1845	2036	2299	355	69	306	306	456	525	311
9	1276	552	2297	5675	1155	529	242	253	334	338	159	373
1	437	330	384	115	252	1541	1231	137	263	1018	206	631
2	246	199	259	395	115	415	671	905	102	463	188	204
3	102	326	186	72	112	169	983	230	353	792	512	424
4	313	257	219	371	261	506	317	82	399	319	623	736
5	62	340	199	168	245	575	440	451	306	288	396	436
6	384	192	126	388	126	746	401	122	295	588	314	344
7	665	196	275	518	653	381	460	261	549	719	1193	705
8	279	316	313	504	669	556	536	84	456	464	763	753
9	289	141	294	454	301	397	501	68	619	857	487	439
	Spirilla (cells/ μ l)											
1	194	24	29	9	15	31	67	26	28	23	57	35
2	113	13	12	10	8	29	189	32	57	29	41	51
3	301	78	6	6	8	51	100	34	39	49	70	23
4	52	35	8	9	20	285	213	99	106	55	59	174
5	116	179	32	34	24	108	281	69	93	36	116	236
6	53	18	8	8	6	30	89	63	52	41	25	23
7	9	9	11	36	11	39	158	76	14	44	44	27
8	22	9	6	23	9	74	29	45	33	44	19	34
9	21	18	6	14	11	58	95	35	21	24	14	19
1	17	10	21	6	18	69	123	60	33	20	24	10
2	39	36	56	46	13	39	118	408	63	70	55	38
3	8	32	16	15	13	46	88	39	40	29	22	18
4	31	52	124	61	34	31	30	23	17	9	24	9
5	36	124	51	68	27	31	177	25	38	15	31	20

6	30	20	7	16	11	44	51	18	15	11	11	13
7	29	12	28	58	107	28	47	93	45	105	92	33
8	18	38	43	92	107	78	47	36	53	49	73	58
9	27	10	38	67	36	42	19	46	63	75	54	25
	Rods (cells/μl)											
1	43	14	57	32	24	11	18	5	5	4	10	1
2	88	112	103	75	28	13	53	9	4	10	4	5
3	89	44	2	52	20	10	31	6	3	6	3	5
4	36	39	35	49	50	13	52	4	11	12	15	8
5	128	149	93	53	27	12	59	10	3	4	8	6
6	16	8	9	18	14	9	19	3	4	7	2	3
7	11	94	10	114	31	13	74	39	0	1	9	4
8	18	4	4	27	34	15	10	3	3	3	4	3
9	20	3	11	7	8	14	9	3	0	1	1	1
1	3	1	4	6	3	5	4	2	0	1	0	1
2	3	14	8	4	2	3	3	8	1	0	0	1
3	1	6	2	3	3	2	5	1	1	1	0	0
4	3	9	10	6	2	3	0	1	0	0	0	0
5	4	21	8	3	2	5	3	4	1	0	0	0
6	2	3	1	4	2	2	2	0	1	1	0	1
7	4	3	3	1	4	1	3	3	2	1	2	0
8	1	4	2	1	11	4	1	1	1	0	0	2
9	1	2	1	3	1	4	2	0	1	1	0	0

Cocci underwent a precipitous decrease following April 2015, then they had a slight renaissance in the summer of 2016. Like cocci, rods were significantly more abundant at the beginning of the observation period. Their numbers decreased with time, with the exception of a pronounced growth phase in July 2015 when they tripled in comparison to June. Rods were no longer detected at most sites by the end of 2016. Unlike cocci and rods, spirilla showed consistent seasonal trends in both years (with the exception of shallow sites 7-9, which nearly fell dry in August 2016), reaching the highest numbers in the summer months and lowest in spring and autumn. Spirilla also underwent a second, less pronounced peak of growth during the winter months at several sites.

MTB populations evolved quite distinctly between the pond and the control beaker (Figure 3-2). Initially, all morphotypes were less abundant in the control environment relative to the pond.

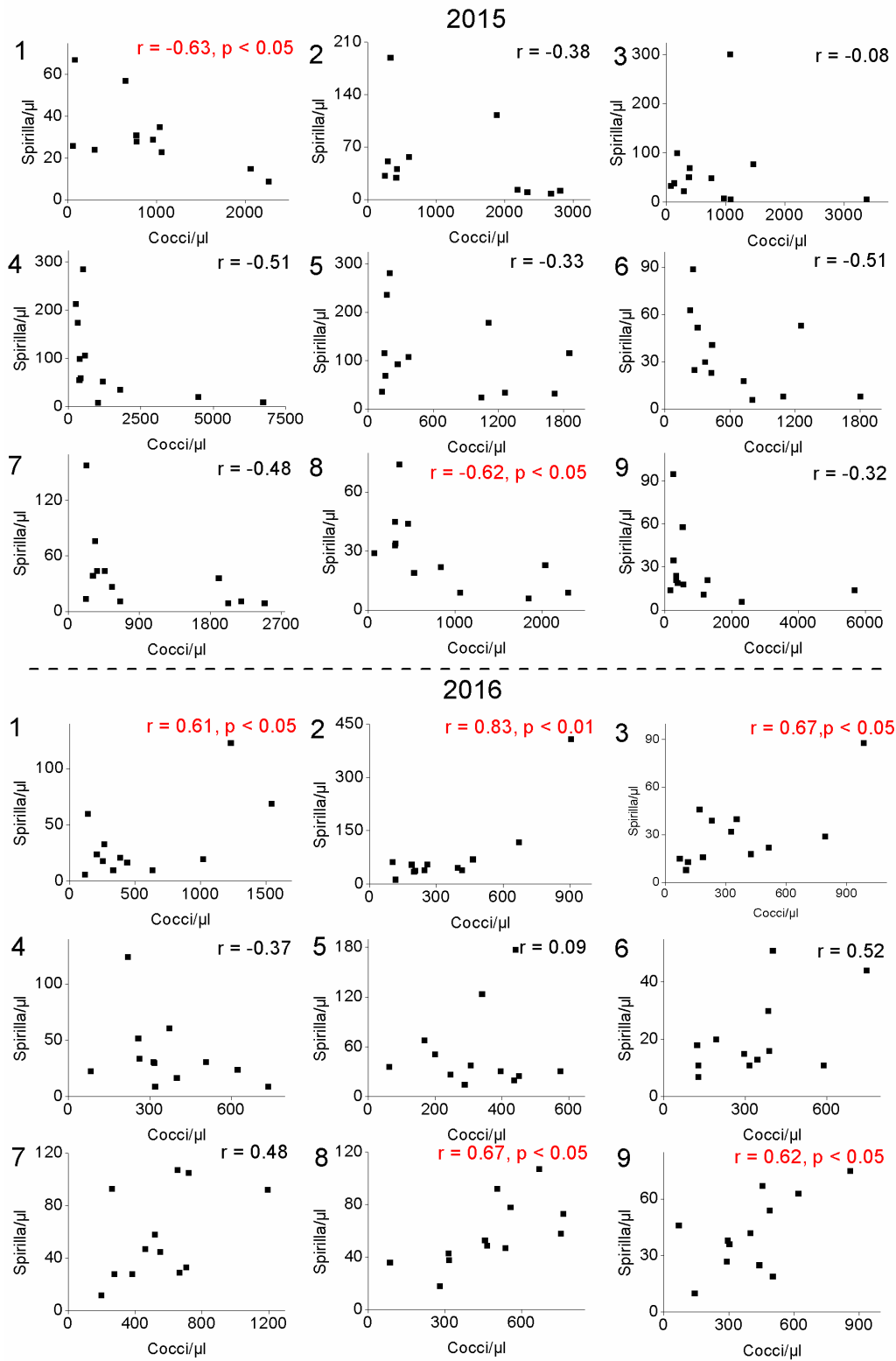


Figure 3 - 4 Relationship between spirilla and cocci abundances at each site for each month during 2015 and 2016. Correlation coefficients in red are significant at 95% or 99% confidence limits.

Within several months cocci concentrations in the beaker rose $\sim 10\times$ higher than those in the pond and peaked in the summer of 2015 and potentially in the summer of 2016 albeit not as clear. Rods numbers in the beaker exhibited a pronounced peak in winter 2015 and then decreased gradually until the end of the experiment. Spirilla boomed in spring and late autumn-early winter in contrast to the pond where population maxima occurred in the summer. Spirilla and cocci numbers in the pond were negatively correlated in 2015 ($r = -0.28$, $p < 0.01$, $n = 108$) and positively correlated in 2016 ($r = 0.38$, $p < 0.01$, $n = 108$), although there was a high degree of variability between sites (Figure 3-4). Interestingly, cocci abundance was significantly positively correlated with O_2 concentration in 2015, but not in 2016 (Figure 3-5), whereas spirilla exhibited a significant negative correlation with O_2 in 2015 but not in 2016 (Figure 3-5). Rods had no significant relationship with O_2 in either year.

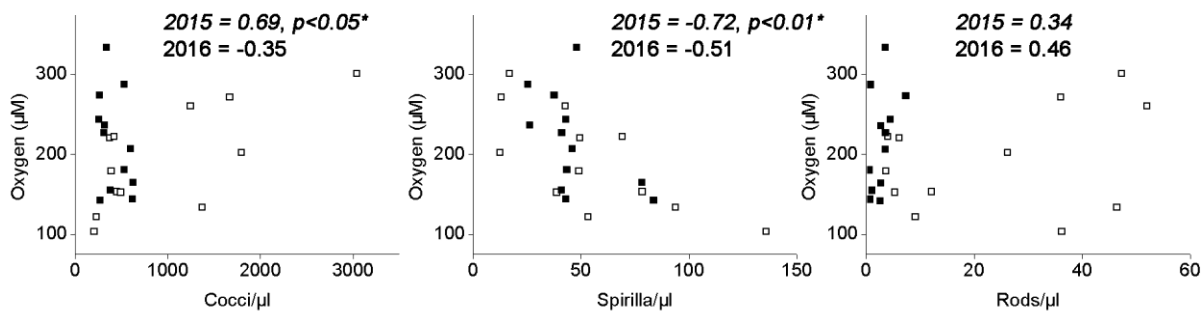


Figure 3 - 5 Relationship between bottom water O_2 and MTB concentrations of the three morphotypes. Open symbols = 2015; solid symbols = 2016. The r values with asterisks are significant at 95% ($p < 0.05$) and 99% ($p < 0.01$) confidence limits, respectively.

Previous work in the pond identified magnetite as the sole ferrimagnetic mineral in the sediment [Zhao, 2015]. We further confirmed this with low temperature experiments that revealed a broad Verwey transition around 110 K (Figure 3-6 a), characteristic of non-stoichiometric (oxidized) magnetite. The temperature dependence of the magnetic remanence and susceptibility defined single Curie temperatures around 575°C (Figure 3-6 b). First order reversal curves showed a distinct central ridge with no hint of magnetostatic interactions diagnostic of authigenic greigite (Figures 3-6c and 3-6d).

The magnetic properties of the pond surface sediments were not related to the number of living MTB, nor did they change through time, but instead varied as a function of water depth (Figures 3-7a and 3-7b). Sites from deeper water had higher M_s and were magnetically harder (higher

Bcr), being more displaced toward the single domain region on the Day plot [Day *et al.*, 1977] then sites from shallow water (Figure 3-7c). TOC, TN and bottom water O₂ concentrations

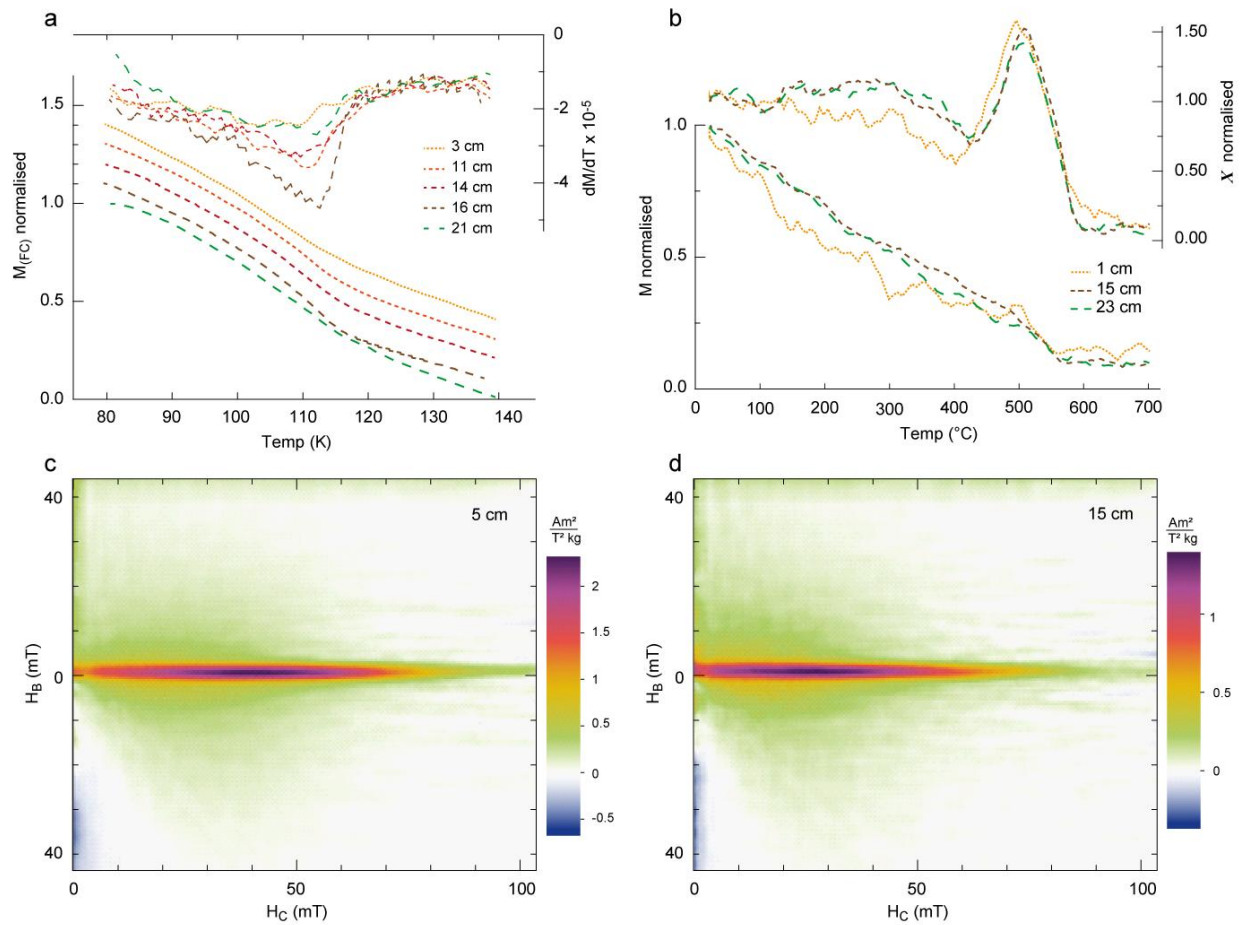


Figure 3 - 6 Field cooled SIRM curves, temperature dependence of the magnetic remanence and susceptibility and FORCs. (a) Field cooled (1 T) SIRM curves measured (Princeton Instruments, MicroMag 3900 vibrating sample magnetometer) upon warming in a null field of the August 2016 core sediments from 3, 11, 14, 16 and 21 cm depth. (b) Temperature dependence of the magnetic remanence (M) and susceptibility (X) of the August core sediments at 1, 15 and 23 cm depth (Petersen Instruments, variable force translation balance). (c and d) First order reversal curve diagrams of the August core sediments at 5 cm and 15 cm depth obtained with VARIFORC [Egli, 2013] (data acquired on a Princeton Instruments, MicroMag 3900 vibrating sample magnetometer).

were also depth dependent, albeit with some scatter. All three chemical parameters showed higher values at the shallow sites close to the inflow and exhibited higher values on average in August 2016 than in January 2015 (Figures 3-7d to 3-7f). The carbon-to-nitrogen ratio (C:N) was nearly constant in space and time (January 2015: 13.2 ± 0.8 ; August 2016: 13.8 ± 1.3 , 1σ uncertainties). The $\delta^{13}C_{TOC}$ isotopic composition of the sediments was $-29.2 \pm 0.1\%$ and

-28.7±0.1‰, while $\delta^{15}\text{N}_{\text{TN}}$ was 2.1±0.2‰ and 1.9±0.3‰ in January 2015 and August 2016, respectively. The rather homogenous geochemical data indicate that the type of organic matter was similar at all times and locations sampled in the pond.

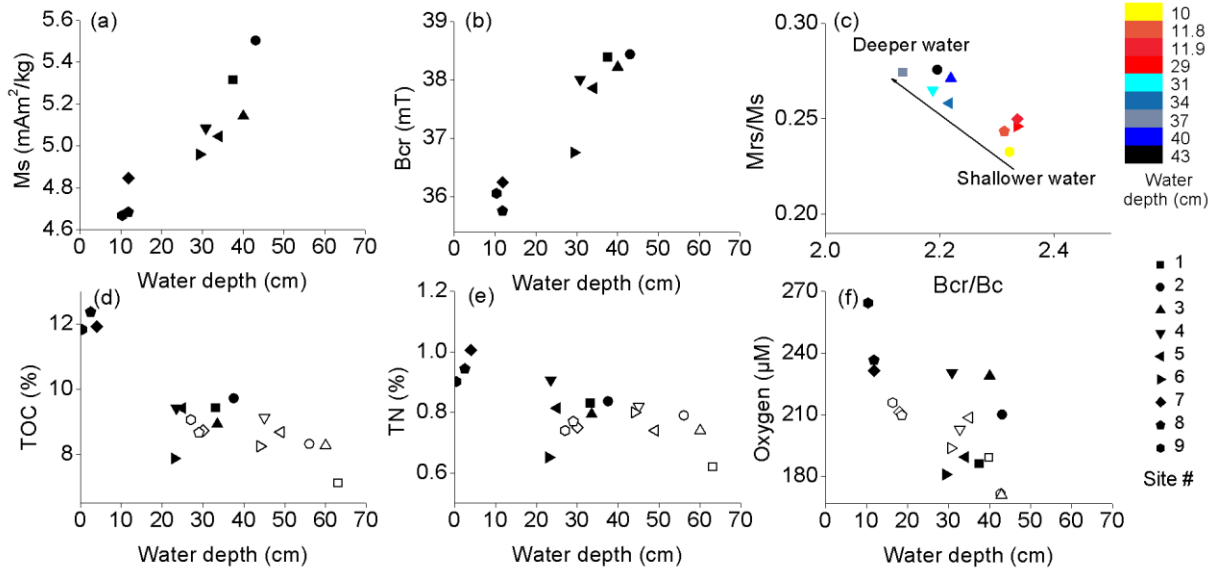


Figure 3-7 Magnetic and chemical parameters of the upper 1 cm of sediment from the pond (averages of 12 months for each of the 9 sites). Symbol types are identical for each individual site (legend in f). (a) Average saturation magnetization (Ms) for 2016. (b) Coercivity of remanence (Bcr) for 2016. (c) Day plot (Day et al., 1977) from 2016 color coded by average depth. (d) Total organic carbon (TOC) in January 2015 (open symbols) and August 2016 (solid symbols). (e) Total nitrogen (TN) in January 2015 (open symbols) and August 2016 (solid symbols). (f) Average bottom water oxygen concentration in 2015 (open symbols) and 2016 (solid symbols). Data in Tables 3-2, 3-4, 3-5.

Figure 3-8 shows vertical profiles of the MTB and the magnetic properties of the sediment measured at different places and times. Cocci and spirilla were bimodally distributed with maximum numbers around 1-2 cm depth and a second less pronounced peak around 4-6 cm depth. Spirilla were generally skewed deeper than cocci, although both were found within the same depth range, as deep as 15 cm. Ms, which serves a proxy for magnetite concentration, and Mrs/Ms, which can indicate grain size, were uncorrelated with the number of live MTB (Figure 3-8).

Table 3 - 4 Magnetic hysteresis and back field parameters for the nine sites in each month of 2016

Site	J	F	M	A	M	J	J	A	S	O	N	D
Mrs (mAm ² /kg)												
1	1.67	1.41	1.45	1.27	1.37	1.38	1.71	1.64	1.57	1.29	1.32	1.46
2	1.76	1.54	1.44	1.30	1.48	1.35	1.57	1.61	1.51	1.35	1.87	1.46
3	1.54	1.60	1.27	1.44	1.32	1.10	1.44	1.43	1.47	1.35	1.25	1.52
4	1.57	1.68	1.40	1.44	1.57	1.21	1.34	1.31	1.20	1.03	1.20	1.24
5	1.52	1.28	1.43	1.39	1.21	1.19	1.44	1.25	1.31	1.18	1.21	1.22
6	1.33	1.16	1.12	1.13	1.27	1.15	1.42	1.10	1.17	1.26	1.28	1.23
7	1.28	1.18	1.04	1.07	1.30	1.03	1.25	1.25	1.19	1.32	1.48	1.16
8	0.96	0.94	1.05	1.04	1.15	1.14	1.38	1.35	1.11	1.30	1.11	1.19
9	1.26	0.96	1.05	1.05	1.01	0.97	1.26	1.12	1.04	1.07	1.14	1.08
Ms (mAm ² /kg)												
1	5.56	5.22	5.40	4.92	5.09	5.34	5.84	5.40	5.93	4.89	4.85	5.36
2	6.01	5.59	5.43	5.19	5.17	5.31	5.45	5.61	5.84	5.10	5.75	5.60
3	5.51	5.78	5.09	4.90	4.94	4.61	5.48	5.09	5.02	5.25	4.94	5.11
4	6.03	5.90	5.18	4.96	5.28	5.01	4.87	4.86	4.56	4.29	5.05	5.03
5	5.42	5.11	5.05	5.03	5.19	4.84	5.36	4.63	5.03	4.85	5.07	4.96
6	5.17	4.97	4.29	5.33	5.20	4.88	5.76	4.48	4.86	4.82	4.87	4.88
7	4.90	4.73	4.27	4.56	4.97	4.33	5.01	5.08	5.13	5.17	5.08	4.92
8	4.48	4.05	4.25	4.37	4.71	4.78	5.10	4.98	4.58	5.17	4.84	4.89
9	5.65	4.75	4.38	4.69	4.48	4.28	4.67	4.46	4.56	4.62	4.81	4.68
Mrs/Ms												
1	0.30	0.27	0.27	0.26	0.27	0.26	0.29	0.30	0.26	0.26	0.27	0.27
2	0.29	0.28	0.27	0.25	0.29	0.25	0.29	0.29	0.26	0.27	0.32	0.26
3	0.28	0.28	0.25	0.29	0.27	0.24	0.26	0.28	0.29	0.26	0.25	0.30
4	0.26	0.29	0.27	0.29	0.30	0.24	0.28	0.27	0.26	0.24	0.24	0.25
5	0.28	0.25	0.28	0.28	0.23	0.25	0.27	0.27	0.26	0.24	0.24	0.25
6	0.26	0.23	0.26	0.21	0.24	0.23	0.25	0.25	0.24	0.26	0.26	0.25
7	0.26	0.25	0.24	0.23	0.26	0.24	0.25	0.25	0.23	0.26	0.29	0.23
8	0.21	0.23	0.25	0.24	0.24	0.24	0.27	0.27	0.24	0.25	0.23	0.24
9	0.22	0.20	0.24	0.23	0.23	0.23	0.27	0.25	0.23	0.23	0.24	0.23
Bcr (mT)												
1	38.2	38.1	38.9	38.9	38.5	37.9	39.9	37.9	38.2	38.7	38.1	37.5
2	37.6	37.9	39.2	38.7	38.2	38.3	38.4	38.3	38.7	38.9	39.6	37.5
3	38.8	38.8	38.5	38.0	38.1	37.6	38.4	36.7	38.5	38.1	38.5	38.7
4	39.0	38.1	40.3	38.3	37.3	37.3	38.9	36.7	38.8	36.8	36.9	37.8
5	37.5	38.5	39.2	38.8	37.1	38.6	38.3	36.3	37.9	37.2	37.6	37.3
6	37.8	36.9	36.9	36.1	37.7	37.2	36.1	36.5	37.0	36.5	36.3	36.1
7	35.8	36.8	37.1	37.5	38.2	35.7	36.2	35.4	35.1	36.9	34.8	35.6

8	36.8	35.2	36.1	37.7	36.7	35.2	35.5	34.1	35.8	34.8	34.7	36.5
9	36.6	36.1	36.4	37.9	35.9	36.0	36.6	34.1	35.7	35.8	35.3	36.4
	Bc (mT)											
1	19.5	16.6	18.5	17.2	17.1	16.7	18.8	17.3	18.0	19.8	18.5	18.6
2	18.6	18.0	18.6	17.0	18.1	16.6	17.7	17.7	16.0	17.7	17.4	17.1
3	17.7	17.7	18.1	17.4	17.6	15.9	15.7	16.4	16.7	17.0	17.7	19.2
4	18.2	18.9	19.2	18.1	18.3	16.8	16.7	15.4	17.6	16.6	16.3	17.2
5	17.3	17.4	17.3	17.3	18.1	17.1	19.0	16.7	16.8	16.0	14.9	17.6
6	16.8	15.7	15.8	14.5	16.2	16.5	15.3	15.7	14.0	15.8	16.5	16.8
7	15.9	16.8	16.0	15.7	16.1	12.9	14.8	16.0	14.4	17.0	15.7	15.8
8	15.3	15.3	15.8	15.7	16.4	15.1	16.0	15.2	15.7	14.5	14.7	15.9
9	15.0	15.1	16.0	17.8	16.3	14.1	15.9	14.0	15.1	15.7	15.7	16.1
	Bcr/Bc											
1	1.96	2.30	2.11	2.26	2.25	2.27	2.13	2.19	2.12	1.96	2.06	2.02
2	2.02	2.11	2.11	2.27	2.11	2.31	2.17	2.16	2.42	2.20	2.27	2.19
3	2.19	2.19	2.13	2.18	2.17	2.37	2.45	2.23	2.31	2.24	2.17	2.02
4	2.15	2.02	2.10	2.12	2.04	2.22	2.34	2.38	2.21	2.22	2.26	2.20
5	2.17	2.22	2.26	2.25	2.05	2.26	2.01	2.17	2.25	2.32	2.52	2.11
6	2.26	2.36	2.34	2.50	2.32	2.25	2.37	2.32	2.65	2.31	2.19	2.16
7	2.25	2.19	2.32	2.38	2.37	2.78	2.44	2.21	2.44	2.18	2.22	2.25
8	2.41	2.30	2.28	2.41	2.23	2.33	2.22	2.25	2.28	2.40	2.36	2.29
9	2.43	2.39	2.27	2.13	2.20	2.55	2.30	2.44	2.36	2.29	2.25	2.25

Table 3 - 5 Carbon and nitrogen isotopic data for each sample at each site in January 2015 and August 2016 (data in figures are the averages of the two samples/site)

Site	$\delta^{15}\text{N}$ vs AIR	%TN	%TC	$\delta^{13}\text{C}$ vs VPDB	%TOC	%TIC	TOC/TN
January 2015							
1a	2.27	0.69	8.77	-28.97	7.93	0.84	13.33
1b	2.08	0.55	7.45	-29.32	6.31	1.14	13.28
2a	2.21	0.78	9.92	-29.24	8.24	1.68	12.27
2b	2.13	0.79	9.69	-29.15	8.40	1.29	12.42
3a	2.44	0.71	9.49	-29.32	7.79	1.71	12.82
3b	1.99	0.77	9.96	-29.38	8.74	1.21	13.19
4a	2.12	0.82	10.99	-29.42	9.36	1.63	13.30
4b	1.97	0.81	10.60	-29.09	8.89	1.72	12.79
5a	1.73	0.84	11.18	-29.19	9.81	1.37	13.62
5b	2.33	0.64	8.29	-29.19	7.55	0.75	13.69
6a	2.01	0.80	10.29	-29.30	8.88	1.41	12.95

6b	2.43	0.79	9.20	-29.06	7.61	1.60	11.23
7a	2.16	0.78	9.96	-29.33	9.27	0.69	13.81
7b	2.24	0.71	9.09	-29.38	8.19	0.89	13.42
8a	1.76	0.77	10.41	-29.43	8.36	2.05	12.64
8b	1.80	0.76	10.19	-29.21	8.97	1.22	13.72
9a	1.74	0.82	11.15	-29.13	10.19	0.96	14.49
9b	2.05	0.80	10.72	-29.42	9.66	1.05	14.04
9c	1.83	0.59	7.76	-29.19	7.32	0.44	14.43
August 2016							
1a	2.33	0.75	10.45	-28.51	8.82	1.63	13.64
1b	2.27	0.91	11.59	-28.51	10.06	1.53	12.90
2a	2.05	0.90	11.96	-28.69	9.65	2.31	12.55
2b	2.06	0.78	10.77	-28.68	9.79	0.98	14.71
3a	1.99	0.87	12.23	-28.84	8.70	3.53	11.74
3b	2.11	0.72	10.41	-28.69	9.14	1.27	14.76
4a	1.92	0.92	12.84	-28.84	9.04	3.80	11.42
4b	2.08	0.89	12.40	-28.55	9.78	2.62	12.82
5a	2.06	0.75	10.66	-28.60	9.15	1.50	14.23
5b	2.01	0.88	12.23	-28.59	9.68	2.55	12.88
6a	2.14	0.67	9.76	-28.58	7.67	2.09	13.41
6b	2.21	0.64	10.30	-28.59	8.07	2.23	14.83
7a	1.08	1.03	13.08	-28.59	11.75	1.34	13.33
7b	1.84	0.98	13.33	-28.97	12.07	1.26	14.32
8a	2.10	0.88	12.57	-28.78	12.22	0.35	16.21
8b	1.39	1.01	14.34	-28.59	12.51	1.83	14.48
9a	1.54	0.93	13.07	-28.52	12.20	0.87	15.27
9b	1.58	0.87	11.96	-28.53	11.45	0.50	15.35

3.4. Discussion

Two years of observations showed distinct seasonal cycles in MTB populations in the pond. Despite differences between morphotypes, the relative trends of individual morphotypes appear coherent from site to site, which indicates an overall sensitivity of MTB populations to the pond's environment (Figure 3-3). Spirilla were most abundant in the summer months when water temperatures peaked and O₂ concentrations were lowest. A subsidiary spirilla growth phase occurred in the winter.

Population trends of spirilla were in antipathy with cocci in 2015, when absolute numbers varied strongly, yet coincided in 2016 when temporal variations in cocci abundance were more subdued (Figure 3-4). Significant anti-correlation in time and space between spirilla and cocci populations was also found by *He et al.* [2017] who measured MTB abundances at 72 points in two aquaria each month for 198 days. Such antipathy between cocci and spirilla might be related to differences in their magnetotactic behavior [*Mao et al.*, 2014a]. Alternatively, antipathy could be related to disparate mechanisms coping in chemical environments, as suggested by the

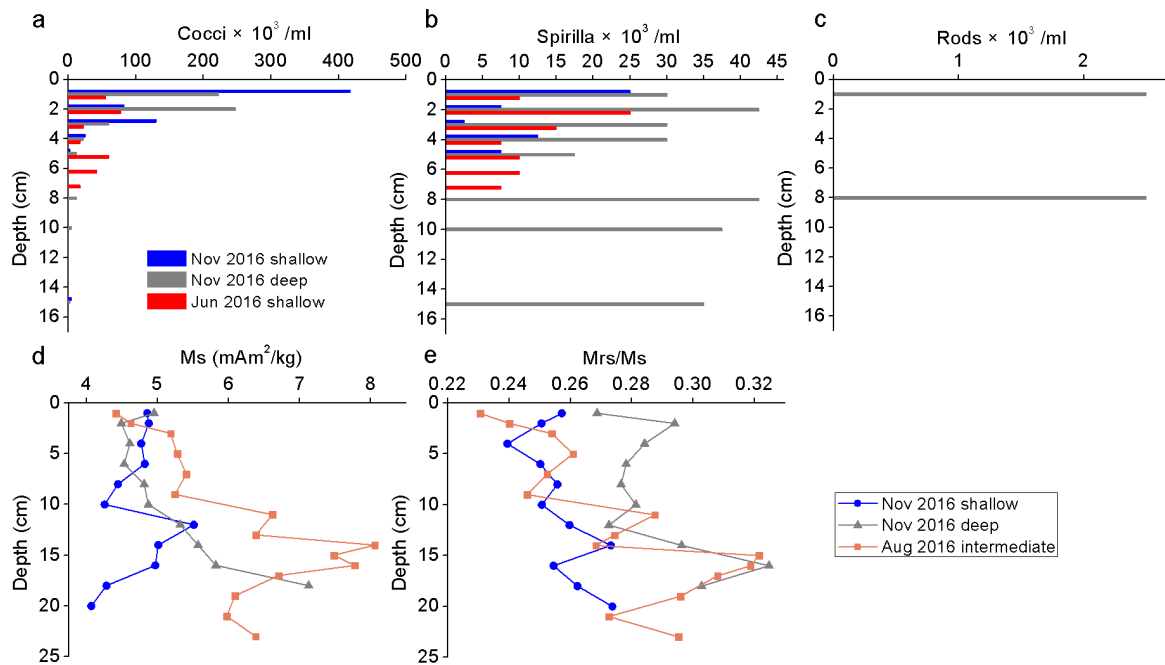


Figure 3 - 8 Vertical distribution of magnetotactic bacteria abundance and magnetic parameters. (a-c) Vertical distribution of magnetotactic bacteria abundance in three cores. 0 cm represents the water-sediment interface. Core locations shown in Figure 1b. Note that the three colored bars at the top five centimeters were measured at the same depth each centimeter—the bars are displaced for clarity. (d-e) Saturation magnetization (Ms) and the remanence ratio (Mrs/Ms) as a function of depth for three vertical profiles. Note that no MTB were counted in the core collected in August 2016 and magnetic profiles were not made on the core from June 2016. Data in Table 3-6 and 3-7.

differential depth range where the morphotypes were detected in the vertical profiles, with spirilla being skewed lower in the sediment column than cocci (Figure 3-8), consistent with the observations of *Lefèvre et al.* [2011a]. Interestingly, the anti-correlation was significant when both morphotypes correlated distinctly negative (spirilla) or positive (cocci) with O₂ (Figure 3-5). We cannot exclude that the observed changes in MTB abundances are related to the changes on the species level of cocci and spirilla/vibrios, since we can only distinguish them on the

Table 3 - 6 Vertical distribution of magnetotactic bacteria abundance

Depth cm	Cocci			Spirilla			Bavaricum		
	Nov shallow	Nov deep	June	Nov shallow	Nov deep	June	Nov shallow	Nov deep	June
	Cells/ μ l								
1	418	223	55	25	30	10	0	3	0
2	83	248	78	8	43	25	0	0	0
3	130	60	23	3	30	15	0	0	0
4	25	23	18	13	30	8	0	0	0
5	3	13	60	8	18	10	0	0	0
6	--	--	43	--	--	10	--	--	0
7	--	--	18	--	--	8	--	--	0
8	--	13	--	--	43	--	--	3	--
10	0	5	--	0	38	--	0	0	--
15	5	3	--	0	35	--	0	0	--

Table 3 - 7 Vertical distribution of magnetic parameters

Depth cm	Ms			Mrs/Ms		
	Nov 2016 shallow	Nov 2016 deep	Aug 2016	Nov 2016 shallow	Nov 2016 deep	Aug 2016
	mAm^2/kg					
1	4.85	4.95	4.41	0.26	0.27	0.23
2	4.88	4.49	4.62	0.25	0.29	0.24
3	4.77	4.61	5.18	0.24	0.28	0.25
5	4.82	4.53	5.28	0.25	0.28	0.26
7	4.44	4.81	5.41	0.26	0.28	0.25
9	4.25	4.87	5.24	0.25	0.28	0.25
11	5.51	5.32	6.62	0.26	0.27	0.29
13	5.01	5.57	6.38	0.27	0.30	0.27
14	4.97	5.82	8.06	0.25	0.32	0.27
15	4.28	7.13	7.48	0.26	0.30	0.32
16	4.07	--	7.78	0.27	--	0.32
17	--	--	6.70	--	--	0.31
19	--	--	6.09	--	--	0.30
21	--	--	5.97	--	--	0.27
23	--	--	6.38	--	--	0.30

morphotype level with the viable cell count technique [Faivre and Schüler, 2008; Lefèvre and Bazylinski, 2013]. Moreover, the three depth profiles suggest that the MTB might have, at times,

migrated vertically and escaped detection (Figure 3-8). This could eventually bear on our measurements and interpretations of the MTB abundances, as the surface samples integrated over the upper 1 cm of the sediment column.

Within the scope of the measured chemical parameters, none can singularly explain the variability in MTB population. The fact that O₂ trends in the control beaker and pond were fairly similar over the two-year period, yet the MTB trends of the two environments did not correlate, suggests that there is no universal relationship between O₂ and MTB concentrations across different ecosystems, following the conclusions of *Flies et al.* [2005] and *Jogler et al.* [2010]. *Du et al.* [2015] found that unicellular MTB abundances at two brackish water sites peaked just after the period with the highest temperatures (~23°C), similar to our findings for spirilla but opposite of cocci whose lowest abundances occurred in summer 2015 (Figure 3-2). Excessive warmth will be detrimental, as *Lin et al.* [2012a] found that temperatures of 37°C reduced cocci abundance to 1% of those living at 26°C. The more moderate temperature variations during the course of our study likely had little influence on MTB populations in the pond and were negligible in the control beaker. The C:N ratios and isotopic values indicate that the organic matter consists of a rather homogenous mixture of algal and vascular terrestrial organic matter throughout the pond [*Meyers*, 1994]. TOC and TN percentages were rather constant, which suggests nutrient type or availability did not drive the observed changes in MTB populations in the pond. The changes among the morphotype populations could therefore represent internal fluctuations driven by competition with other organisms.

The magnetic parameters Ms and Mrs/Ms of the sediments were uncorrelated with live MTB abundance, but instead varied in proportion with water depth, with deeper sites possessing ~15% higher Ms and Mrs/Ms than sites from shallower water (Figure 3-7). Live MTB abundance did not correlate with water depth, except only slightly for rods whose abundance was minimal (Figure 3-11). Because the magnetosomes of the living cells represent <1% of the total Ms, the magnetization of the sediment should reflect the cumulative magnetofossil concentration in the pond. This is in agreement with FORC diagrams that contain a central ridge characteristic of non-interacting single domain (SD) particles that account for ~50% of the magnetization [*Mao et al.*, 2014b] (Figure 3-6).

The ranges in Mrs/Ms (0.21-0.27) and Bcr/Bc (2.1-2.4) are displaced away from the wholly single domain (SD) character of pure MTB extracts with $Mrs/Ms \sim 0.5$ and $Bcr/Bc \sim 1.0-1.5$ [Lin and Pan, 2009; Moskowitz *et al.*, 1988; Pan *et al.*, 2005]. Lower values than those expected for pure-SD particle distributions can stem from dilution by non-SD detrital magnetite and/or from oxidation. Low temperature oxidation of SD magnetite lowers M_s [Readman and O'Reilly, 1972]. Although higher O_2 concentrations existed in shallower water where M_s was lower (Figure 3-7), a change in domain state is required to explain the reduction in Mrs/Ms . Reducing Mrs/Ms by low temperature oxidation of SD grains can be feasible when SD particles close to the SD-superparamagnetic (SP) limit become SP thereby lowering their spontaneous magnetizations. However, the FORC diagrams showed no signature characteristic of magnetic viscosity related to SP particles (Figure 3-6). On the other hand, sediment accumulated more rapidly during the two-year period in the shallow area, so greater dilution should be expected there, which would lower M_s . Diluting with material impoverished in SD particles would lower Mrs/Ms preferentially in the shallow sites and hence lowering Mrs/Ms can be fully explained by a mixing trend between SD magnetosomes and a non-SD (detrital) end-members.

That M_s and Mrs/Ms increase with depth in the sediment (Figure 3-8) may be attributed to an increase in magnetofossil concentration and/or to the reduction of oxidized magnetite back to stoichiometric magnetite in more reducing environments. The former agrees with the higher MTB abundances at the start of the experiment that decreased by a factor of ten within several months. Less oxidized magnetite at greater depth in the sediment is in agreement with our low temperature experiments that show a better definition of the Verwey transition with increasing depth (Figure 3-6).

Our two-year study shows that environmental factors drive MTB abundance as reflected by coherent trends throughout the pond, but neither dissolved O_2 nor temperature variations can singularly explain changes in MTB populations. Several other factors that were not measured in our study have been shown to affect MTB abundance such as sulfur, salinity and iron [Lin and Pan, 2009, 2010; Lin *et al.*, 2012b; Postec *et al.*, 2012; Sobrinho *et al.*, 2011]. However, we can conclude that MTB populations in the freshwater pond, particularly spirilla, vary with season.



Figure 3 - 9 Photos of the Niederrlippach pond during different months in 2015



Figure 3 - 10 Photos of the Niederrlippach pond during different months in 2016.

Although absolute MTB concentrations differed in space, all three morphotypes underwent similar relative changes in the time domain, hence long-term trends of MTB populations in natural ecosystems are likely indicative of the ecosystem as a whole. This is in distinct contrast to artificial habitats in the laboratory that have not reached steady-state conditions [He *et al.*, 2017]. Magnetite concentrations and relative grain sizes of the surface sediments do not reflect

trends in MTB abundance but are related to water depth, likely due to enhanced dilution of the SD magnetofossil fraction by detrital material at the shallow sites that were situated proximal to the pond's inflow.

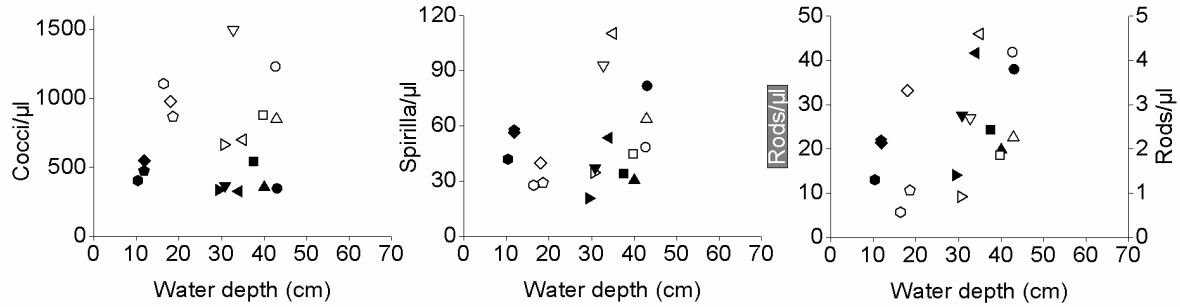


Figure 3 - 11 Monthly averaged MTB concentrations in the pond for 2015 (open symbols) and 2016 (solid symbols) as a function of water depth. Note that rods have two different scales for each year (2015 on left, 2016 on right).

Chapter 4 Perspectives

Some researchers found MMPs exhibit phototaxis. Thus it would be interesting to see whether unicellular MTB are also light-sensitive. In the future, I also want to measure MTB abundances in a sediment profiles over different seasons. For instance, the redox level may change in different seasons. Therefore, it is interesting to investigate whether MTB abundance also changed in vertical direction in different seasons. Through observing the variation of MTB abundance in vertical profiles, we will learn more about the preferred habitat of different species of MTB in sediment.

Magnetofossils were detected in Oligocene-Miocene marine sediments [*Channell et al.*, 2013]. However, there is no report on magnetofossils in Oligocene-Miocene continental sediments. In central western part of China, there is abundant red clay, from which the heavy minerals can be extracted in search of magnetofossils using a high-resolution transmission electronic microscope.

I would also like to investigate the relationship between MTB abundance and the grain size, and to know whether the abundance of MTB was affected by variation of pH, NH_4^+ and SO_4^{2-} .

Magnetotactic bacteria can form magnetosomes which can be preserved in sediment over geological times, which gives rise to the term “magnetofossils”. In warmer periods, more magnetofossils were detected [*Hesse*, 1994]. Therefore, they can be seen as a potential proxy for reconstructing paleoclimatic change. However, the preservation environment of magnetofossils also has an effect on their abundance [*Suk*, 2016]. *Mandernack et al.* [1999] found that oxygen-18 isotope values of magnetite produced by cultured MTB can be useful in paleoenvironmental studies. However, there are very few studies about reconstructing paleotemperature using oxygen isotope analysis from magnetofossils [*Schumann et al.*, 2008]. During the Cenozoic era, there are several warm periods such as the Paleocene Eocene Thermal Maximum (PETM) and the Middle Miocene Climatic Optimum (MMCO) and relative colder period like Middle Miocene Climate Transition (MMCT) [*Zachos et al.*, 2008]. I plan to enrich and purify as many magnetofossils as I can from the IODP cores with known age, and these magnetofossils will be used for oxygen isotope analysis using Nanosecondary Ion Mass Spectrometry (NanoSIMS). I hope I can rebuild the water temperature of above-mentioned periods when MTB lived. After that, a comparison will be made with other temperature proxies

such as the TEX-86 organic biomarker [Zachos *et al.*, 2006]. In addition, I will try to find whether different morphologies of magnetosomes produced by different species of MTB have different oxygen isotope values under the same cultured temperature. On the other hand, we can take sediment samples in winter or in summer from lakes and measure the oxygen isotopes of the magnetosomes to see whether the oxygen isotope values are different in different seasons.

Magnetofossils can be seen as a paleoxygen indicator [Chang and Kirschvink, 1984]. Hesse [1994] and Yamazaki [2012] found more isotropic magnetofossils dominated in relative oxidized conditions, whereas more anisotropic magnetofossils predominated in more reduced conditions. However, Lean and McCave [1998] observed an increase in the proportion of equidimensional magnetofossils during glacial stages. Therefore, it is important to know which factors cause the different proportion of magnetofossils in sediment.

According to my previous research in Munich, I have found that different morphotypes of MTB have different variation trends in both controlled environments and a natural environment over time. However, I did not examine the relationship between MTB morphotypes with their magnetosomes. In the future, I would like to see whether the proportion of different morphotypes of magnetosomes varies with environmental factors such as temperature, oxygen concentration, nitrate, sulfur, pH, and so on. I would take sediment samples from a pond that contains a high MTB population density and transfer them into aquaria. Different kinds of microsensors will be used to monitor chemical condition of the sediments in the aquaria. Meanwhile, I would quantify the abundance of MTB using qPCR analysis [Simmons *et al.*, 2007]. High-resolution transmission electron microscope (HRTEM) will be used to detect the morphology of magnetosomes produced by different species of MTB.

Chapter 5 The relationship between magnetic field strength and remanence anisotropy through redeposition experiments

Abstract

Redeposition experiments were performed over a range of magnetic field intensities and inclinations using magnetite-bearing, natural sediments. Paleointensity values defined by NRM over SIRM, ARM or susceptibility systematically increase with applied magnetic field, yet relative paleointensities from 25 repeat redeposition experiments performed at identical field conditions vary by a factor of two. The question arises as to what accounts for the variability and what can we do to diminish/remove the variability to improve the precision of relative paleointensity estimates? Recalling that M_s lies in the long axis direction of a magnetite grain, then the maximum axis of the magnetic anisotropy ellipsoid should parallel the paleomagnetic direction if the magnetization reflects a true depositional remanence acquired via torque. As higher external fields increase NRM by tightening the alignment of the grains, magnetic anisotropy should become increasingly prolate proportional to field strength. This effect is indeed demonstrated in our new experiments using anisotropy of anhysteretic remanent magnetization (AARM): nearly all AARM indices vary in proportion with magnetic field strength. Conversely, anisotropy of magnetic susceptibility does not, as it is overwhelmed by the paramagnetic fraction that shows a sedimentary fabric. AARM thus holds promise to improve relative paleointensity estimates from sediments.

5.1 Introduction

The geomagnetic field can be approximated as a dipole. During geological time, the geomagnetic field direction underwent reversals. When the geomagnetic field starts to reverse, the paleointensity becomes weaker. Therefore, paleointensity research is better for us to understand the mechanism of geodynamo. Since magnetostratigraphy can be seen as a chronology tool to date sediment effectively, researchers also try to build a chronology tool based on the variation of paleointensity if geomagnetic field can be approximated seen as a magnetic dipole. Volcanic

rocks and fired archeological materials are ideal materials to reconstruct absolute paleointensity. However, the distribution of volcanic and archeological materials are not continuous compared to sediments. Sediment, especially marine sediment can be preserved continuously in a long geological history. They contain abundant paleoclimatic and paleomagnetic information. Researchers have done a series of redeposition experiment in laboratory to explore whether sediment can be a potential material to rebuild paleointensity [*Kent and Opdyke, 1977; King et al., 1983; Levi and Banerjee, 1976; Tauxe, 1993; Tauxe and Wu, 1990*]. *Johnson et al.* [1948] firstly found the relationship between magnetization and external field was linear. *Jackson et al.* [1991] found that inclination error of detrital remanent magnetization (DRM) can be corrected by anhysteretic remanent magnetization (ARM) anisotropy using synthetic sediments (silica, kaolin, and sized magnetite powders). *Tauxe et al.* [2006] found that the salinity and floc size have an effect on the paleointensity through the redeposition experiment using clay from the Siwaliks. *Jezeck and Gilder* [2006] made a viscous model trying to understand better how the sediments obtain their remanent magnetizations. They described that how the ellipsoidal magnetic particles rotated in the viscous fluid with hydrodynamic and magnetic forces. *Tauxe et al.* [2006] summarized that relative paleointensity based on sediment can be affected by many factors such as grain size, magnetic particles concentration, pH, salinity, flocs size and magnetic types.

Single domain magnetite produced by magnetotactic bacteria, is well situated to record the magnetic field. *Paterson et al.* [2013] used cultured *Magnetospirillum magneticum* strain AMB-1 to do a series of deposition experiment at different field strength and direction. They found that the NRM magnetosome recorded was aligned with magnetic field during the range of 0-120 μT . When they increased the concentration of MTB, NRM can be obtained by correct factor, whereas ARM and saturation isothermal remanent magnetization (SIRM) did not respond to as expected for the interaction caused by high concentration of MTB. *Ouyang et al.* [2014] and *Chen et al.* [2017] found that nanoparticle inclusions and biogenic magnetite have different ability to record the geomagnetic field. They found that biogenic magnetite has 2-4 times higher efficiency on recording geomagnetic field than detrital magnetite.

Since the first anisotropy of magnetic susceptibility (AMS) measurement has been done in 1954, AMS has been seen as a rapid, effective and simple technique to identify the magnetic fabric of

samples. The anisotropy of magnetic susceptibility is the tensor that relates the intensity of external field (H) to the acquired magnetization (M) of a material. The AMS of a crystal is the resultant of mineralogical composition, grain shape [Uyeda *et al*, 1963] and preferred orientation. However, AMS mostly reflects the superparamagnetic (SP) and coarse grain, multidomain sized magnetic particles. Afterwards, anisotropy of magnetic remanence (AMR) is being used, particularly in paleomagnetic studies of anisotropic rocks to compare the ancient field vector and accurate determinations of paleointensity. Anisotropy of anhysteretic remanent magnetization (AARM) reflects the ferromagnetic particles. Moreover, Jackson [1991] found that pARM can distinguish the different grain size of ferromagnetic particles. For instance, 10 mT window of pARM mainly reflect the coarse size of ferromagnetic particles whereas 50 mT window of pARM mostly reflect the fine size of ferromagnetic particles. The results from AMS and AARM can be combined together to obtain effectively subfabrics [Hrouda, 2002].

Although many researches have focused on inclination shallowing from the sediment, very few researchers tried to find whether there are some parameters to decrease the scatter of reconstructed paleointensity. So far, there are no researches about the relationship between anisotropy of ARM and field strength. Can AARM be seen as a potential parameter to decrease the scatter degree of paleointensity? Therefore, in our study, we used magnetosome-rich sediment for redeposition experiments in known field direction and strength to find the ability for recording external field and try to find the relationship between magnetic fabric and external field strength.

5.2 Methods

5.2.1 Sample preparation

The samples were taken in July 2014 at the pond near Niederlippach, 80 km northeast of Munich. The magnetosome-rich sediment was transferred into two similar aquaria (A and B). These two aquaria were stored at 20-25°C during the experimental period.

The redeposition experiments were conducted in a magnetically controlled space consisting of a two-dimensional array of home-made Helmholtz coils which were placed in magnetic north-south direction (See Figure 5-1). Helmholtz coils produced the magnetic field through

adjusting the current of coils. The field strength used in the experiments was 1 μT , 10 μT , 50 μT , 100 μT and 150 μT . The declination and inclination at each kind of field are both 0° . In addition, for 50 μT , 100 μT and 150 μT external fields, we also set up each field through adjusting current with declination and inclination as 180° and 60° , respectively. We put 25 pilot plastic paleomagnetic cups at the centre of the Helmholtz coils (See Figure 5-1a, b). We made all the arrows which were marked at the bottom of the paleomagnetic cups directing to north direction. To obtain stronger external magnetic field strength, we made a permanent magnet that produces a 300 mT field at its centre. We put the magnet on a table, ensuring that the field direction is the same with the arrow marked at the bottom of the cup. 8 paleomagnetic cups were placed at 2 layers in the centre of the magnetic ring. All these cups were filled with slurry by pipette every two days. After the slurry layer was nearly dry, new slurry was added until the cups were completely filled. Each round of experiment took about 40 days to finish filling the cup with sediment. After the whole sediment in the cups was dry, we added the lids to these 25 or 8 cups, and placed them on the sushibar to do next step of experiment [Wack, 2012]. To get different

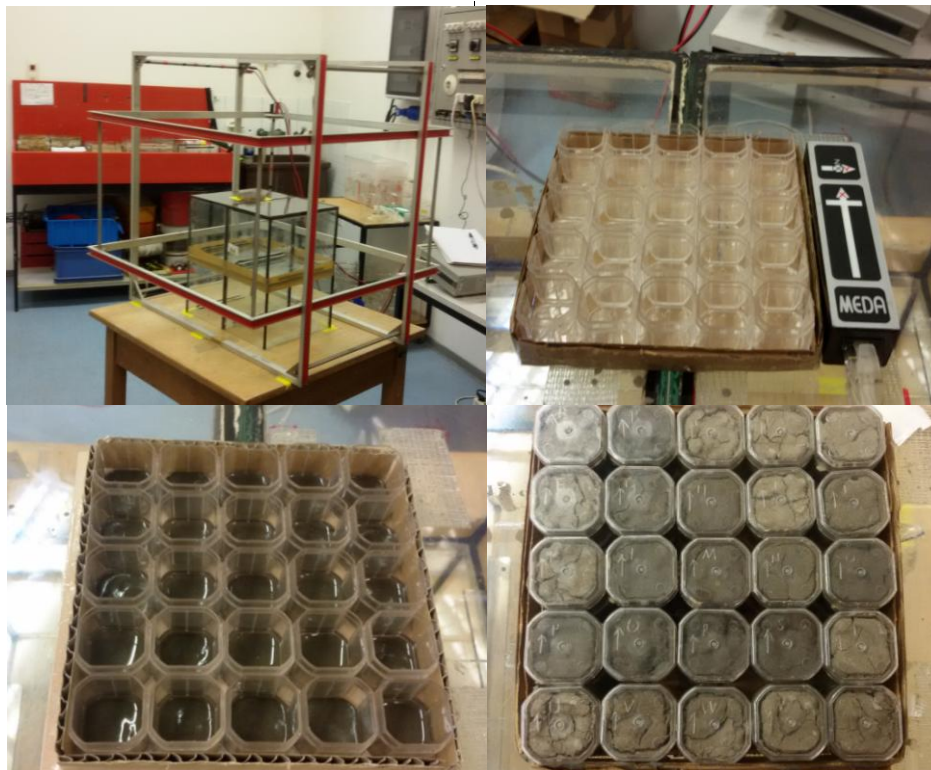


Figure 5 - 1 Redeposition experiment. (a) The set up of redeposition experiment. (b) The magnetic field produced by Helmholtz coils was measured using fluxgator. (c) The slurry was put into 25 plastic boxes. (d) The filled air-dry samples were prepared to receive the measurement on sushibar

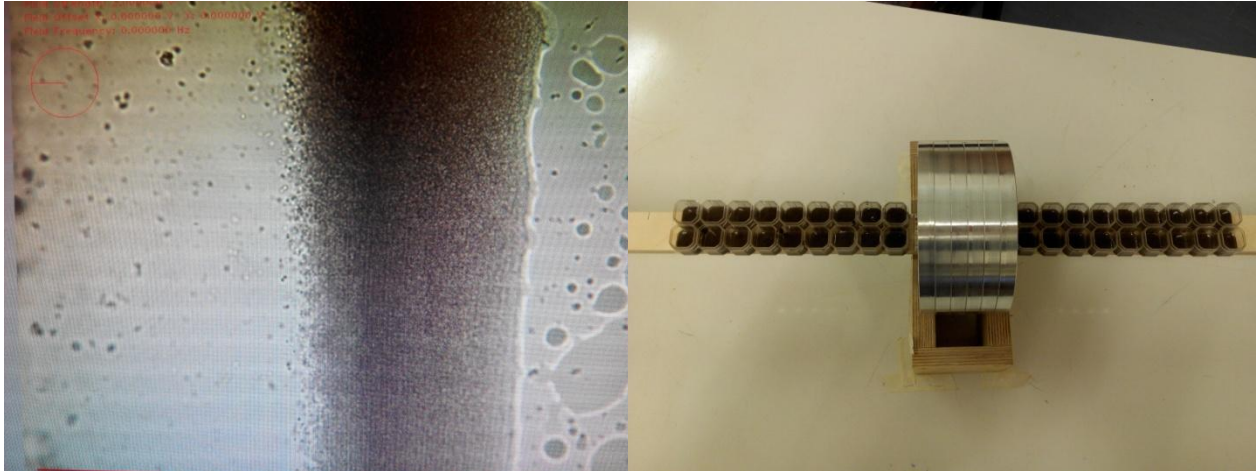


Figure 5 - 2 The enrichment of MTB and set up of redeposition experiment produced by magnet. (a) The enrichment of MTB-cocci at the edge of water drop. (b) 36 samples were placed on the wood board which going through the strong magnetic ring.

field strength between $150 \mu\text{T}$ and 300 mT , we put a magnetic ring on a wood holder to make sure the inside field direction was parallel to geomagnetic field. We made a wood board going through the centre of the standing ring in horizontal direction, and make sure the wood board was horizontal and fixed. The magnetic field produced by the big magnetic ring has been measured at every 1 cm space by LakeShore probe in x, y and z axes following to a Cartesian coordinate system in three height level (0 cm, 1 cm and 2 cm) (See figure 5-3) on the wood board. Then, we used these original data to draw the spatial distribution of magnetic field produced by the magnetic ring with Golden Software Surfer 12. 18 cylinder plastic paleomagnetic cups were placed at each side of magnetic ring on the board, respectively (See figure 5-2b). The average field strength and directions (declination and inclination) responding to each sample were calculated, respectively. The field strength decreased as the distance between samples and magnetic ring became larger. Finally, the range of field strength is from $\sim 71.1 \text{ mT}$ to 0.3 mT . The range of average declination and inclination at each site are $-33\text{-}41^\circ$ and $60\text{-}70^\circ$, respectively. For every round experiment, these cups were filled with sediment which was rich in magnetotactic bacteria and magnetofossils every 2 days. Each experiment lasted about 40 days.

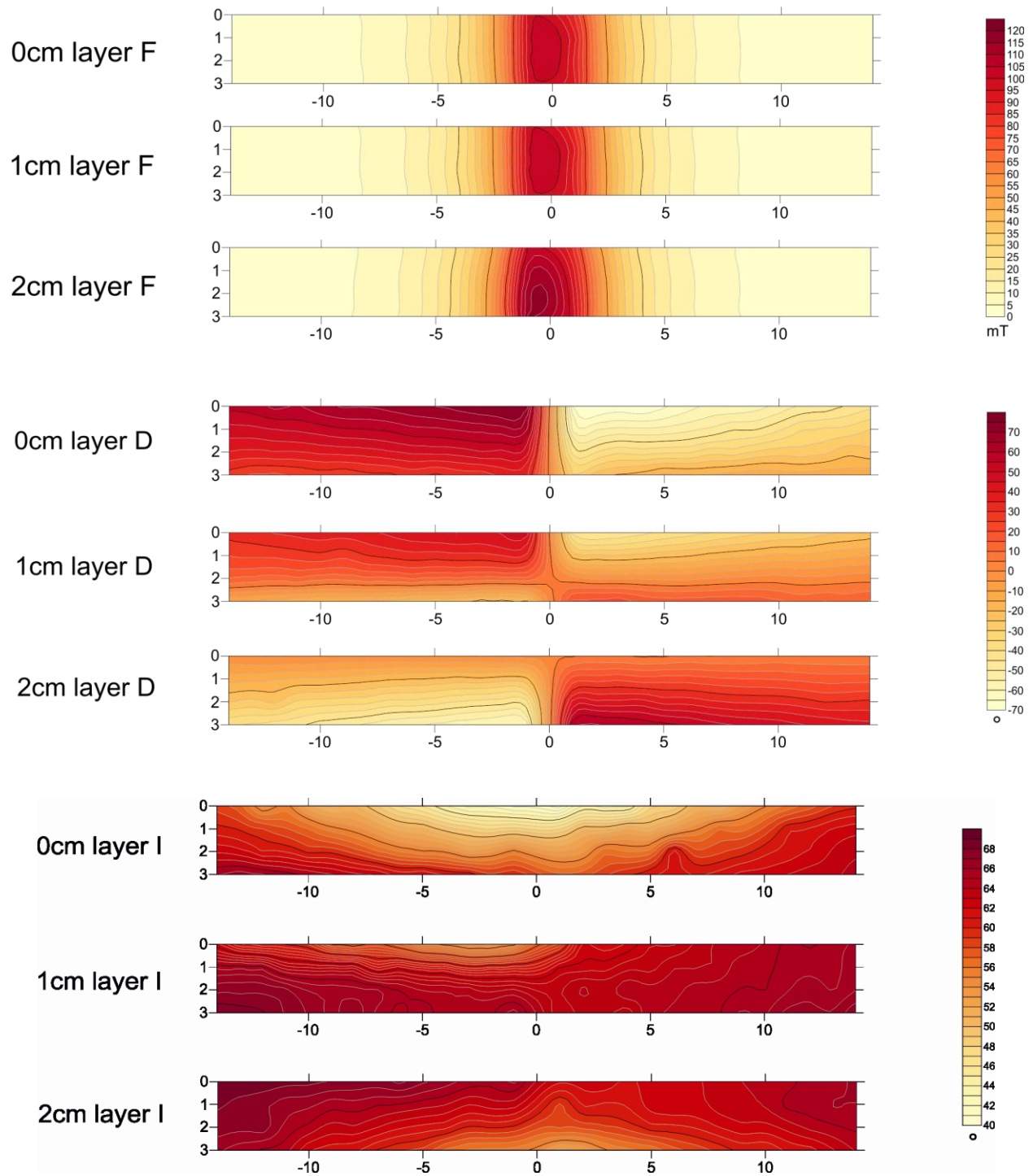


Figure 5 - 3 The spatial distribution of external field strength and directions on the wood board

5.2.2 Magnetic measurements

After these samples were air-dried, these samples were placed on a vertical 2G cryogenic magnetometer with an automated system for paleomagnetic investigations (sushibar) to measure natural remanent magnetization (NRM) and alternating-field (AF) demagnetized at 2, 4, 7, 11, 16, 20, 30, 40, 55, 70 and 90 mT, respectively [Wack, 2012]. The goal of AF demagnetization is to find the magnetization direction these magnetosome-rich sediments recorded under the external magnetic field. AF demagnetization was conducted using a 3-axis tumbler system with a peak alternating field of 90 mT. Then, the samples were given a partial ARM (pARM) in a DC field of 100 μ T with an AF field window between 30 and 70 mT. We gave each sample pARM at 12 directions. After the sample was given a pARM at one direction, we AF demagnetized the sample at this direction and gave a pARM at next direction. Therefore, anisotropy of anhysteretic remanent magnetization (AARM) were obtained through measuring pARM at 12, 1, 2, 3, 4, 5, 6, 7, 8, 9, 10, 11 and 12 directions, respectively. The tensor of AARM was calculated. After that, these samples were given an isothermal remanent magnetization (IRM) using electromagnet (See figure 5-4a). Afterwards, we measured the IRM values of these samples using AGICO-JR 6A spinner magnetometer. For partial samples, we also gave them -300 mT magnetization before giving them SIRM. Finally, all these samples were measured weight and low frequency magnetic susceptibility with scale and Bartington MS2 magnetometer, respectively. To identify whether these samples were affected by interaction, we chose part of these samples to be measured ARM acquisition with bias DC field of 10 μ T, 50 μ T, 100 μ T and 150 μ T, respectively. The maximum AF field is 90 mT. After each round, we cleared the paleomagnetic cups and AF demagnetized them in three directions using the AF demagnetizer.

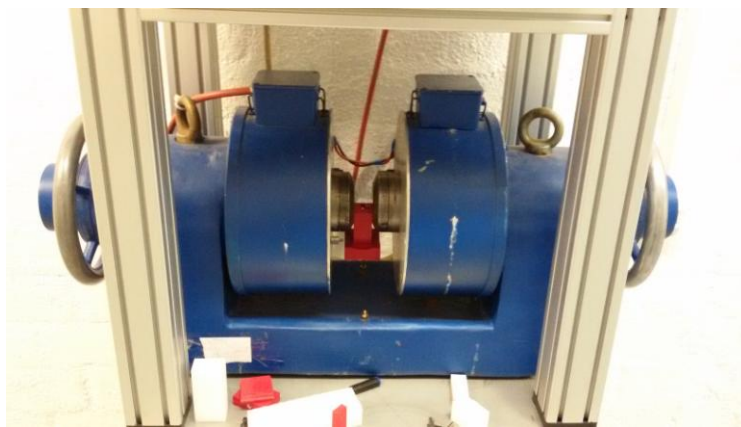


Figure 5 - 4 The electromagnet

Some samples were measured for AMS using a MFK FA Kappabridge at the University of Tuebingen. Anisotropy of a sample was determined by measurement of susceptibility along about 200 directions so that the susceptibility ellipsoid can be calculated.

5.3 Results and Discussion

Figure 5-2 shows many MTB at the edge of a water drop. This means that there are large amounts of live MTB in our sediment. We also demonstrate there are enough magnetofossils in the sediment through biplots of $\chi_{\text{ARM}}/\text{SIRM}$ vs. χ_{ARM}/χ (Figure 5-5). It shows that our data are in the limited area where the ratios of lake sediments with inferred magnetosomes were in [Kodama *et al.*, 2013; Snowball *et al.*, 2002]. S ratio, which is defined as $\text{IRM-300 mT}/\text{IRM 800 mT}$, the value are more than 0.9, which means the magnetization carrier are mostly soft coercive component (magnetite).

All average of AF demagnetization curves of each round of experiment are shown in Figure 5-6. We found the sediments under inclination of 60° have higher coercivity than those samples under 0° inclination. The reason may be that all the samples with inclination of 60° were collected from one aquarium and those samples with inclination of 0° were from another aquarium. Although these two aquaria were taken from the same pond, however, their sampling positions were different: one is close to the input of the pond, and another one was near center of the pond. That may cause the different grain size of magnetic minerals in sediment.

The magnetic behaviour of typical samples during AF demagnetization were plotted on Zijderveld diagram (See Figure 5-7). The Zijderveld and stereogram plots were produced by PMGSC 4.2 software [Enkin, 2004]. 25 pilot samples show the consistent demagnetization behaviour at each round of redeposition experiment. Zijderveld plots show that the direction of demagnetization was not stable for those samples under $1 \mu\text{T}$. However, for other samples in stronger external field, the demagnetization direction is going to the origin. Similarly, from the stereogram plots, both the points from NRM and 30 mT steps were more scattered for $1 \mu\text{T}$ samples. These stereogram figures show that sediments can record the declination and inclination of external field very well. We take all NRM and 30 mT steps and put them into the stereonet, respectively. A characteristic remanence (ChRM) was isolated by 30 mT. The average remanent declination and inclination after 30 mT AF demagnetization are close to the external

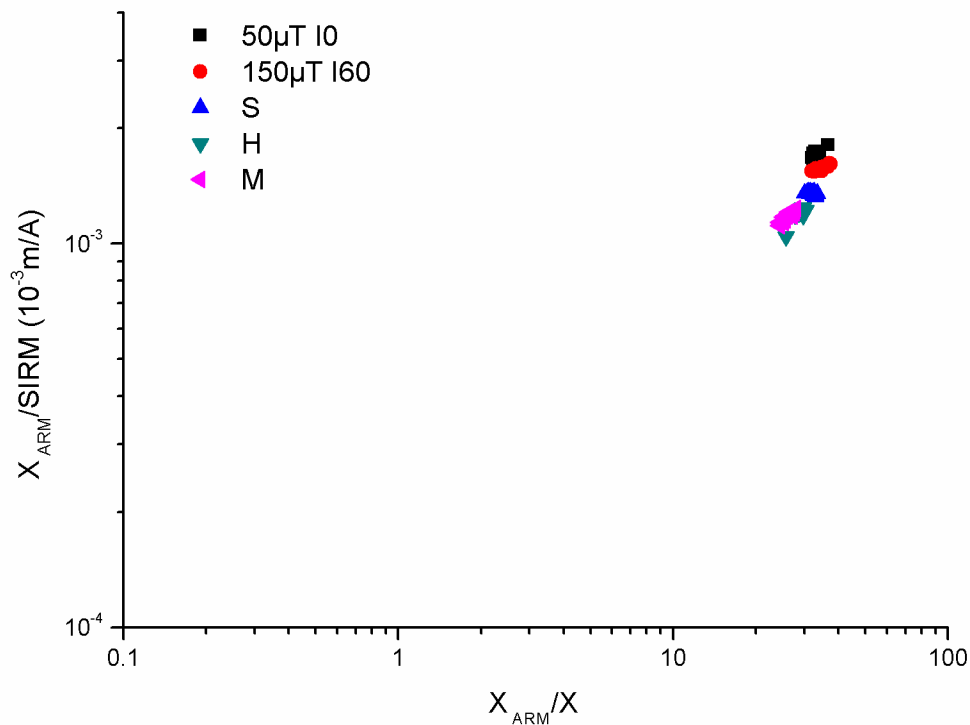


Figure 5 - 5 Biplots of $\chi_{ARM}/SIRM$ vs. χ_{ARM}/χ

field direction. For inclination, there are a little ($\sim 3^\circ$) inclination shallowing. The reason may be from the compaction [Anson and Kodama, 1987; Blow and Hamilton, 1978], coagulation effects [Lu et al., 1990], electrostatic effects [Shcherbakov and Shcherbakova, 1987] and surface tension phenomena [Nöel, 1980]. For the strong magnetic field, the sediment can also record the field direction (Figure 5-8).

It was found that the remanent magnetization first decreased but then increased after demagnetization in successively higher fields (40 mT steps) for redeposition samples at 1 μ T.

We found that there is some gap between SIRM and χ . The reason may be that the humidity degree of sample is different. Wet samples have lower χ , because water is diamagnetic material. Another reason may be from the grain size changed among different round of experiment. When the value was higher, that means small particles are more abundant. It shows that the sediment was more or less similar from the same environment. It reflects the relative uniform of source of sediments during different round of experiment.

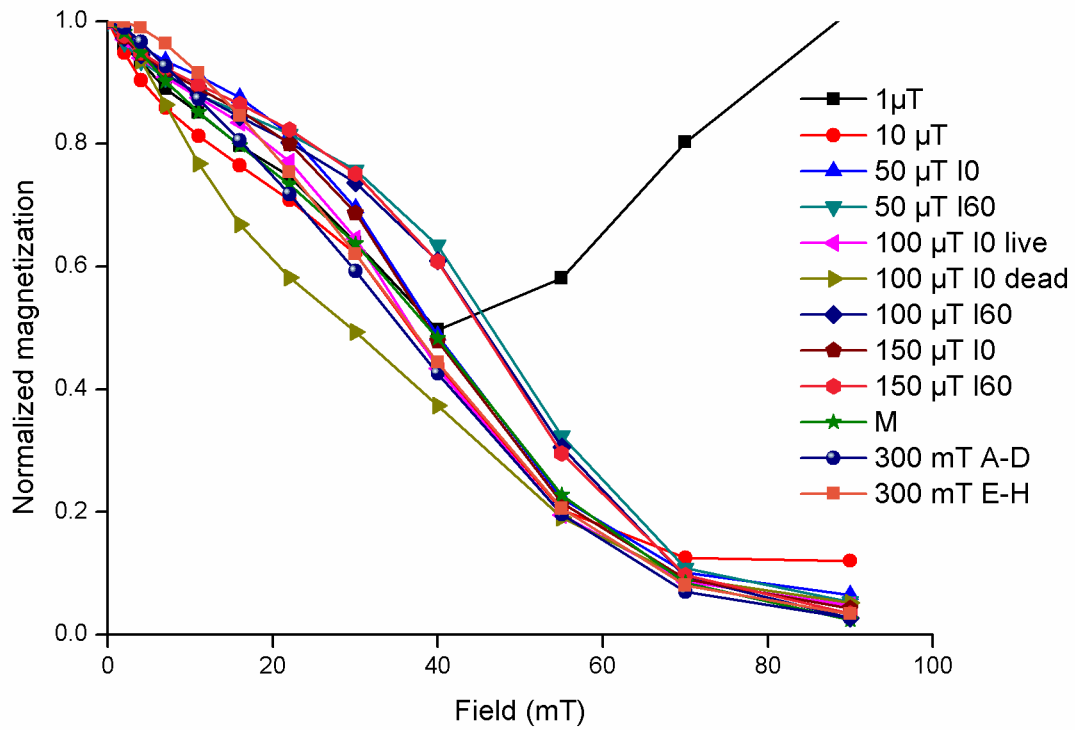
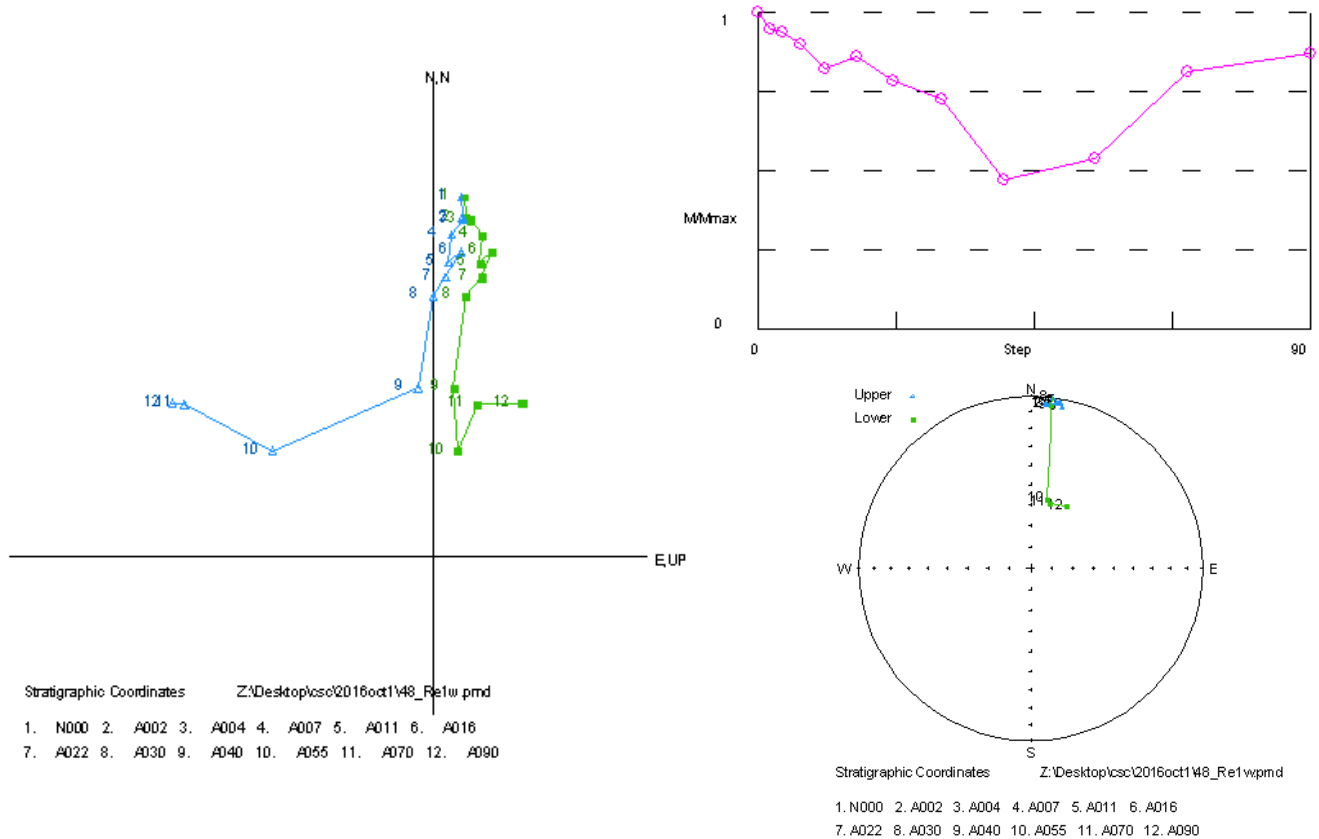
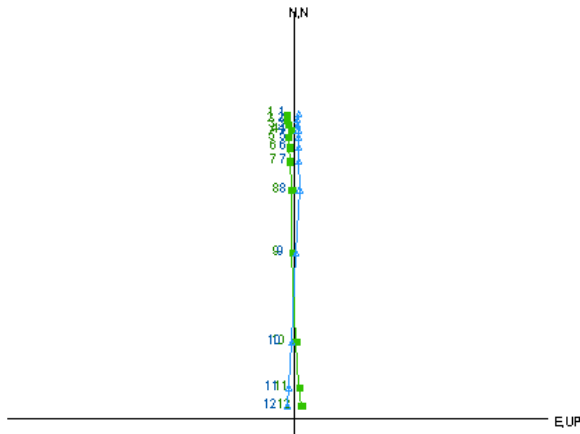
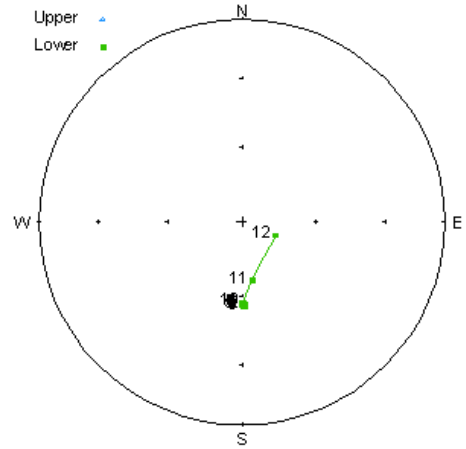


Figure 5 - 6 The average normalized AF demagnetization curves of NRM at different external field strength

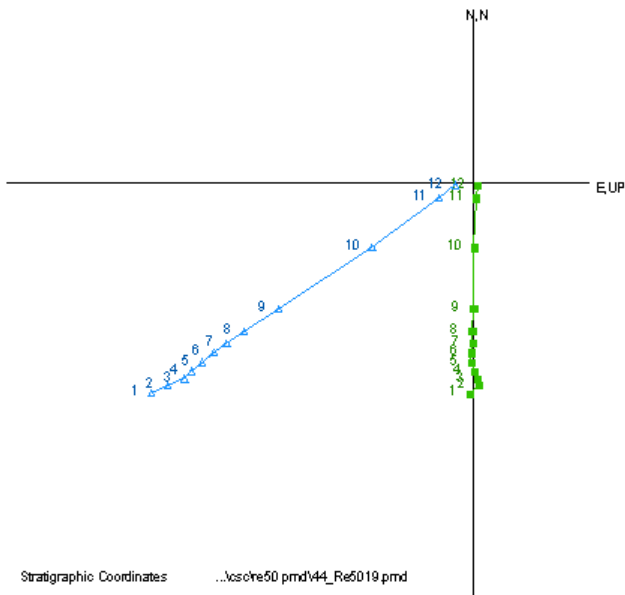




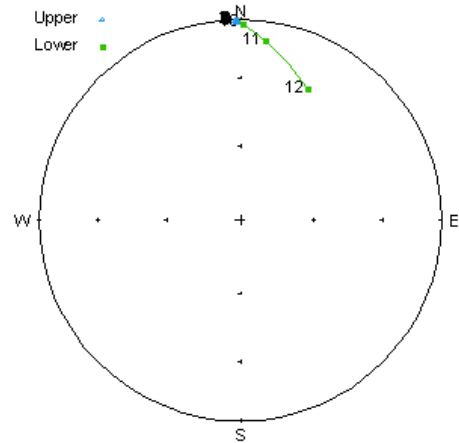
Stratigraphic Coordinates ...lcscre50 pmd\12_Re501.pmd
 1. N000 2. A002 3. A004 4. A007 5. A011 6. A016
 7. A022 8. A030 9. A040 10. A055 11. A070 12. A090



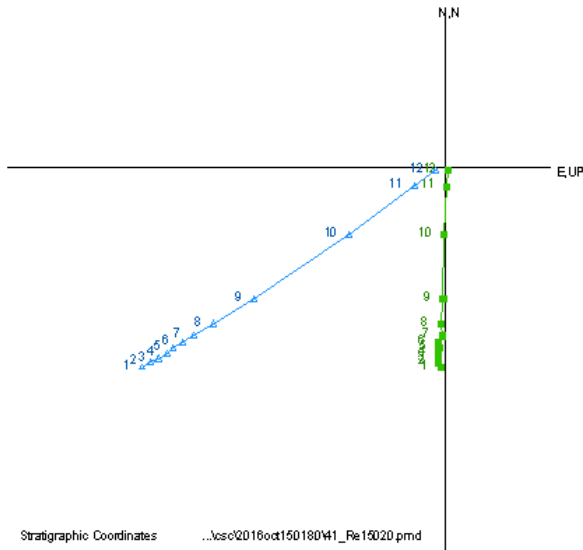
Stratigraphic Coordinates ...lcscre50 pmd\44_Re5019.pmd
 1. N000 2. A002 3. A004 4. A007 5. A011 6. A016
 7. A022 8. A030 9. A040 10. A055 11. A070 12. A090



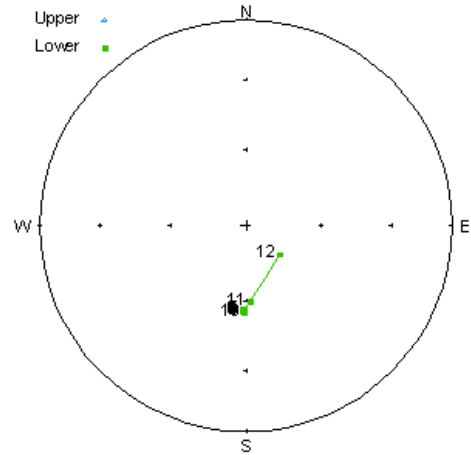
Stratigraphic Coordinates ...lcscre50 pmd\44_Re5019.pmd
 1. N000 2. A002 3. A004 4. A007 5. A011 6. A016
 7. A022 8. A030 9. A040 10. A055 11. A070 12. A090



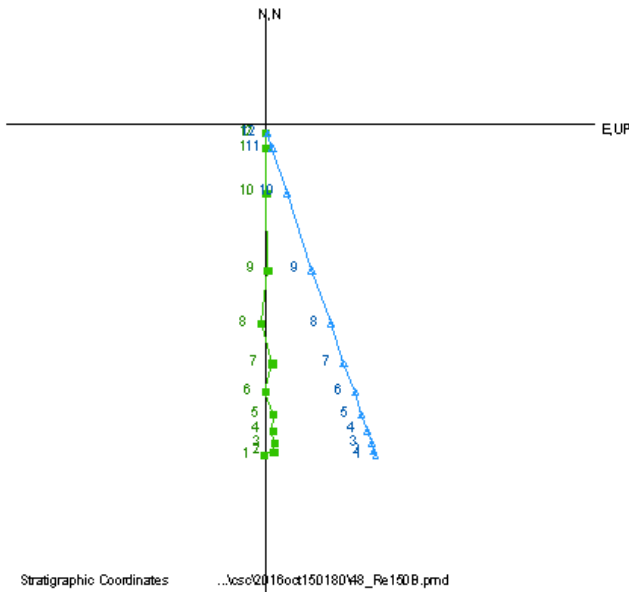
Stratigraphic Coordinates ...lcscre50 pmd\12_Re501.pmd
 1. N000 2. A002 3. A004 4. A007 5. A011 6. A016
 7. A022 8. A030 9. A040 10. A055 11. A070 12. A090



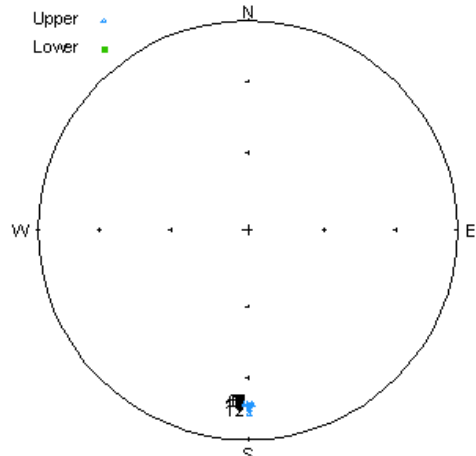
1. N000
2. A002
3. A004
4. A007
5. A011
6. A016
7. A022
8. A030
9. A040
10. A055
11. A070
12. A090



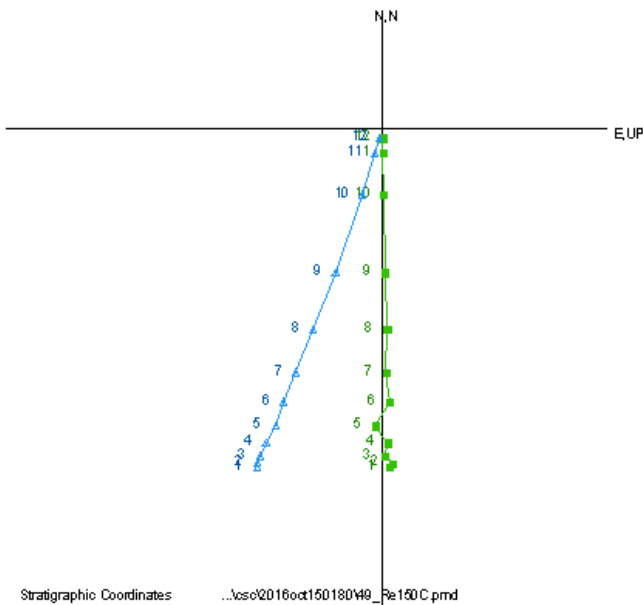
1. N000
2. A002
3. A004
4. A007
5. A011
6. A016
7. A022
8. A030
9. A040
10. A055
11. A070
12. A090



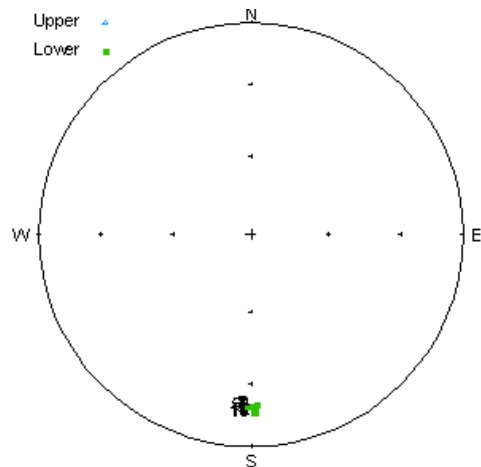
1. N000
2. A002
3. A004
4. A007
5. A011
6. A016
7. A022
8. A030
9. A040
10. A055
11. A070
12. A090



1. N000
2. A002
3. A004
4. A007
5. A011
6. A016
7. A022
8. A030
9. A040
10. A055
11. A070
12. A090



1. N000
2. A002
3. A004
4. A007
5. A011
6. A016
7. A022
8. A030
9. A040
10. A055
11. A070
12. A090



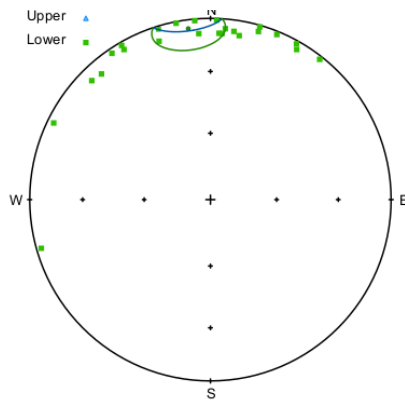
1. N000
2. A002
3. A004
4. A007
5. A011
6. A016
7. A022
8. A030
9. A040
10. A055
11. A070
12. A090

Figure 5 - 7 Alternating-field demagnetization of the NRM of one sample at different field strength

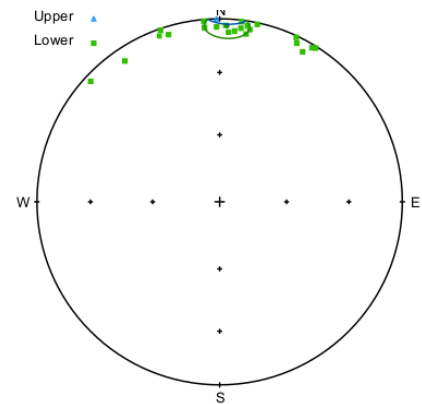
1 μT

Declination: 0°

Inclination: 0°



NRM

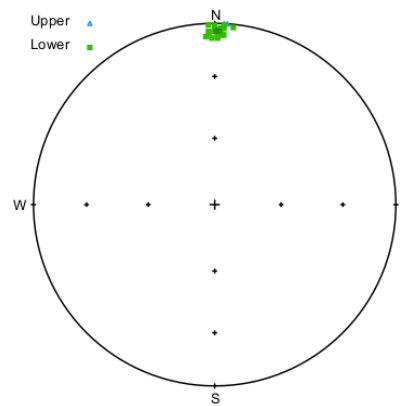


AF30 mT

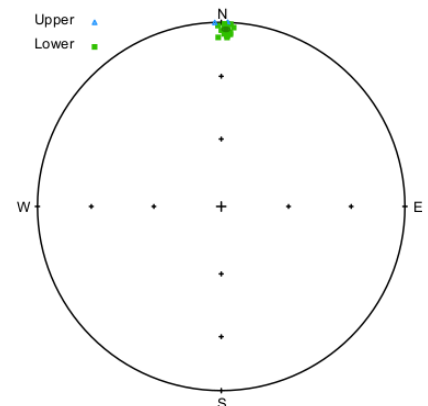
50 μT

Declination: 0°

Inclination: 0°



NRM

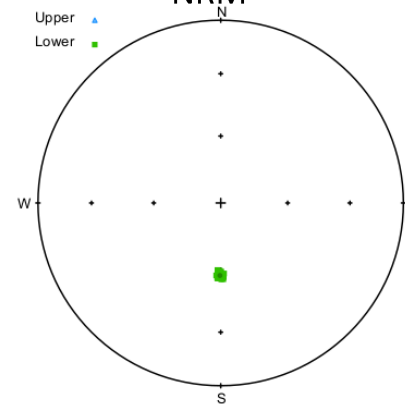


AF30 mT

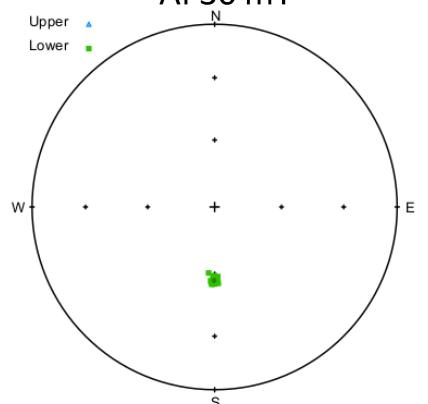
50 μT

Declination: 180°

Inclination: 60°



NRM

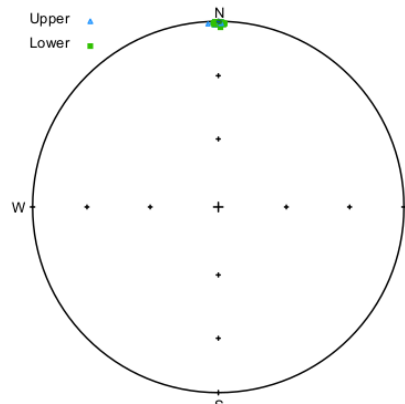


AF30 mT

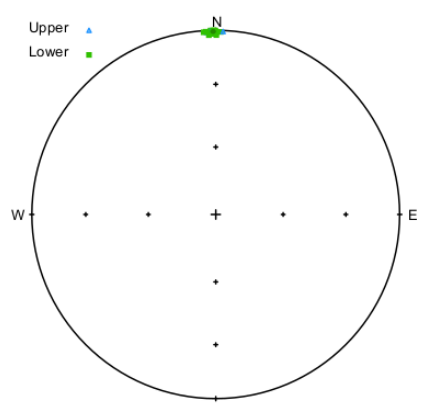
100 μT

Declination: 0°

Inclination: 0°



NRM

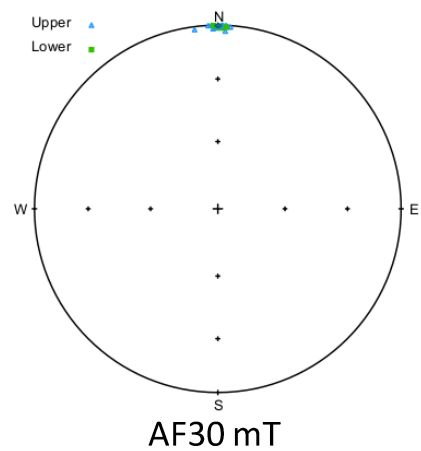
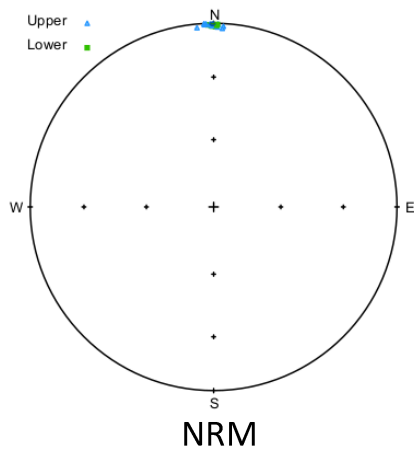


AF30 mT

150 μ T

Declination: 0°

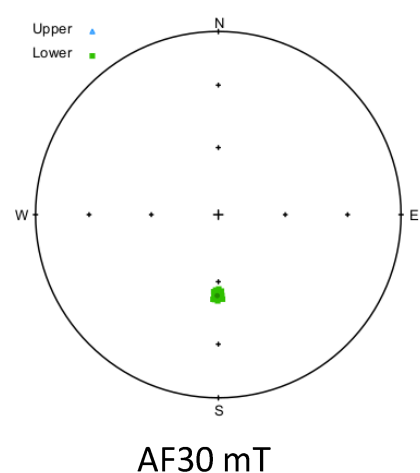
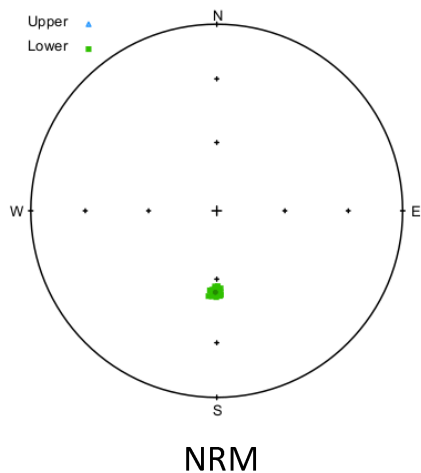
Inclination: 0°



150 μ T

Declination: 180°

Inclination: 60°



300 mT

Declination: 180°

Inclination: $\pm 20^\circ$

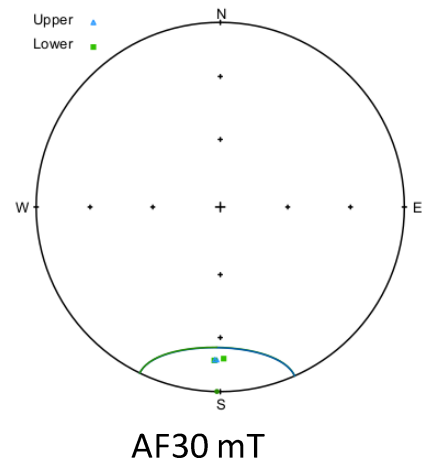
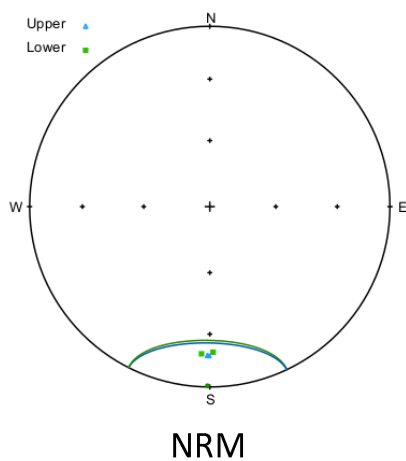


Figure 5 - 8 Stereonet plots for NRM and AF 30 mT

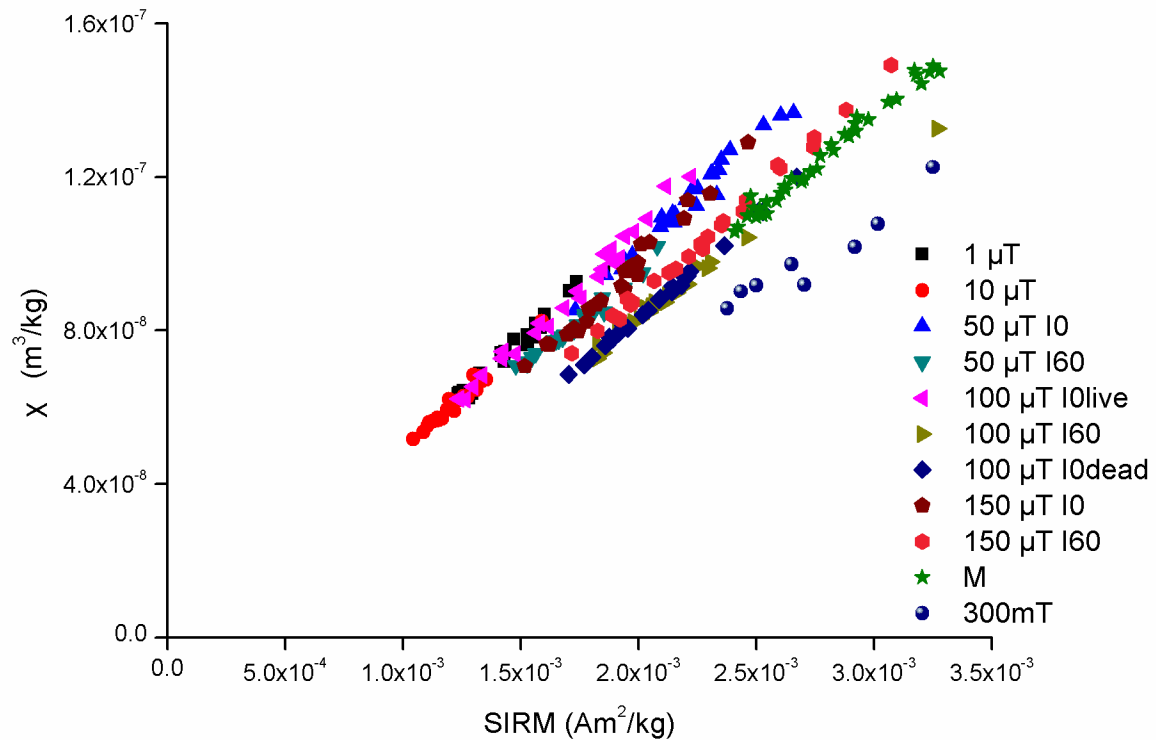


Figure 5 - 9 Plot of SIRM versus χ for samples

No previous research has done so many pilot redeposition experiments under one external field. *King et al.* [1983] concluded that uniformity of the DRM/ARM ratio is that the difference between maximum and minimum magnetite concentration should not exceed the by more than 20-30 times. In all of our samples, the maximum value of SIRM is $3.28 \times 10^{-3} \text{ Am}^2/\text{kg}$, the minimum value of SIRM is $1.04 \times 10^{-3} \text{ Am}^2/\text{kg}$, which means the difference is only about 3 times. Therefore, the samples in our experiment can be seen as uniform.

NRM can be affected by the concentration of magnetic minerals. SIRM, χ and ARM are the parameters reflecting the concentration of magnetic minerals. NRM/SIRM, NRM/ χ and NRM/ARM are the parameters which can rebuild the relative paleointensity. We found that the values of NRM/ χ , NRM/ARM and NRM/SIRM scattered under the same field strength from 1 to 150 μT (Figure 5-10 and 5-12). The range of NRM/pARM was from 0 to 0.5 and the range of NRM/SIRM was from 0 to 0.03. Because the AF window of pARM is from 30 to 70 mT, therefore, it mainly reflects the character of SD particles. We assume that the long axis of

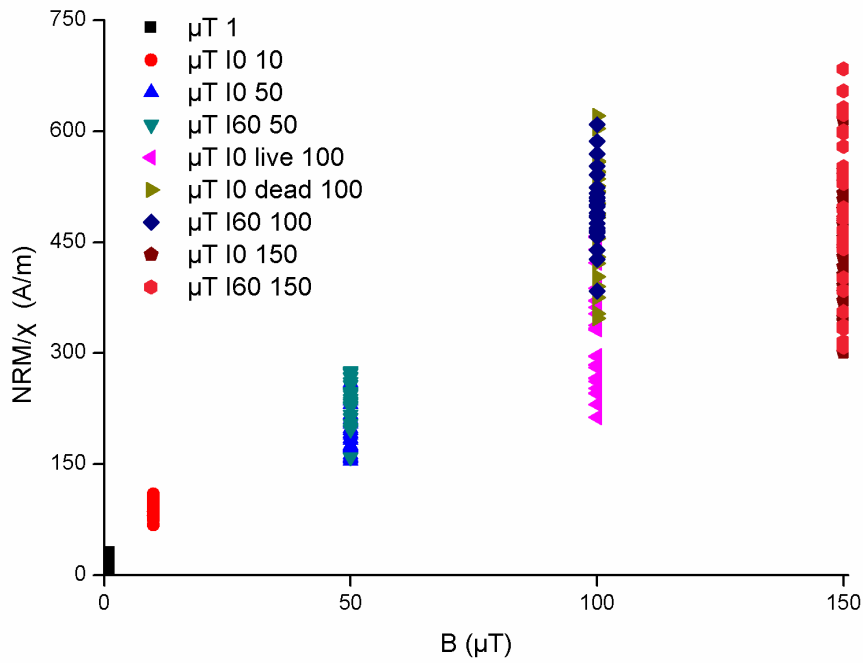


Figure 5 - 10 The relationship between NRM/χ and B

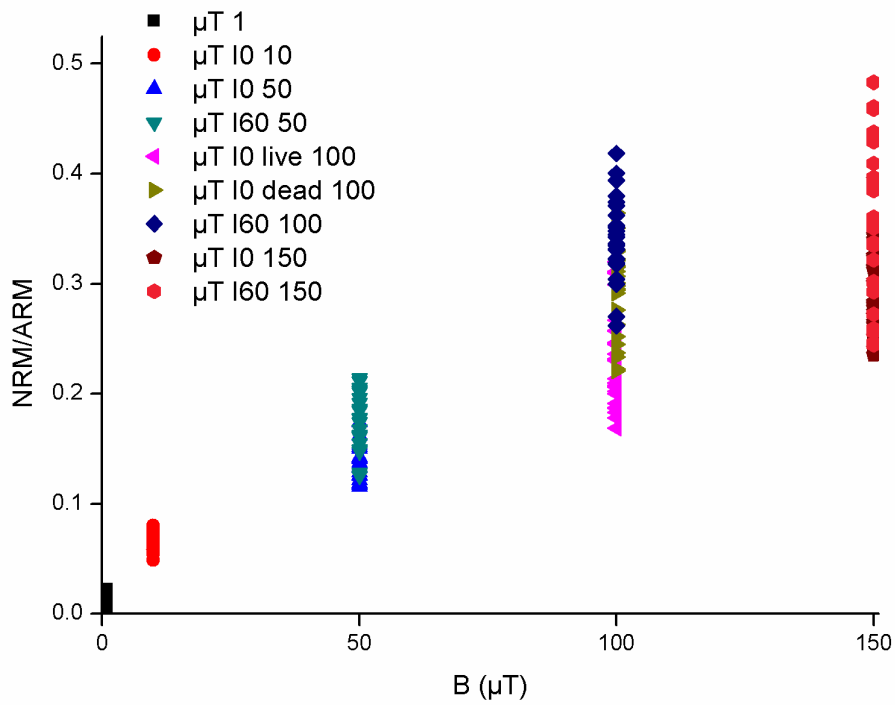


Figure 5 - 11 The relationship between NRM/ARM and B

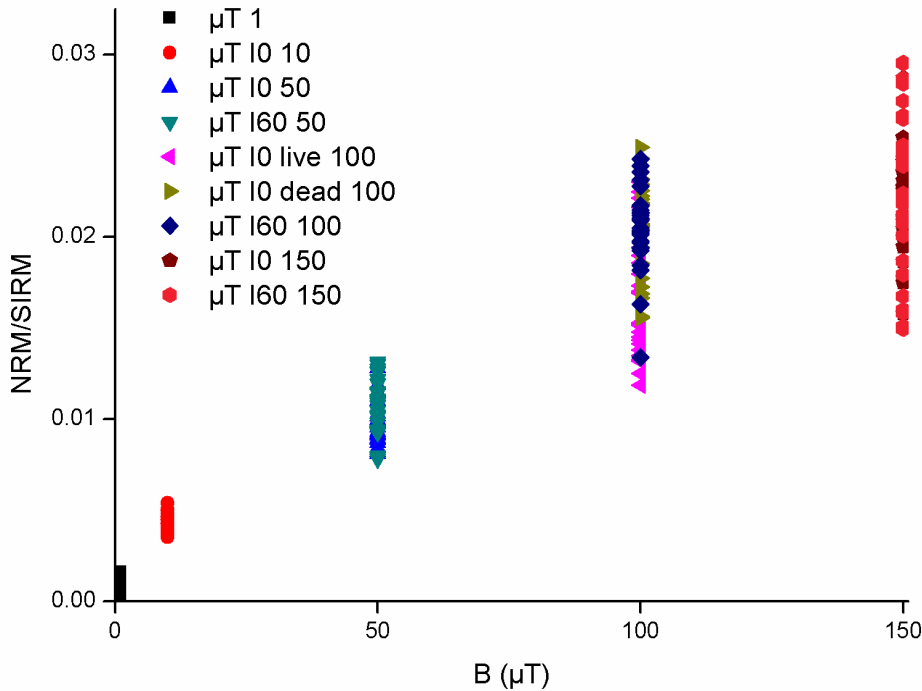


Figure 5 - 12 The relationship between NRM/SIRM and B

magnetite will be aligned with magnetic field lines when the external field was strong enough. However, from these values, we infer that the alignment efficiency of SD magnetic particles was only 3% when the sediment was magnetized under 150 μT .

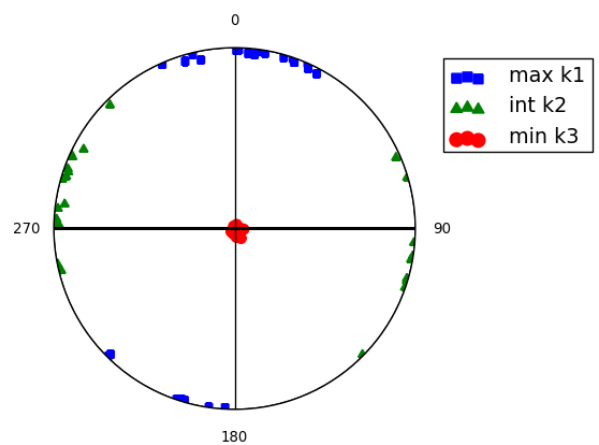
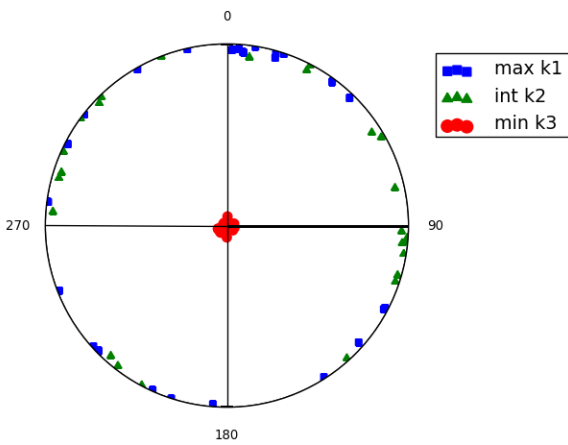
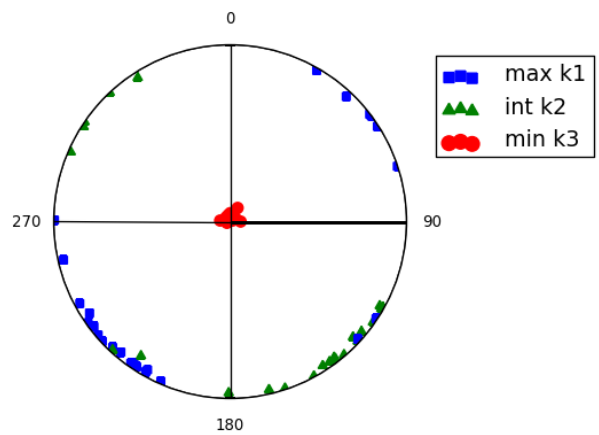
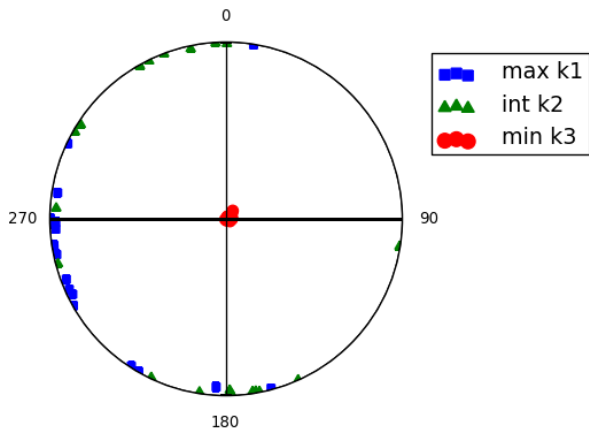
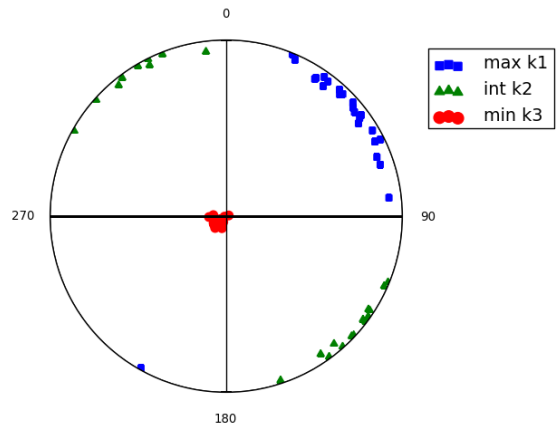
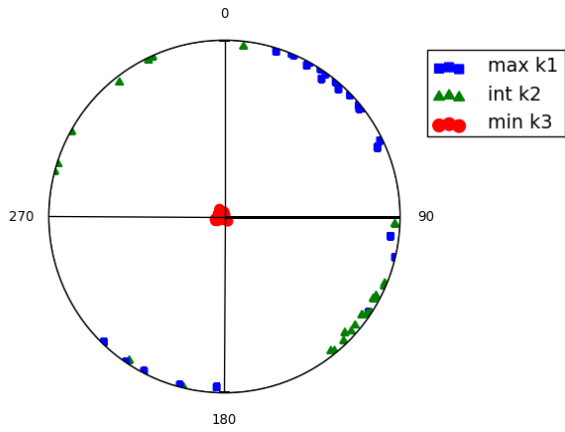
In addition, our results show that from 0 to 150 μT , the paleointensity is not linear with field strength. *Tucker* [1980] found that when the sediment was stirred, they can change linearly with the variation of field strength. *Tauxe et al.* [2006] found that DRM has non-linear relationship with applied field, even in the range of geomagnetic field, which is consist with this result. They think the reason is that the small size of flocs (several microns), which have a strong effect on the efficiency of DRM. *Mao et al.* [2014b] did the redeposition experiment and found they are proportional to the field strength between 0.4 and 160 μT . *Valet et al.* [2017] used cultured MTB and carbonate sediments to do redeposition experiments. They found that magnetization acquisition is linear to the external field strength.

The tensor of AARM/AMS is k_1 , k_2 and k_3 . The tensor can be described geometrically as a triaxial ellipsoid. Lination (L) is defined as k_1/k_2 , foliation (F) is defined as k_2/k_3 . The anisotropy degree (P) is k_1/k_3 . The anisotropy of partial ARM and AMS at different field

strength can be seen in Figure 5-13 and 5-14, respectively. In the Helmholtz setup experiment, k3 direction was mostly in the centre of the stereogram plot, which means the static deposition environment. When the shape parameter T is between 0 and 1, the ellipsoid is oblate. Whereas $-1 < T < 0$, the ellipsoid is prolate. The P-T plot of AMS data shows that most samples are oblate. When the external field was stronger than 10 mT, the k3 direction can reflect the inclination of the field. The relationship between L or F and B for M samples is shown in Figure 5-15. During the range from 0 to 10 mT, L of pARM and B have a positive relationship, whereas L of AMS and B has no obvious relationship. On the other hand, F of pARM and B have a negative relationship, similarly, F of AMS and B has no obvious relationship. The AF demagnetization window for pARM was from 30 to 70 mT, which means the single domain of magnetite was our target. The relationship between degree of anisotropy (P) and field strength (B) for M samples is shown in Figure 5-16. We found the degree of anisotropy of pARM has a strong positive relationship with external field strength when it was bigger than 10 mT. However, the anisotropy of AMS performs different with the anisotropy of ARM. The reason may be that AARM are more sensitive to single domain particles, whereas AMS are more affected by paramagnetic particles [Parés, 2004; Rochette, 1987].

ARM ratio is more useful tool for identifying magnetic interactions [Paterson *et al.*, 2013]. Figure 5-17 shows the ARM acquisition curves at different bias field. The results indicate that the samples were between non-interacting [Kopp *et al.*, 2006a] and interacting extremes [Cisowski, 1981]. Although the interaction exist, however, it is weaker than Paterson *et al.* [2013] found.

Tauxe [1993] mentioned that normalization should be preferably done by several methods, all yielding consistent results. We found NRM/ARM has a better evaluation than NRM/ χ and NRM/SIRM. Because IRM and susceptibility are sensitive to coarser grains, therefore, ARM is used to normalize the paleointensity. Tauxe [1993] thought that magnetic minerals concentration, grain size and the properties of nonmagnetic matrix can have an effect on the paleointensity reconstruction. According to Figure 5-11, we found that there is very low alignment efficiency for single domain chains in sediment. The reason is maybe magnetite particles paste on the clay minerals. Therefore, they cannot align with magnetic lines effectively because of the limit of clay minerals. Similarly, Valet *et al.* [2017] found that kaolinite matrix is more easily to inhibit



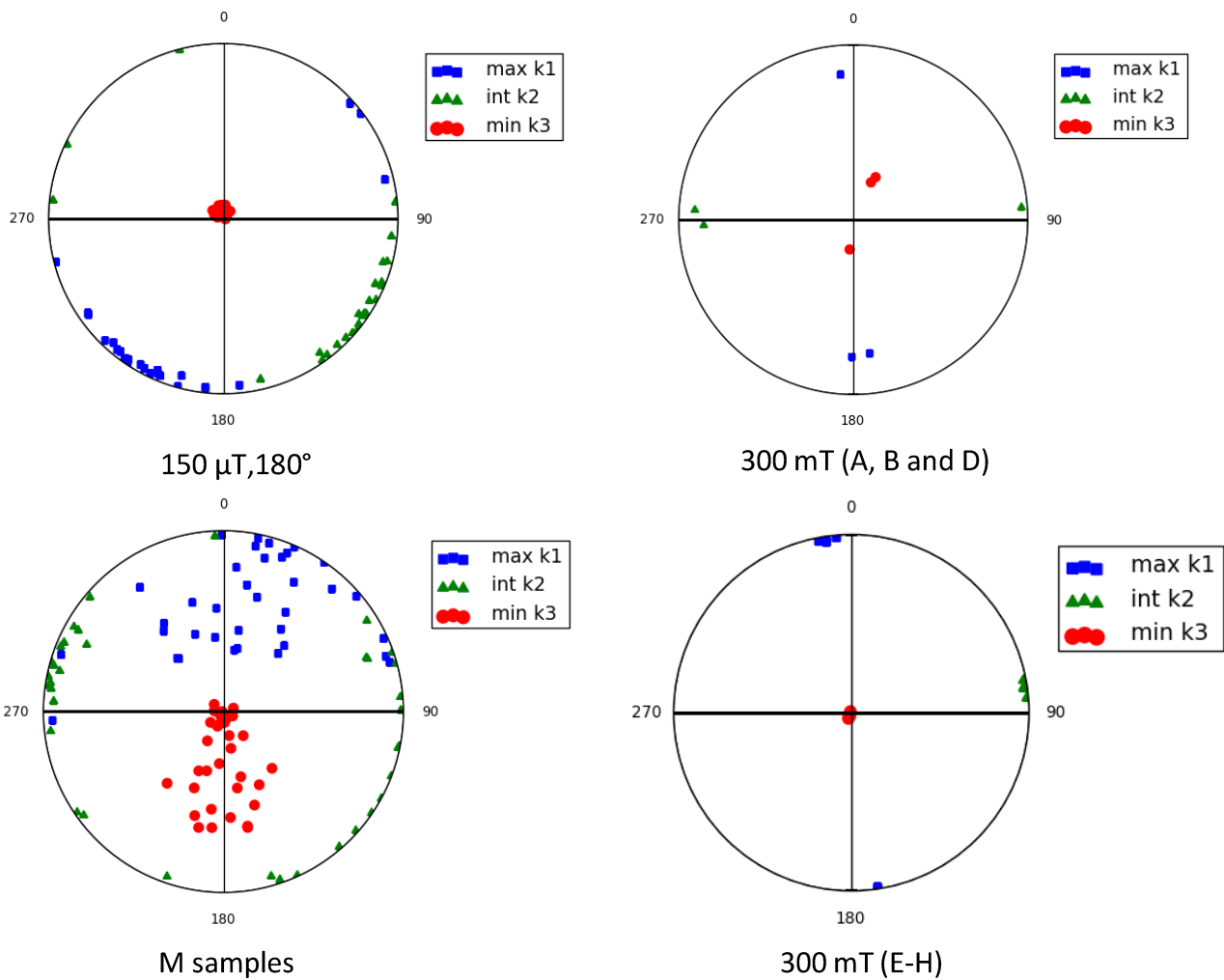
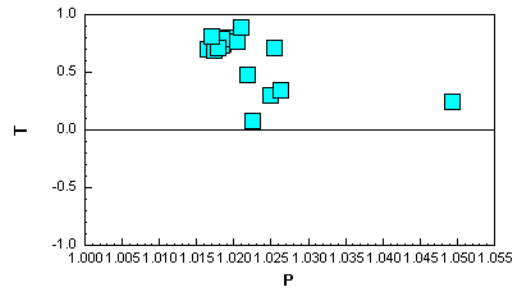
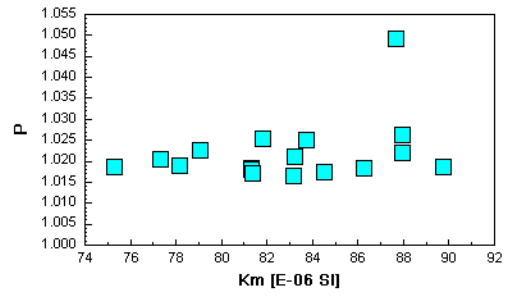
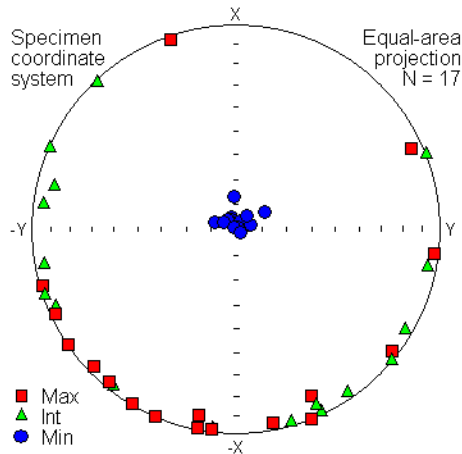


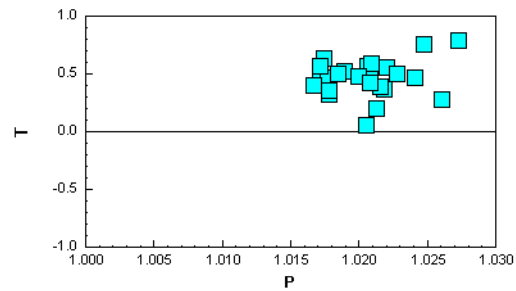
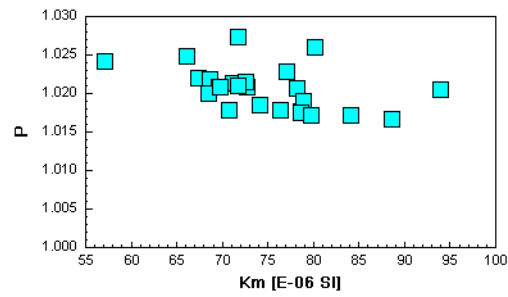
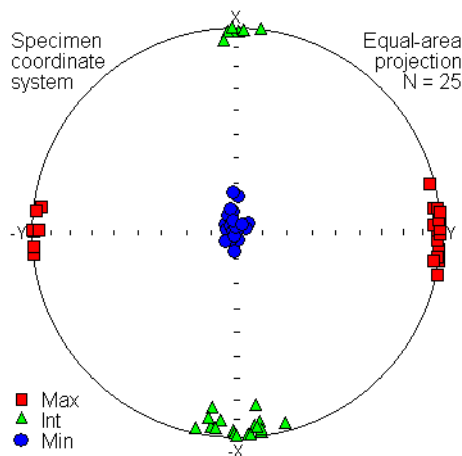
Figure 5 - 13 The AARM ellipsoid at different field strength. Plotting of anisotropy directional data on a stereographic projection. The standard projection is polar, for instance, the center corresponds to an inclination of 90° and the circumference corresponds to the horizontal plane. The directions of maximum principal axes, k_1 , are plotted as squares, of intermediate principal axes, k_2 , as triangles, and of minimum principal axes, k_3 , as circles.

paleointensity. In addition, the drying of the sample can alter magnetic remanence [Henshaw and Merrill, 1979].

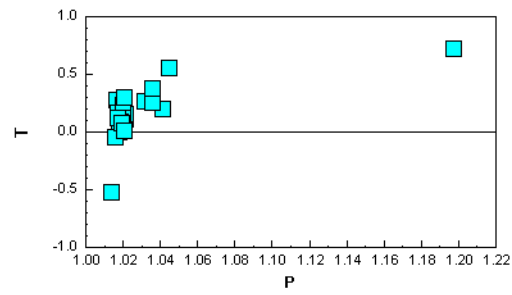
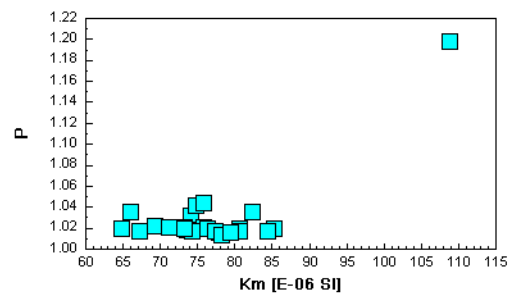
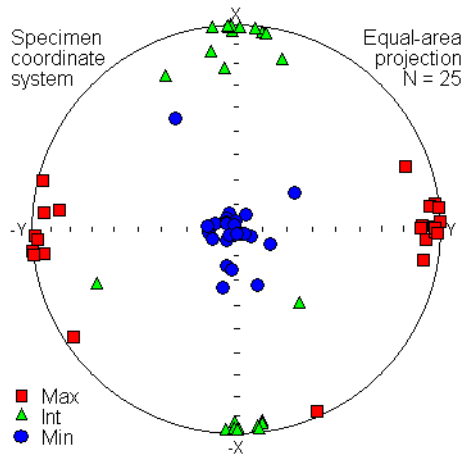
Although our experiment identified that all AARM indices vary in proportion with magnetic field strength, however, from 1 to $150 \mu\text{T}$, our experiments did not show a strong relationship between L or F and B . Similarly, the ratio of eigenvalues of the maximum and intermediate axes for the ARM anisotropy tensors has no obvious changing trend from 0 to $120 \mu\text{T}$ in the research of Paterson *et al.* [2013]. Next step, we will update the Sushibar and measure the sample's magnetic grains alignment below 40-45 percent sediment concentration comparing to carbonate



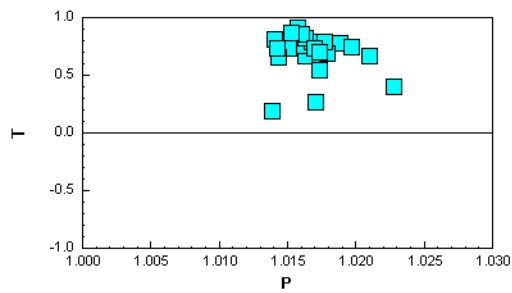
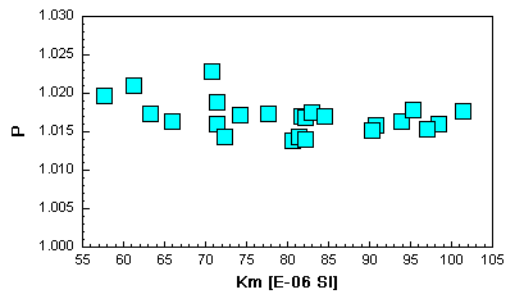
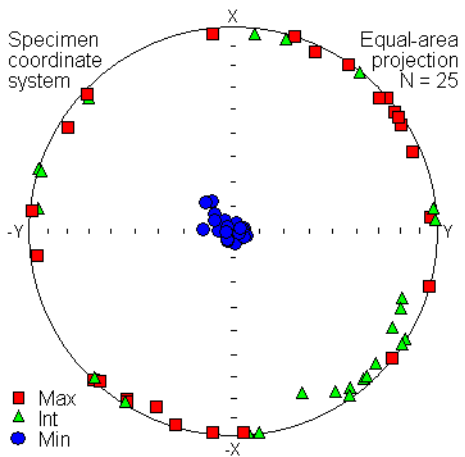
50 μ T I=0°



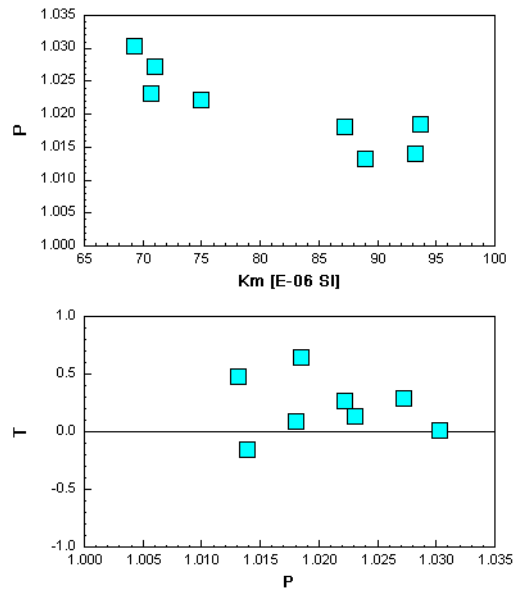
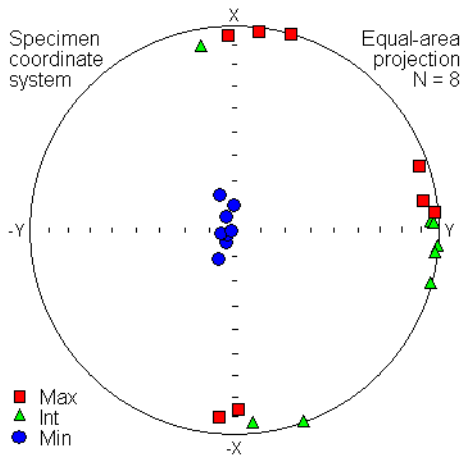
100 μ T dead MTB



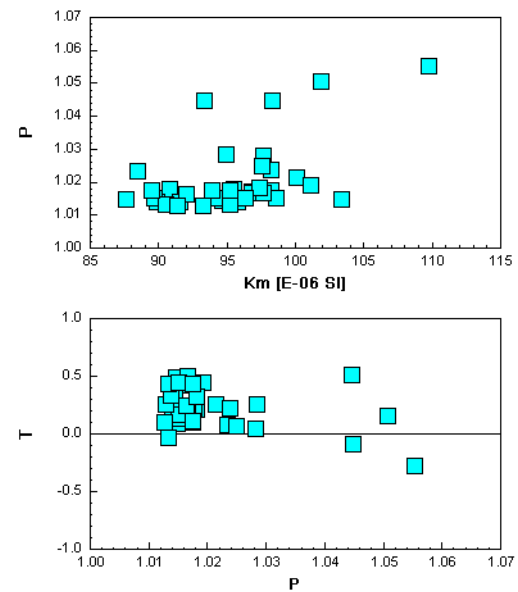
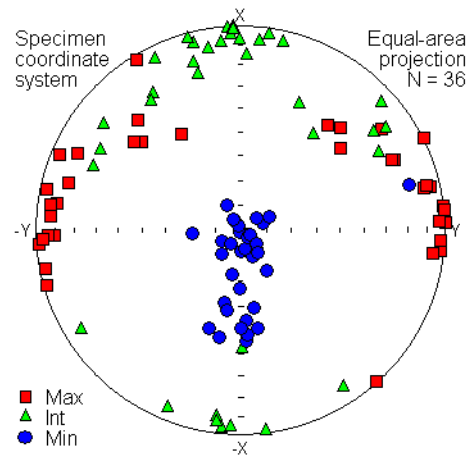
100 μ T live MTB D=180°, I=60°



150 μ T D=180°, I=60°.



300 mT



From 300 μ T to 70 mT

Figure 5 - 14 The stereographic projection of principal susceptibility axes, P-Km plot and P-T plot of AMS

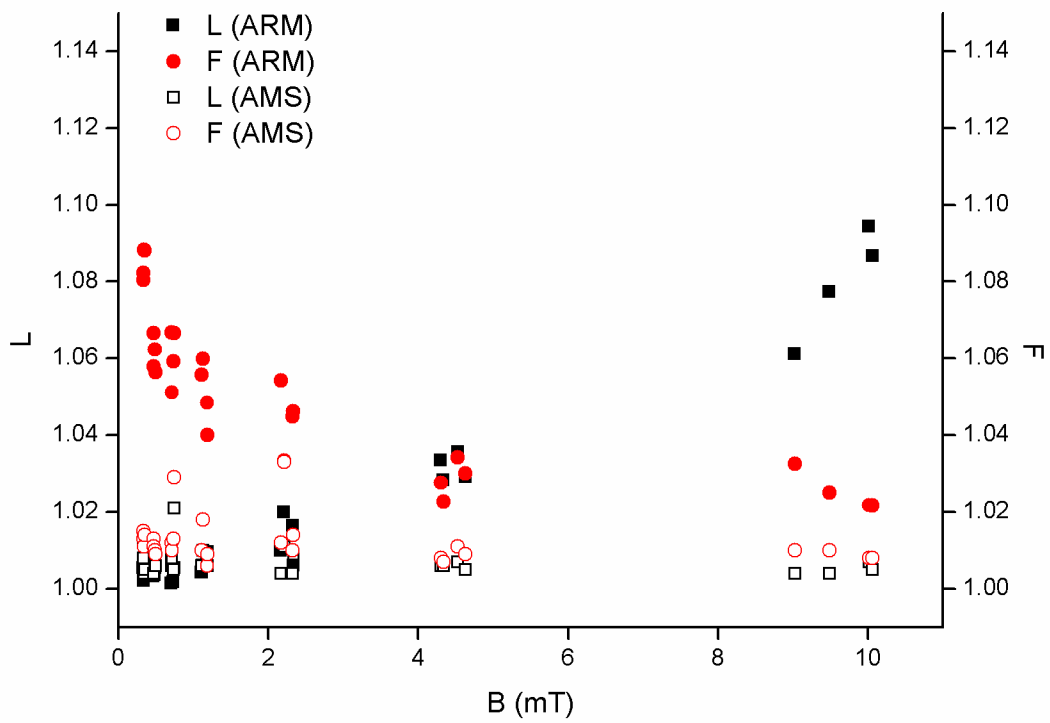


Figure 5 - 15 The relationship between F, L and B

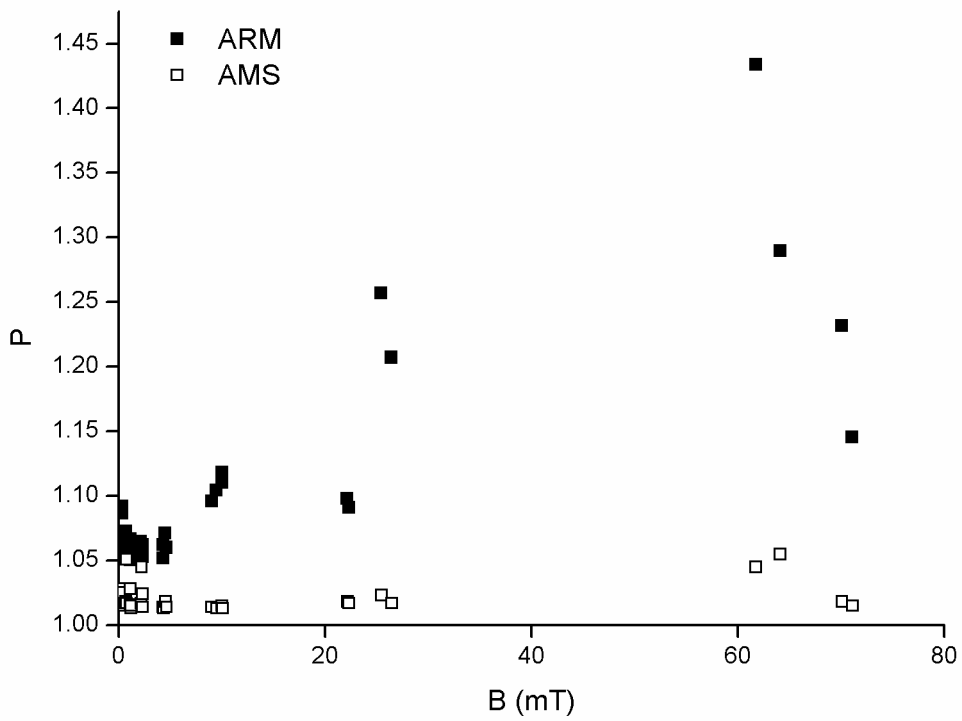


Figure 5 - 16 The relationship between external field strength and P

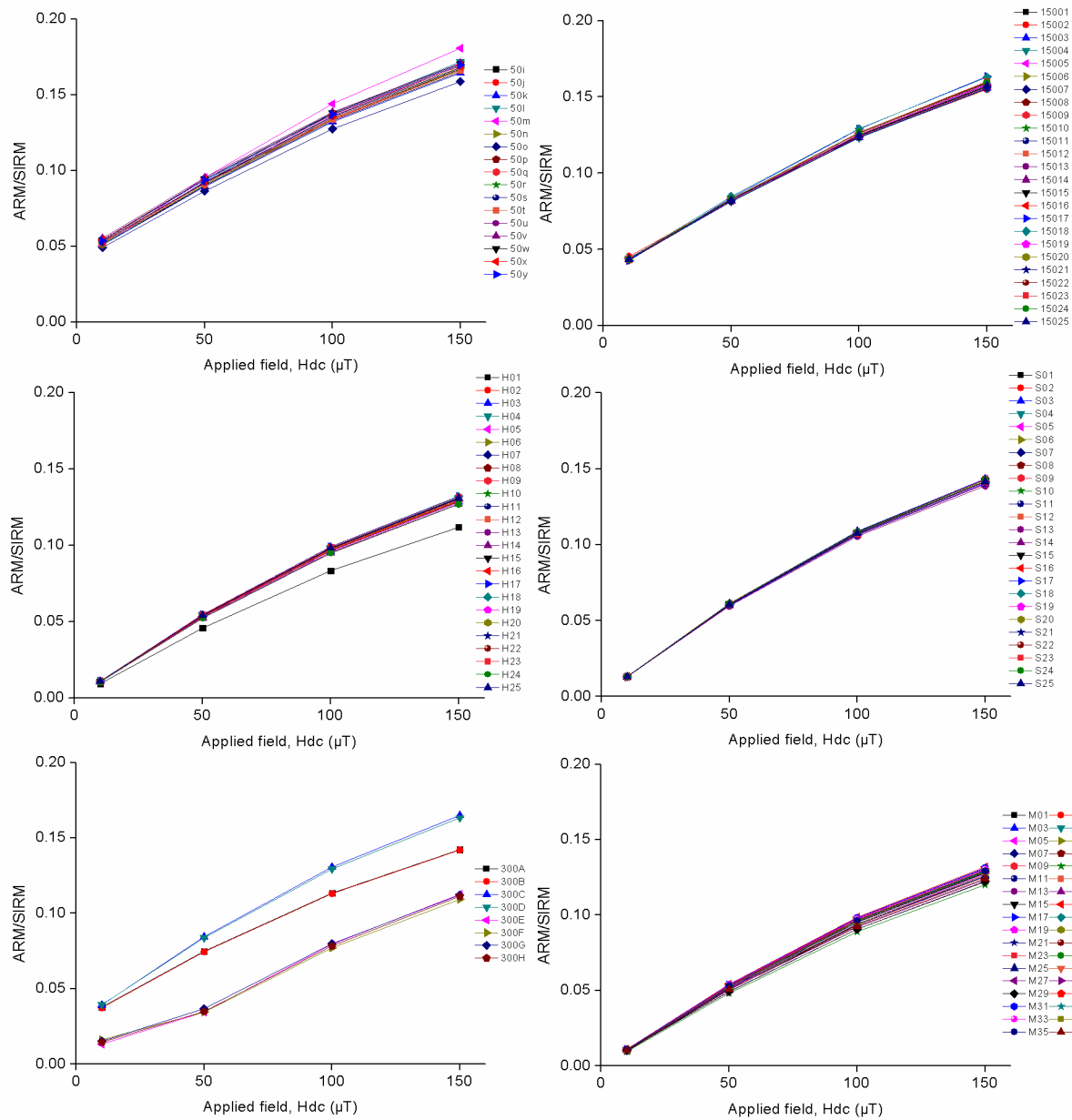


Figure 5 - 17 SIRM normalized ARM acquisition versus the bias field applied during alternating field demagnetization for the redeposition samples

powders.

What factors lead to the scatter of paleointensity during the 25 pilot samples at each round of experiment? *Tauxe et al.* [2006] think that the floc size have a profound effect on the scatter of AARM at more directions. In that case, the result will be more accurate. Besides, we will consider using a special material for carrying sediment samples, whose magnetic signal can be

better distinguished. The relative proportions of paramagnetic materials and single domain magnetic particles should be calculated according to magnetic measurement. We will put known-sized magnetite into clay and do the same experiment, and try to see whether there will be the same result as we did using the magnetofossil-rich sediment.

References

- Amor, M., V. Busigny, P. Louvat, A. Gélabert, P. Cartigny, M. Durand-Dubief, G. Ona-Nguema, E. Alphandéry, I. Chebbi, and F. Guyot (2016), Mass-dependent and-independent signature of Fe isotopes in magnetotactic bacteria, *Science*, 352(6286), 705-708.
- Anson, G., and K. Kodama (1987), Compaction-induced inclination shallowing of the post-depositional remanent magnetization in a synthetic sediment, *Geophysical Journal International*, 88(3), 673-692.
- Ardelean, I., C. Moisescu, M. Ignat, M. Constantin, and M. Virgolici (2009), Magnetospirillum Gryphiswaldense: Fundamentals and applications, *Biotechnology and Biotechnological Equipment*, 23(sup1), 751-754.
- Bazylinski, D. A., and R. B. Frankel (2004), Magnetosome formation in prokaryotes, *Nature Reviews Microbiology*, 2(3), 217-230.
- Bazylinski, D. A., R. B. Frankel, B. R. Heywood, S. Mann, J. W. King, P. L. Donaghay, and A. K. Hanson (1995), Controlled Biomineralization of Magnetite (Fe_3O_4) and Greigite (Fe_3S_4) in a Magnetotactic Bacterium, *Applied and Environmental Microbiology*, 61(9), 3232-3239.
- Bazylinski, D. A., B. R. Heywood, S. Mann, and R. B. Frankel (1993), Fe_3O_4 and Fe_3S_4 in a bacterium, *Nature*, 366(6452), 218-218.
- Bellini, S. (1963a), Su di un particolare comportamento di batteri d'acqua dolce, *Istituto di Microbiologia dell'Università di Pavia*.
- Bellini, S. (1963b), Ulteriori studi sui "batteri magnetosensibili" (Further studies on magnetosensitive bacteria). Institute of Microbiology, University of Pavia Rep., Italy. internal report.
- Blakemore, R. P. (1975), Magnetotactic bacteria, *Science*, 190(4212), 377-379.
- Blakemore, R. P., and R. B. Frankel (1981), Magnetic navigation in bacteria, *Scientific American*.
- Blakemore, R. P., R. B. Frankel, and A. J. Kalmijn (1980), South-seeking magnetotactic bacteria in the Southern Hemisphere, *Nature*, 286, 384-385.
- Blow, R., and N. Hamilton (1978), Effect of compaction on the acquisition of a detrital remanent magnetization in fine-grained sediments, *Geophysical Journal International*, 52(1), 13-23.
- Buerger, S., A. Spoering, E. Gavriš, C. Leslin, L. Ling, and S. Epstein (2012), Microbial scout hypothesis, stochastic exit from dormancy, and the nature of slow growers, *Applied and Environmental Microbiology*, 78(9), 3221-3228.

Chang, L., D. Heslop, A. P. Roberts, D. Rey, and K. J. Mohamed (2016), Discrimination of biogenic and detrital magnetite through a double Verwey transition temperature, *Journal of Geophysical Research: Solid Earth*, *121*(1), 3-14.

Chang, S.-B. R., and J. L. Kirschvink (1985), Possible biogenic magnetite fossils from the Late Miocene Potamida clays of Crete, in Magnetite biomineralization and magnetoreception in organisms, edited, pp. 647-669, Springer

Chang, S.-B. R., and J. L. Kirschvink (1989), Magnetofossils, the magnetization of sediments, and the evolution of magnetite biomineralization, *Annual Review of Earth and Planetary Sciences*, *17*, 169-195.

Chang, S., and J. Kirschvink (1984), Bacterial magnetofossils as probes of Precambrian ecological and biochemical evolutionary events, paper presented at 97th annual meeting, Geological Society of America.

Channell, J., C. Ohneiser, Y. Yamamoto, and M. Kesler (2013), Oligocene-Miocene magnetic stratigraphy carried by biogenic magnetite at sites U1334 and U1335 (equatorial Pacific Ocean), *Geochemistry, Geophysics, Geosystems*, *14*(2), 265-282.

Chen, A., V. Berounsky, M. Chan, M. Blackford, C. Cady, B. Moskowitz, P. Kraal, E. Lima, R. Kopp, and G. Lumpkin (2014), Magnetic properties of uncultivated magnetotactic bacteria and their contribution to a stratified estuary iron cycle, in *Nature Communications*, edited, Nature Research.

Chen, L., D. Heslop, A. P. Roberts, L. Chang, X. Zhao, H. V. McGregor, G. Marino, L. Rodriguez-Sanz, E. J. Rohling, and H. Pälike (2017), Remanence acquisition efficiency in biogenic and detrital magnetite and recording of geomagnetic paleointensity, *Geochemistry, Geophysics, Geosystems*, *18*(4), 1435-1450.

Cisowski, S. (1981), Interacting vs. non-interacting single domain behavior in natural and synthetic samples, *Physics of the Earth and Planetary Interiors*, *26*, 56-62.

Coskun, Ö. K., S. Roud, K. He, N. Petersen, S. Gilder, and W. D. Orsi (2017), Tracking heterotrophic and autotrophic carbon cycling by magnetotactic bacteria in freshwater sediments using DNA stable isotope probing, paper presented at EGU General Assembly Conference Abstracts.

Day, R., M. Fuller, and V. Schmidt (1977), Hysteresis properties of titanomagnetites: grain-size and compositional dependence, *Physics of the Earth and Planetary Interiors*, *13*(4), 260-267.

D'Onofrio, A., J. M. Crawford, E. J. Stewart, K. Witt, E. Gavriš, S. Epstein, J. Clardy, and K. Lewis (2010), Siderophores from neighboring organisms promote the growth of uncultured bacteria, *Chemistry and Biology*, *17*(3), 254-264.

DeLong, E. F., R. B. Frankel, and D. A. Bazylinski (1993), Multiple evolutionary origins of magnetotaxis in bacteria, *Science*, *259*(5096), 803-806.

Du, H. J., Y. R. Chen, R. Zhang, H. M. Pan, W. Y. Zhang, K. Zhou, L. F. Wu, and T. Xiao (2015), Temporal distributions and environmental adaptations of two types of multicellular magnetotactic prokaryote in the sediments of Lake Yuehu, China, *Environmental Microbiology Reports*, 7(3), 538-546.

Dziuba, M., T. Kolganova, V. Gorlenko, and B. Kuznetsov (2013), Species diversity of magnetotactic bacteria from the Ol'khovka River, Russia, *Microbiology*, 82(3), 335-340.

Egli, R. (2004), Characterization of individual rock magnetic components by analysis of remanence curves, 1. Unmixing natural sediments, *Studia Geophysica et Geodaetica*, 48(2), 391-446.

Egli, R. (2013), VARIFORC: An optimized protocol for calculating non-regular first-order reversal curve (FORC) diagrams. *Global Planetary Change*, 110(C), 302–320.

Egli, R., and W. Lowrie (2002), Anhysteretic remanent magnetization of fine magnetic particles, *Journal of Geophysical Research: Solid Earth*, 107(B10).

Egli, R., A. P. Chen, M. Winklhofer, K. P. Kodama, and C. S. Horng (2010), Detection of noninteracting single domain particles using first-order reversal curve diagrams, *Geochemistry, Geophysics, Geosystems*, 11(1).

Enkin, R. (2004), Paleomagnetism data analysis: Version 4.2, *Geol. Surv. of Can., Sidney, BC (Available at <http://www.pgc.nrcan.gc.ca/tectonic/enkin.htm>)*.

Faivre, D., and D. Schüler (2008), Magnetotactic bacteria and magnetosomes, *Chemical Reviews*, 108(11), 4875-4898.

Faivre, D., N. Menguy, M. Pósfai, and D. Schüler (2008), Environmental parameters affect the physical properties of fast-growing magnetosomes, *American Mineralogist*, 93(2-3), 463-469.

Farina, M., D. M. S. Esquivel, and H. G. Lins de Barros (1990), Magnetic iron-sulphur crystals from a magnetotactic microorganism, *Nature*, 343(6255), 256.

Fassbinder, J. W., H. Stanjek, and H. Vali (1990), Occurrence of magnetic bacteria in soil, *Nature*, 343(6254), 161-163.

Flies, C. B., H. M. Jonkers, D. de Beer, K. Bosselmann, M. E. Böttcher, and D. Schüler (2005), Diversity and vertical distribution of magnetotactic bacteria along chemical gradients in freshwater microcosms, *FEMS Microbiology Ecology*, 52(2), 185-195.

Frankel, R. B., and D. A. Bazylinski (2004), Magnetosome mysteries, *ASM news*, 70(4), 176.

Frankel, R. B., D. A. Bazylinski, M. S. Johnson, and B. L. Taylor (1997), Magneto-aerotaxis in marine coccoid bacteria, *Biophysical Journal*, 73(2), 994-1000.

Frankel, R. B., R. Blakemore, F. Torres de Araujo, D. M. S. Esquivel, and J. Danon (1981), Magnetotactic bacteria at the geomagnetic equator, *Science*, 212(4500), 1269.

Gehring, A. U., H. Fischer, M. Charilaou, and I. García-Rubio (2011), Magnetic anisotropy and Verwey transition of magnetosome chains in *Magnetospirillum gryphiswaldense*, *Geophysical Journal International*, 187(3), 1215-1221.

Hanzlik, M., M. Winklhofer, and N. Petersen (1996), Spatial arrangement of chains of magnetosomes in magnetotactic bacteria, *Earth and Planetary Science Letters*, 145(1-4), 125-134.

He, K., S. A. Gilder, W. D. Orsi, X. Zhao, and N. Petersen (2017), Constant Flux of Spatial Niche Partitioning through High-Resolution Sampling of Magnetotactic Bacteria, *Applied and Environmental Microbiology*, 83(20), e01382-01317.

Henshaw, P. C., and R. T. Merrill (1979), Characteristics of drying remanent magnetization in sediments, *Earth and Planetary Science Letters*, 43(2), 315-320.

Heslop, D., A. P. Roberts, and L. Chang (2014), Characterizing magnetofossils from first-order reversal curve (FORC) central ridge signatures, *Geochemistry, Geophysics, Geosystems*, 15(6), 2170-2179.

Heslop, D., A. P. Roberts, L. Chang, M. Davies, A. Abrajevitch, and P. De Deckker (2013), Quantifying magnetite magnetofossil contributions to sedimentary magnetizations, *Earth and Planetary Science Letters*, 382, 58-65.

Hesse, P. P. (1994), Evidence for bacterial palaeoecological origin of mineral magnetic cycles in oxic and sub-oxic Tasman Sea sediments, *Marine Geology*, 117(1-4), 1-17.

Heyen, U., and D. Schüler (2003), Growth and magnetosome formation by microaerophilic *Magnetospirillum* strains in an oxygen-controlled fermentor, *Applied Microbiology and Biotechnology*, 61(5-6), 536-544.

Heywood, B. R., D. A. Bazylinski, A. Garratt-Reed, S. Mann, and R. B. Frankel (1990), Controlled biosynthesis of greigite (Fe_3S_4) in magnetotactic bacteria, *Naturwissenschaften*, 77(11), 536-538.

Hrouda, F. (2002), The use of the anisotropy of magnetic remanence in the resolution of the anisotropy of magnetic susceptibility into its ferromagnetic and paramagnetic components, *Tectonophysics*, 347(4), 269-281.

Jackson, M. (1991), Anisotropy of magnetic remanence: a brief review of mineralogical sources, physical origins, and geological applications, and comparison with susceptibility anisotropy, *Pure and Applied Geophysics*, 136(1), 1-28.

Jackson, M. J., S. K. Banerjee, J. A. Marvin, R. Lu, and W. Gruber (1991), Detrital remanence, inclination errors, and anhysteretic remanence anisotropy: quantitative model and experimental results, *Geophysical Journal International*, 104(1), 95-103.

Jermy, A. (2012), Bacterial physiology: environment shapes magnetic personality, *Nature Reviews Microbiology*, 10(2), 84-84.

Jezek, J., and S. a. Gilder (2006), Competition of magnetic and hydrodynamic forces on ellipsoidal particles under shear: Influence of the Earth's magnetic field on particle alignment in viscous media, *Journal of Geophysical Research: Solid Earth*, 111, 1-18.

Jogler, C., M. Niebler, W. Lin, M. Kube, G. Wanner, S. Kolinko, P. Stief, A. Beck, D. De Beer, and N. Petersen (2010), Cultivation-independent characterization of 'Candidatus Magnetobacterium bavaricum' via ultrastructural, geochemical, ecological and metagenomic methods, *Environmental Microbiology*, 12(9), 2466-2478.

Johnson, E., T. Murphy, and O. Torreson (1948), Pre-history of the Earth's magnetic field, *Journal of Geophysical Research*, 53(4), 349-372.

Kawaguchi, R., J. G. Burgess, T. Sakaguchi, H. Takeyama, R. H. Thornhill, and T. Matsunaga (1995), Phylogenetic analysis of a novel sulfate-reducing magnetic bacterium, RS-1, demonstrates its membership of the δ -Proteobacteria, *FEMS Microbiology Letters*, 126(3), 277-282.

Kent, D. V., and N. D. Opdyke (1977), Palaeomagnetic field intensity variation recorded in a Brunhes epoch deep-sea sediment core, *Nature*, 266(5598), 156-159.

Kind, J., A. U. Gehring, M. Winklhofer, and A. M. Hirt (2011), Combined use of magnetometry and spectroscopy for identifying magnetofossils in sediments, *Geochemistry, Geophysics, Geosystems*, 12(8).

King, J. W., S. K. Banerjee, and J. Marvin (1983), A new rock-magnetic approach to selecting sediments for geomagnetic paleointensity studies: Application to paleointensity for the last 4000 years, *Journal of Geophysical Research: Solid Earth*, 88(B7), 5911-5921.

Kirschvink, J. (1980), South-seeking magnetic bacteria, *Journal of Experimental Biology*, 86(1), 345-347.

Kirschvink, J. L., and S.-B. R. Chang (1984), Ultrafine-grained magnetite in deep-sea sediments: Possible bacterial magnetofossils, *Geology*, 12(9), 559-562.

Kodama, K., R. Moeller, D. Bazylinski, R. Kopp, and A. Chen (2013), The mineral magnetic record of magnetofossils in recent lake sediments of Lake Ely, PA, *Global and Planetary Change*, 110, 350-363.

Kopp, R. E., and J. L. Kirschvink (2008), The identification and biogeochemical interpretation of fossil magnetotactic bacteria, *Earth-Science Reviews*, 86(1), 42-61.

Kopp, R. E., C. Z. Nash, A. Kobayashi, B. P. Weiss, D. A. Bazylinski, and J. L. Kirschvink (2006a), Ferromagnetic resonance spectroscopy for assessment of magnetic anisotropy and magnetostatic interactions: A case study of mutant magnetotactic bacteria, *Journal of Geophysical Research: Solid Earth*, 111(B12).

Kopp, R. E., B. P. Weiss, A. C. Maloof, H. Vali, C. Z. Nash, and J. L. Kirschvink (2006b), Chains, clumps, and strings: Magnetofossil taphonomy with ferromagnetic resonance spectroscopy, *Earth and Planetary Science Letters*, 247(1), 10-25.

Kopp, R. E., T. D. Raub, D. Schumann, H. Vali, A. V. Smirnov, and J. L. Kirschvink (2007), Magnetofossil spike during the Paleocene-Eocene thermal maximum: Ferromagnetic resonance, rock magnetic, and electron microscopy evidence from Ancora, New Jersey, United States, *Paleoceanography*, 22(4).

Lean, C. M. B., and I. N. McCave (1998), Glacial to interglacial mineral magnetic and palaeoceanographic changes at Chatham Rise, SW Pacific Ocean, *Earth and Planetary Science Letters*, 163(1), 247-260.

Lefèvre, C. T., and D. A. Bazylinski (2013), Ecology, diversity, and evolution of magnetotactic bacteria, *Microbiology and Molecular Biology Reviews*, 77(3), 497-526.

Lefèvre, C. T., R. B. Frankel, F. Abreu, U. Lins, and D. A. Bazylinski (2011a), Culture-independent characterization of a novel, uncultivated magnetotactic member of the Nitrospirae phylum, *Environmental Microbiology*, 13(2), 538-549.

Lefèvre, C. T., N. Menguy, F. Abreu, U. Lins, M. Pósfai, T. Prozorov, D. Pignol, R. B. Frankel, and D. A. Bazylinski (2011b), A cultured greigite-producing magnetotactic bacterium in a novel group of sulfate-reducing bacteria, *Science*, 334(6063), 1720-1723.

Lefèvre, Christopher T., M. Bennet, L. Landau, P. Vach, D. Pignol, Dennis A. Bazylinski, Richard B. Frankel, S. Klumpp, and D. Faivre (2014), Diversity of Magneto-Aerotactic Behaviors and Oxygen Sensing Mechanisms in Cultured Magnetotactic Bacteria, *Biophysical Journal*, 107(2), 527-538.

Levi, S., and S. K. Banerjee (1976), On the possibility of obtaining relative paleointensities from lake sediments, *Earth and Planetary Science Letters*, 29(1), 219-226.

Li, J., and Y. Pan (2012), Environmental factors affect magnetite magnetosome synthesis in *Magnetospirillum magneticum* AMB-1: implications for biologically controlled mineralization, *Geomicrobiology Journal*, 29(4), 362-373.

Lin, W., and Y. Pan (2009), Uncultivated magnetotactic cocci from Yuandadu park in Beijing, China, *Applied and Environmental Microbiology*, 75(12), 4046-4052.

Lin, W., and Y. Pan (2010), Temporal variation of magnetotactic bacterial communities in two freshwater sediment microcosms, *FEMS Microbiology Letters*, 302(1), 85-92.

Lin, W., Y. Wang, and Y. Pan (2012a), Short-term effects of temperature on the abundance and diversity of magnetotactic cocci, *MicrobiologyOpen*, 1(1), 53-63.

Lin, W., Y. Wang, B. Li, and Y. Pan (2012b), A biogeographic distribution of magnetotactic bacteria influenced by salinity, *The ISME journal*, 6(2), 475-479.

Lin, W., J. Li, D. Schöler, C. Jogler, and Y. Pan (2009), Diversity analysis of magnetotactic bacteria in Lake Miyun, northern China, by restriction fragment length polymorphism, *Systematic and Applied Microbiology*, 32(5), 342-350.

Lin, W., D. A. Bazylinski, T. Xiao, L.-F. Wu, and Y. Pan (2013a), Life with compass: diversity and biogeography of magnetotactic bacteria, *Environmental Microbiology*, 86.

Lin, W., Y. Wang, Y. Gorby, K. Nealson, and Y. Pan (2013b), Integrating niche-based process and spatial process in biogeography of magnetotactic bacteria, *Scientific Reports*, 3, 1643.

Lin, W., A. Deng, Z. Wang, Y. Li, T. Wen, L.-F. Wu, M. Wu, and Y. Pan (2014), Genomic insights into the uncultured genus 'Candidatus Magnetobacterium' in the phylum Nitrospirae, *The ISME Journal*, 8(12), 2463-2477.

Lins, U., M. R. McCartney, M. Farina, R. B. Frankel, and P. R. Buseck (2005), Habits of magnetosome crystals in coccoid magnetotactic bacteria, *Applied and Environmental Microbiology*, 71(8), 4902-4905.

Liu, S., C. Deng, J. Xiao, J. Li, G. A. Paterson, L. Chang, L. Yi, H. Qin, Y. Pan, and R. Zhu (2015), Insolation driven biomagnetic response to the Holocene Warm Period in semi-arid East Asia, *Scientific reports*, 5.

Lu, R., S. K. Banerjee, and J. Marvin (1990), Effects of clay mineralogy and the electrical conductivity of water on the acquisition of depositional remanent magnetization in sediments, *Journal of Geophysical Research: Solid Earth*, 95(B4), 4531-4538.

Maher, B. A. (1988), Magnetic properties of some synthetic sub-micron magnetites, *Geophysical Journal International*, 94(1), 83-96.

Mandernack, K. W., D. A. Bazylinski, W. C. Shanks, and T. D. Bullen (1999), Oxygen and iron isotope studies of magnetite produced by magnetotactic bacteria, *Science*, 285(5435), 1892-1896.

Mann, S., N. H. Sparks, R. B. Frankel, D. A. Bazylinski, and H. W. Jannasch (1990), Biomineralization of Ferrimagnetic Greigite (Fe_3S_4) and Iron Pyrite (FeS_2) in a Magnetotactic Bacterium, *Nature*, 343(6255), 258.

Mao, X. (2013), Magnetotactic bacteria in sediment: Magnetotaxis, chemotaxis, and paleomagnetic implications, München, Ludwig-Maximilians-Universität, Diss., 2013.

Mao, X., R. Egli, N. Petersen, M. Hanzlik, and X. Liu (2014a), Magneto-chemotaxis in sediment: first insights, *PLoS ONE*, 9(7), e102810.

Mao, X., R. Egli, N. Petersen, M. Hanzlik, and X. Zhao (2014b), Magnetotaxis and acquisition of detrital remanent magnetization by magnetotactic bacteria in natural sediment: First experimental results and theory, *Geochemistry, Geophysics, Geosystems*, 15(1), 255-283.

Martel, S., M. Mohammadi, O. Felfoul, Z. Lu, and P. Pouponneau (2009), Flagellated magnetotactic bacteria as controlled MRI-trackable propulsion and steering systems for medical nanorobots operating in the human microvasculature, *The International Journal of Robotics Research*, 28(4), 571-582.

Martins, J. L., T. S. Silveira, K. T. Silva, and U. Lins (2010), Salinity dependence of the distribution of multicellular magnetotactic prokaryotes in a hypersaline lagoon, *International Microbiology*, 12(3), 193-201.

Martins, J. L., T. S. Silveira, F. Abreu, F. P. de Almeida, A. S. Rosado, and U. Lins (2012), Spatiotemporal distribution of the magnetotactic multicellular prokaryote *Candidatus Magnetoglobus multicellularis* in a Brazilian hypersaline lagoon and in microcosms, *International Microbiology*, 15(3), 141-149.

Mayr, C., G. Försterra, V. Häussermann, A. Wunderlich, J. Grau, M. Zieringer, and A. Altenbach (2011), Stable isotope variability in a Chilean fjord food web: implications for N-and C-cycles, *Marine Ecology Progress Series*, 428, 89-104.

Meyers, P. A. (1994), Preservation of elemental and isotopic source identification of sedimentary organic matter, *Chemical Geology*, 114(3-4), 289-302.

Moiescu, C., I. I. Ardelean, and L. G. Benning (2014), The effect and role of environmental conditions on magnetosome synthesis, *Frontiers in Microbiology*, 5(February), 1-12.

Morillo, V., F. Abreu, A. C. Araujo, L. G. de Almeida, A. Enrich-Prast, M. Farina, A. T. de Vasconcelos, D. A. Bazylinski, and U. Lins (2014), Isolation, cultivation and genomic analysis of magnetosome biomineralization genes of a new genus of South-seeking magnetotactic cocci within the Alphaproteobacteria, *Frontiers in Microbiology*, 5.

Moskowitz, B., R. B. Frankel, P. Flanders, R. Blakemore, and B. B. Schwartz (1988), Magnetic properties of magnetotactic bacteria, *Journal of Magnetism and Magnetic Materials*, 73(3), 273-288.

Moskowitz, B. M. (1995), Biomineralization of magnetic minerals, *Reviews of geophysics*, 33(S1), 123-128.

Moskowitz, B. M., R. B. Frankel, and D. A. Bazylinski (1993), Rock magnetic criteria for the detection of biogenic magnetite, *Earth and Planetary Science Letters*, 120(3-4), 283-300.

Murat, D., A. Quinlan, H. Vali, and A. Komeili (2010), Comprehensive genetic dissection of the magnetosome gene island reveals the step-wise assembly of a prokaryotic organelle, *Proceedings of the National Academy of Sciences*, 107(12), 5593-5598.

Nöel, M. (1980), Surface tension phenomena in the magnetization of sediments, *Geophysical Journal International*, 62(1), 15-25.

- Oldfield, F. (2007), Sources of fine-grained magnetic minerals in sediments: a problem revisited, *The Holocene*, 17(8), 1265-1271.
- Ouyang, T., D. Heslop, A. P. Roberts, C. Tian, Z. Zhu, Y. Qiu, and X. Peng (2014), Variable remanence acquisition efficiency in sediments containing biogenic and detrital magnetites: implications for relative paleointensity signal recording, *Geochemistry, Geophysics, Geosystems*, 15(7), 2780-2796.
- Paasche, Ø., R. Løvlie, S. O. Dahl, J. Bakke, and A. Nesje (2004), Bacterial magnetite in lake sediments: late glacial to Holocene climate and sedimentary changes in northern Norway, *Earth and Planetary Science Letters*, 223(3), 319-333.
- Pan, Y., N. Petersen, M. Winklhofer, A. F. Davila, Q. Liu, T. Frederichs, M. Hanzlik, and R. Zhu (2005), Rock magnetic properties of uncultured magnetotactic bacteria, *Earth and Planetary Science Letters*, 237(3), 311-325.
- Parés, J. M. (2004), How deformed are weakly deformed mudrocks? Insights from magnetic anisotropy, *Geological Society, London, Special Publications*, 238(1), 191-203.
- Paterson, G. a., Y. Wang, and Y. Pan (2013), The fidelity of paleomagnetic records carried by magnetosome chains, *Earth and Planetary Science Letters*, 383, 82-91.
- Petermann, H., and U. Bleil (1993), Detection of live magnetotactic bacteria in South Atlantic deep-sea sediments, *Earth and Planetary Science Letters*, 117(1-2), 223-228.
- Petersen, N., T. von Dobeneck, and H. Vali (1986), Fossil bacterial magnetite in deep-sea sediments from the South Atlantic Ocean, *Nature*, 320(6063), 611-615.
- Petersen, N., D. G. Weiss, and H. Vali (1989), Magnetic bacteria in lake sediments, in *Geomagnetism and Palaeomagnetism*, edited, pp. 231-241, Springer.
- Popa, R., W. Fang, K. H. Nealson, V. Souza-Egipsy, T. S. Berquó, S. K. Banerjee, and L. R. Penn (2009), Effect of oxidative stress on the growth of magnetic particles in *Magnetospirillum magneticum*, *International Microbiology*, 12, 49-57.
- Postec, A., N. Tapia, A. Bernadac, M. Joseph, S. Davidson, L.-F. Wu, B. Ollivier, and N. Pradel (2012), Magnetotactic bacteria in microcosms originating from the French Mediterranean coast subjected to oil industry activities, *Microbial Ecology*, 63(1), 1-11.
- Potter, D. K., and A. Stephenson (1988), Single-domain particles in rocks and magnetic fabric analysis, *Geophysical Research Letters*, 15(10), 1097-1100.
- Readman, P., and W. O'reilly (1972), Magnetic Properties of Oxidized (Cation-Deficient) Titanomagnetites, *Journal of Geomagnetism and Geoelectricity*, 24(1), 69-90

Reinholdsson, M., I. Snowball, L. Zillén, C. Lenz, and D. Conley (2013), Magnetic enhancement of Baltic Sea sapropels by greigite magnetofossils, *Earth and Planetary Science Letters*, 366, 137-150.

Roberts, A. P., D. Heslop, X. Zhao, and C. R. Pike (2014), Understanding fine magnetic particle systems through use of first-order reversal curve diagrams, *Reviews of Geophysics*, 52(4), 557-602.

Roberts, A. P., L. Chang, D. Heslop, F. Florindo, and J. C. Larrasoña (2012), Searching for single domain magnetite in the “pseudo-single-domain” sedimentary haystack: implications of biogenic magnetite preservation for sediment magnetism and relative paleointensity determinations, *Journal of Geophysical Research: Solid Earth*, 117(B8).

Roberts, A. P., Q. Liu, C. J. Rowan, L. Chang, C. Carvallo, J. Torrent, and C. S. Horng (2006), Characterization of hematite (α -Fe₂O₃), goethite (α -FeOOH), greigite (Fe₃S₄), and pyrrhotite (Fe₇S₈) using first-order reversal curve diagrams, *Journal of Geophysical Research: Solid Earth*, 111(B12).

Roberts, A. P., F. Florindo, G. Villa, L. Chang, L. Jovane, S. M. Bohaty, J. C. Larrasoña, D. Heslop, and J. D. F. Gerald (2011), Magnetotactic bacterial abundance in pelagic marine environments is limited by organic carbon flux and availability of dissolved iron, *Earth and Planetary Science Letters*, 310(3), 441-452.

Rochette, P. (1987), Magnetic susceptibility of the rock matrix related to magnetic fabric studies, *Journal of Structural Geology*, 9(8), 1015-1020.

Rodgers, F. G., R. P. Blakemore, N. A. Blakemore, R. B. Frankel, D. A. Bazylinski, D. Maratea, and C. Rodgers (1990), Intercellular structure in a many-celled magnetotactic prokaryote, *Archives of Microbiology*, 154(1), 18-22.

Sakaguchi, T., J. G. Burgess, and T. Matsunaga (1993), Magnetite formation by a sulphate-reducing bacterium, *Nature*, 365(6441), 47-49.

Savian, J. F., L. Jovane, M. Giorgioni, F. Iacoviello, D. Rodelli, A. P. Roberts, L. Chang, F. Florindo, and M. Sprovieri (2016), Environmental magnetic implications of magnetofossil occurrence during the Middle Eocene Climatic Optimum (MECO) in pelagic sediments from the equatorial Indian Ocean, *Palaeogeography, Palaeoclimatology, Palaeoecology*, 441, 212-222.

Schüler, D. (2006), *Magnetoreception and magnetosomes in bacteria*, Springer Science and Business Media.

Schüler, D., and E. Baeuerlein (1998), Dynamics of iron uptake and Fe₃O₄ biomineralization during aerobic and microaerobic growth of *Magnetospirillum gryphiswaldense*, *Journal of Bacteriology*, 180(1), 159-162.

Schüler, D., and R. B. Frankel (1999), Bacterial magnetosomes: microbiology, biomineralization and biotechnological applications, *Applied Microbiology and Biotechnology*, 52(4), 464-473.

Schumann, D., T. D. Raub, R. E. Kopp, J.-L. Guerquin-Kern, T.-D. Wu, I. Rouiller, A. V. Smirnov, S. K. Sears, U. Lücken, and S. M. Tikoo (2008), Gigantism in unique biogenic magnetite at the Paleocene–Eocene Thermal Maximum, *Proceedings of the National Academy of Sciences*, 105(46), 17648-17653.

Shcherbakov, V., and V. Shcherbakova (1987), On the physics of acquisition of post-depositional remanent magnetization, *Physics of the Earth and planetary interiors*, 46(1-3), 64-70.

Simmons, S. L., and K. J. Edwards (2007), Unexpected diversity in populations of the many-celled magnetotactic prokaryote, *Environmental Microbiology*, 9(1), 206-215.

Simmons, S. L., D. A. Bazylinski, and K. J. Edwards (2006), South-seeking magnetotactic bacteria in the Northern Hemisphere, *Science*, 311(5759), 371-374.

Simmons, S. L., D. A. Bazylinski, and K. J. Edwards (2007), Population dynamics of marine magnetotactic bacteria in a meromictic salt pond described with qPCR, *Environmental microbiology*, 9(9), 2162-2174.

Simmons, S. L., S. M. Sievert, R. B. Frankel, D. A. Bazylinski, and K. J. Edwards (2004), Spatiotemporal distribution of marine magnetotactic bacteria in a seasonally stratified coastal salt pond, *Applied and Environmental Microbiology*, 70(10), 6230-6239.

Snowball, I., P. Sandgren, and G. Petterson (1999), The mineral magnetic properties of an annually laminated Holocene lake-sediment sequence in northern Sweden, *The Holocene*, 9(3), 353-362.

Snowball, I., L. Zillén, and P. Sandgren (2002), Bacterial magnetite in Swedish varved lake-sediments: a potential bio-marker of environmental change, *Quaternary International*, 88(1), 13-19.

Sobrinho, R. L., U. Lins, and M. C. Bernardes (2011), Geochemical characteristics related to the gregite-producing multicellular magnetotactic prokaryote *Candidatus Magnetoglobus multicellularis* in a hypersaline lagoon, *Geomicrobiology Journal*, 28(8), 705-713.

Spring, S., and K.-H. Schleifer (1995), Diversity of magnetotactic bacteria, *Systematic and Applied Microbiology*, 18(2), 147-153.

Spring, S., R. Amann, W. Ludwig, K.-H. Schleifer, and N. Petersen (1992), Phylogenetic diversity and identification of nonculturable magnetotactic bacteria, *Systematic and Applied Microbiology*, 15(1), 116-122.

Spring, S., R. Amann, W. Ludwig, K.-H. Schleifer, H. van Gemerden, and N. Petersen (1993), Dominating role of an unusual magnetotactic bacterium in the microaerobic zone of a freshwater sediment, *Applied and Environmental Microbiology*, 59(8), 2397-2403.

Suk, D. (2016), Environmental conditions for the presence of magnetofossils in the Last Glacial Maximum inferred from magnetic parameters of sediments from the Ulleung Basin, East Sea, *Marine Geology*, 372, 53-65.

Tauxe, L. (1993), Sedimentary records of relative paleointensity of the geomagnetic field: theory and practice, *Reviews of Geophysics*, 31(3), 319-354.

Tauxe, L., and G. Wu (1990), Normalized remanence in sediments of the western equatorial Pacific: relative paleointensity of the geomagnetic field? *Journal of Geophysical Research: Solid Earth*, 95(B8), 12337-12350.

Tauxe, L., J. L. Steindorf, and A. Harris (2006), Depositional remanent magnetization: Toward an improved theoretical and experimental foundation, *Earth and Planetary Science Letters*, 244, 515-529.

Tucker, P. (1980), Stirred remanent magnetization: a laboratory analogue of post-depositional realignment. *Journal of Geophysics*. 48, 153–157.

Uebe, R., and D. Schüler (2016), Magnetosome biogenesis in magnetotactic bacteria, *Nature Reviews Microbiology*, 14(10), 621-637.

Uyeda, S., M. Fuller, J. Belshe, and R. Girdler (1963), Anisotropy of magnetic susceptibility of rocks and minerals, *Journal of Geophysical Research*, 68(1), 279-291.

Valet, J.-P., C. Tany, and J. Carlot (2017), Detrital magnetization of laboratory-redeposited sediments, *Geophysical Journal International*, 210(1), 34-41.

Vasiliev, I., C. Franke, J. D. Meeldijk, M. J. Dekkers, C. G. Langereis, and W. Krijgsman (2008), Putative Greigite Magnetofossils From The Pliocene Epoch, *Nature Geoscience*, 1(November), 782-786.

Vinatier, F., P. Tixier, P. F. Duyck, and F. Lescourret (2011), Factors and mechanisms explaining spatial heterogeneity: a review of methods for insect populations, *Methods in Ecology and Evolution*, 2(1), 11-22.

Wack, M. R. (2012), Anisotropy of Magnetic Remanence Development of an Automated System and Application to Natural Sediments Dissertation Ludwig-Maximilians-Universität München.

Wang, Y., W. Lin, J. Li, and Y. Pan (2013), High diversity of magnetotactic Deltaproteobacteria in a freshwater niche, *Applied and Environmental Microbiology*, 79(8), 2813-2817.

Weiss, B. P., S. S. Kim, J. L. Kirschvink, R. E. Kopp, M. Sankaran, A. Kobayashi, and A. Komeili (2004), Ferromagnetic resonance and low-temperature magnetic tests for biogenic magnetite, *Earth and Planetary Science Letters*, 224(1), 73-89.

- Wenter, R., G. Wanner, D. Schüler, and J. Overmann (2009), Ultrastructure, tactic behaviour and potential for sulfate reduction of a novel multicellular magnetotactic prokaryote from North Sea sediments, *Environmental Microbiology*, 11(6), 1493-1505.
- Yamazaki, T. (2009), Environmental magnetism of Pleistocene sediments in the North Pacific and Ontong-Java Plateau: Temporal variations of detrital and biogenic components, *Geochemistry, Geophysics, Geosystems*, 10(7).
- Yamazaki, T. (2012), Paleoposition of the Intertropical Convergence Zone in the eastern Pacific inferred from glacial-interglacial changes in terrigenous and biogenic magnetic mineral fractions, *Geology*, 40(2), 151-154.
- Yamazaki, T., and H. Kawahata (1998), Organic carbon flux controls the morphology of magnetofossils in marine sediments, *Geology*, 26(12), 1064-1066.
- Yamazaki, T., and M. Ikehara (2012), Origin of magnetic mineral concentration variation in the Southern Ocean, *Paleoceanography*, 27(2).
- Zachos, J. C., G. R. Dickens, and R. E. Zeebe (2008), An early Cenozoic perspective on greenhouse warming and carbon-cycle dynamics, *Nature*, 451(7176), 279-283.
- Zachos, J. C., S. Schouten, S. Bohaty, T. Quattlebaum, A. Sluijs, H. Brinkhuis, S. Gibbs, and T. Bralower (2006), Extreme warming of mid-latitude coastal ocean during the Paleocene-Eocene Thermal Maximum: Inferences from TEX86 and isotope data, *Geology*, 34(9), 737-740.
- Zhao, X. (2015), Natural remanent magnetization acquisition in bioturbated sediments, *Imu*.
- Zhao, X., R. Egli, S. A. Gilder, and S. Müller (2016), Microbially assisted recording of the Earth's magnetic field in sediment, *Nature Communications*, 7.
- Zhou, K., W. Y. Zhang, H. M. Pan, J. H. Li, H. D. Yue, T. Xiao, and L. F. Wu (2013), Adaptation of spherical multicellular magnetotactic prokaryotes to the geochemically variable habitat of an intertidal zone, *Environmental Microbiology*, 15(5), 1595-1605.

Kuang He

Geophysics, Department of Earth and Environmental Sciences,
Ludwig Maximilian University of Munich
Theresienstrasse 41/IV, 80333, Munich, Germany

Education

2018.02 (expected) Ph.D. Geophysics, University of Munich, Germany
2013.07 M.Sc. Physical Geography, Lanzhou University, China
2010.07 B.Sc. Geography, Liaocheng University, China

Research Interests

Magnetotactic Bacteria, Biomagnetism, Paleoclimate Change, Paleomagnetism

Research Experience

2015-2017 Doing redeposition experiment using magnetosome-rich sediment at University of Munich
2014-2016 Measuring the abundance of magnetotactic bacteria in Niederlippach, Landshut
2013-2016 Paleomagnetic experiment using “Sushibar”, rock magnetic experiment using VFTB, Spinner Magnetometer JR6A and AGM/VSM at University of Munich and MFK1-FA Kappabridge at University of Tübingen
2012 Paleomagnetic experiment using 2G 760-R Superconducting (Cryogenic) Rock Magnetometer and MMTD 80A at Lanzhou University
Magnetic susceptibility testing of Miocene sediment using Bartington Meter (Model MS2) at Lanzhou University
2011 Extracting heavy minerals from Miocene sediment at Lanzhou University
2010 Paleosol carbon and oxygen isotope testing of Miocene sediment using Finnigan MAT 252 Isotope Ratio Mass Spectrometer (IRMS) at Lanzhou Center for Oil and Gas Resources, Institute of Geology and Geophysics, Chinese Academic of Sciences

Field Experience

2013 Paleomagnetic sampling in the Tarim basin (7 days)
2012 Loess layer drilling in Lanzhou, Gansu Province (16 days)
Paleomagnetic and detrital zircon sampling in the Qaidam basin

and Tongren basin, Qinghai Province (1 month)
2010 Paleomagnetic and pollen sampling in the Tianshui basin, Gansu Province (1 month)

Honors

2017 LMU Completion Grants (October and November)
2017 LMU Travel Grants for EGU General Assembly 2017
2013-2017 China Scholarship Council (CSC) Scholarship
2012 2nd-class Scholarship of Lanzhou University
2011 1st-class Scholarship of Lanzhou University
2010 1st-class Scholarship of Lanzhou University
2010 Outstanding Graduate of Shandong Province, China (top 5%)
2009 National English Contest for College Students, Second Prize (top 1.5%)
2009 National Endeavor Scholarship of China (top 3%)

Publications

1. **He, K.**, S. Gilder, W. Orsi, X. Zhao and N. Petersen (2017), Temporal and spatial distribution of magnetotactic bacteria in controlled aquaria, *Applied and Environmental Microbiology*, 83, e01382-17. Doi: 10.1128/AEM.01382-17
2. **He, K.**, S. Roud, S. Gilder, R. Egli, C. Mayr and N. Petersen. Seasonal variability of magnetotactic bacteria in a freshwater pond. *Geophysical Research Letters* (in revision)
3. Gilder S., M. Wack, **K. He**, J. Jezek. Can magnetic anisotropy improve relative paleointensity estimates from sediments? (in preparation)
4. Wang, X., J. Li, M. Zattin, **K. He**, A. Song, X. Li and L. Deng. Cyclical tectonic activity dominate the Cenozoic growth of the northeastern Tibetan Plateau (in preparation)
5. Meng, Q., P. Gao, R. Zhang, C. Liu, **K. He** and J. Nie. Rock magnetism and high resolution magnetostratigraphy of the late Miocene Huaitoutala section, the Qaidam Basin. *Chinese Journal of Geophysics* (in Chinese with English abstract) (under review)
6. Lhuillier, F., S. Gilder, M. Wack, **K. He**, N. Petersen, B. Slinger, B. Jicha, A. Schaen and D. Colon (2016), More stable yet bimodal geodynamo during the Cretaceous superchron, *Geophysical Research Letters*, 43, 6170-6177. Doi: 10.1002/2016GL069303
7. Liu, S., J. Li, D. Stockli, C. Song, J. Nie, T. Peng, X. Wang, **K. He**, Z. Hui and J. Zhang (2015), Late Tertiary reorganizations of deformation in northeastern Tibet constrained by stratigraphy and provenance data from eastern Longzhong Basin, *Journal of Geophysical Research: Solid Earth*, 120, 5804-5821. Doi: 10.1002/2015JB011949
8. **He, K.** and X. Wang (2013), The climate change recorded by miocene sediment

colour in Wushan basin, Sciencepaper Online (in Chinese with English abstract)
<http://www.paper.edu.cn/releasepaper/content/201301-817>

9. Liu, S., **K. He**, X. Wu, J. Li and C. Song (2012), Improving the methods of heavy minerals pretreatment and minerals separation in mudstone and siltstone, Geological Science and Technology Information, 31 (1): 131-136. (in Chinese with English abstract)
10. Wang, X., J. Li, C. Song, M. Zattin, Z. Zhao, J. Zhang, Y. Zhang and **K. He** (2012), Late Cenozoic orogenic history of Western Qinling inferred from sedimentation of Tianshui basin, northeastern margin of Tibetan Plateau, International Journal of Earth Sciences, 101(5): 1345-1356. Doi: 10.1007/s00531-011-0724-5

Meeting Abstracts

1. Gilder S., M. Wack, **K. He**, J. Jezek. Can magnetic anisotropy improve relative paleointensity estimates from sediments? EGU meeting, Vienna, Austria, April 2018.
2. Gilder S., M. Wack, **K. He**, J. Jezek, S. Roud. Can magnetic anisotropy improve relative paleointensity estimates from sediments? Santa Fe meeting, Utrecht, Netherlands, July 2017. *Oral presentation.*
3. **He, K.**, S. Gilder and N. Petersen. Temporal and spatial variation of magnetotactic bacteria communities in the Niederlippach pond, EGU meeting, Vienna, Austria, April 2017. *Oral presentation.*
4. Coskun, Ö., S. Roud, **K. He**, N. Petersen, S. Gilder, W. Orsi. Tracking heterotrophic and autotrophic carbon cycling by magnetotactic bacteria in freshwater sediments using DNA stable isotope probing, EGU meeting, Vienna, Austria, April 2017. *Poster presentation.*
5. Zhao, X., R. Egli, **K. He**, S. Gilder, Q. Liu and N. Petersen. Insight into the mechanism of natural remanent magnetization of magnetotactic-bacteria-bearing freshwater sediments, AGU Fall meeting, San Francisco, CA, U.S.A., December 2014. *Poster presentation.*

Personal Interests

Soccer, Geography, Jogging